A Dissertation

entitled

Novel Microtubule-Disrupting Indole-Based Chalcones That Induce Cell Death in

Glioblastoma

by

Shengnan Du

Submitted to the Graduate Faculty as partial fulfillment of the requirements for the

Doctor of Philosophy in Medical Science: Cancer Biology

_____
Dr. William A Maltese, Committee Chair

_____
Dr. Randall Ruch, Committee Member

_____
Dr. Kathryn Eisenmann, Committee Member

_____
Dr Jeffrey G Sarver, Committee Member

_____
Dr. Saori Furuta, Committee Member

_____
Dr. Amanda Bryant-Friedrich, Dean
College of Graduate Studies

The University of Toledo

December 2017

An Abstract of

Novel Microtubule-Disrupting Indole-Based Chalcones That Induce Cell Death in
Glioblastoma

by

Shengnan Du

Submitted to the Graduate Faculty as partial fulfillment of the requirements for the
Doctor of Philosophy Degree in
in Medical Science: Cancer Biology

The University of Toledo

December 2017

The extremely poor prognosis of Glioblastoma multiforme highlights the urgent

need for more efficient drugs to treat this disease. We have developed a series of small

molecules that induce a novel non-apoptotic cell death mechanism, methuosis, in cancer

cells. During the structure-activity relationship study of methuosis-inducing compounds,

we identified a group of unique chalcone derivatives with more potent anti-tumor activity.

The lead compound is 3-(6-methoxy-2-methyl-1H-indol-3-yl)-1-(4-pyridinyl)-2-propene-

1-one (6-MOMIPP). 6-MOMIPP exhibits potent anti-proliferative and cytotoxic activity

in glioblastoma, melanoma, and lung cancer cell lines at concentrations in the nanomolar

range. However, cells treated with the new class of compounds did not morphologically

resemble cells undergoing methuosis. By 24 h, 6-MOMIPP causes the majority of cells to

round up from the culture dish and arrest in mitosis. By 48 h, cell viability is greatly

reduced, correlating with activation of caspases 9, 7, and 3. Caspase inhibitors block the

cell death induced by 6-MOMIPP, suggesting that cell death is caspase-dependent. Phase

contrast images show that the few cells remaining alive after treatment with 6-MOMIPP

are giant, flat, and multiple micronucleated. Whole cell tubulin polymerization assay shows that 6-MOMIPP significantly reduces the amount of polymerized tubulin in living cells. Immunofluorescence staining of microtubules reveals microtubule disruption in U251 cells after treatment with 6-MOMIPP at a concentration of 250 nM or higher. *In vitro* scintillation proximity assay and EBI cross-linking studies of β-tubulin in intact cells both reveal that 6-MOMIPP binds to tubulin on the colchicine binding site. Blocking Cdk1 activity with BMS-265246 greatly reduces cell death induced by 6-MOMIPP, but has no effect on the mitotic arrest, suggesting that blockage of metaphase-anaphase transition by prolonged Cdk1 activation is responsible for the 6-MOMIPP-induced death. Treatment of cells for 24 h with 6-MOMIPP induces phosphorylation of Bcl-2 and Bcl-xL, which could be eliminated by inhibiting Cdk1, suggesting that Cdk1 plays a key role in phosphorylation of the anti-apoptotic Bcl proteins. Cell death induced by 6-MOMIPP is also accompanied by activation of JNK and its downstream substrate c-Jun. Blocking JNK activity with SP600125 reduces the percentage of dead cells, indicating that JNK activation may contribute to the cell death. Cell viability studies have shown the toxicity of 6-MOMIPP is substantially reduced in quiescent human fibroblasts, HUVEC (human umbilical vein endothelial cells) and rat neuronal progenitor cells. Pharmacokinetic studies in mice show that 6-MOMIPP attains brain concentrations that are nearly equal to plasma concentrations at time points up to 8 h after intraperitoneal (i.p.) injection, suggesting that 6-MOMIPP readily crosses the blood-brain barrier. 6-MOMIPP administration at 20 mg/kg every 12 h for 12-15 days significantly decreases the growth of glioblastoma in subcutaneous and intracranial xenograft models without notable toxicities, suggesting that 6-MOMIPP has good anti-tumor activity *in vivo*. These preliminary findings suggest that 6-MOMIPP

merits further preclinical evaluation as a potential therapeutic agent for primary and metastatic brain tumors.

Acknowledgements

I am grateful to the many people that have enabled me to endure the journey of my Ph.D. education. This work wouldn't have been completed without them.

I would like to acknowledge my advisor, Dr. William Maltese, for his guidance throughout my Ph.D. training and the life lessons he has taught me, which will benefit me for years to come. He trained me to grow as a scientist and helped me to improve my skills in scientific presentations and writing. He is one of the most patient and brilliant mentors I have ever met. I'm very grateful to have received my training in his lab.

I would also like to thank Dr. Overmeyer for teaching me most skills and techniques during the course of my training. She has always been there for her students, making my research project much more efficient. I also appreciate valuable insights of Dr. Ruch and Dr. Eisenmann into my projects; they have challenged my thinking in many ways. I thank Dr. Sarver for his professional training and help with the pharmacokinetic studies. Also, I thank Dr. Furuta for agreeing to be on my committee at the last minute, and her wonderful ideas for my project.

I'd like to thank all my friends for supporting and encouraging me through the past years, especially during tough times. We not only supported each other by deliberating over our studies, but also happily talked about things other than just our research. I'm so blessed to have you all in my life.

Many thanks my beloved parents who offer unconditional love and support, and have always been there for me. Their understanding and help have allowed me to be successful in graduate school. Thank you for letting me find my own way. I would not be where I am today without your support. You are the best parents!

Finally, I thank my husband, Sage, for being by my side, he has supported and encouraged me throughout this process. I am truly grateful to have him in my life.

Thank you everyone who has supported and inspired me!

Table of Contents

List of Figures

Chapter 1

Literature Review

1.1   Current Challenges in Treatments for Brain Cancer

1.1.1   Glioblastoma multiforme (GBM)

Malignant brain cancer is one of the most feared cancers due to its extremely poor prognosis. The most common form of brain malignancy is glioma, which includes astrocytomas, ependymomas, oligodendrogliomas, and some other less frequent subtypes [1-4]. Based on the histologic classification from the World Health Organization (WHO), astrocytoma can be divided into four grades: grade I, pilocytic astrocytoma; grade II, diffuse astrocytoma; grade III, anaplastic astrocytoma; and grade IV, glioblastoma [5]. Grade IV astrocytoma or glioblastoma multiforme (GBM) is the most widespread and lethal brain cancer of the central nervous system, accounting for more than 60% of all brain tumors in adults [6]. GBM can occur at any age but is more commonly found between ages 55 to 60. The average survival rate of GBM patients after diagnosis is only15 month [7].

The incidence and treatment outcomes of GBM are influenced by many factors including age, grade, and specific mutation markers. For patients between age 30 to 85, the median survival is reduced by 0.5-4 months with each 5-year increment in age [8]. Primary GBM, which accounts for 90% of GBM, is usually found in patients 50 years old and above. Primary GBM is characterized by overexpression of EGFR (epidermal growth factor receptor), loss of heterozygosity of chromosome 10q (LOH), PTEN (phosphatase and tensin homology gene) mutations, and p16 deletion [9]. Secondary GBM, which evolves from low-grade astrocytomas or oligodendrogliomas is usually found in younger patients and is less common than primary GBM [10]. Secondary GBM generally harbors mutations in TP53 and IDH1, 19p loss, and overexpression of platelet-derived growth factor receptor (PDGFR) and Rb [9-11]. The genetic differences between primary and secondary GBM may lead to different responses to radiotherapy and chemotherapy.

1.1.2 Treatment for Glioblastoma

The current standard treatment for GBM patients is maximal surgical resection when feasible (depending on the location of the tumor), followed by radiotherapy plus daily temozolomide (TMZ) [12-14]. Surgery cannot completely remove the malignant glioma due to its high infiltration, and relapse occurs in approximately 95% of patients within 7-20 months after surgery [15]. Radiotherapy also has its limitations, which include severe neurological disorders, permanent neuronal damage, and radiation therapy resistance of some tumors. Large-scale clinical trials have shown that a combination of radiotherapy and TMZ can increase patients' survival rate [12], but this can also cause

2

severe side effects [13]. In addition to standard chemotherapy, alternative chemotherapies including PVC drug combination (procarbazine-vincristine-CCNU), CAP drug combination (cyclophosphamide-doxorubicin-cisplatin), and BCNU (bis-chloroethyl nitrosourea) have been developed. Also, approaches based on different mechanisms like the anti-VEGF agent, bevacizumab; the anti-EGFR agent, erlotinib; and tyrosine kinase inhibitors have been investigated [14]. However, none of these have been found to significantly improve the outcomes in clinical trials. Immunotherapy, which kills the tumor cells by activating the immune system, and gene therapy, which involves delivering genetically modified virus-based vectors into the cancer cells seem to give promising results in preclinical trials, but further investigations are still needed.

With all the attempts to improve standard therapy, the best treatment can only provide patients with a median survival of 15 months [16]. GBM recurrence occurs in almost all patients, and treatment options for recurrent diseases are even more limited. The recent discovery of cancer stem cells (CSC) may provide one explanation for therapeutic resistance, since traditional therapy that focuses on eliminating the bulk of cancer cells may have no effect on removing CSC [15]. Other factors that may contribute to chemoresistance of GBM may include overexpression of O6-methylguanine-DNA methyltransferase (MGMT), up-regulation of multidrug resistance genes, and defects in the genes that regulate programmed cell death via apoptosis [17-19].

Major challenges in treating GBM include the high infiltration characteristics of the tumor and the rapid proliferation rate of cancer cells, the ability of the blood-brain barrier (BBB) to prevent effective drug delivery to CNS, and specific gene alterations in

the GBM cells (e.g., MGMT methylation, IDH1, IDH2, TERT mutations) [20-22]. Overcoming these difficulties is crucial for improving the overall survival of the patients and should be prioritized in new therapy development.

1.1.3   Brain metastases and treatment

Primary brain tumors arise from cells in the CNS, while secondary brain tumors metastasize from a distant tumor. Brain metastasis (BM) is the most serious clinical complication of cancer given that it is 10 times more common than primary brain tumors. As cancer therapies improve the patient's overall survival, they are at higher risk to develop BM in the long run. Around 20-40% of patients with cancer will develop brain metastases [23]. With limited treatment options, the average survival period of patients with BM is less than 2 months. Brain metastases usually arise from lung, breast, and melanoma malignancies, and account for 67–80% of BM [24, 25]. Current care for patients with BMs includes whole-brain radiation therapy (WBRT), surgery, stereotactic radiosurgery (SRS), and systemic therapy depending on the number, size, and site of metastases [26]. Whole-brain radiation therapy (WBRT) has been considered the main radiation treatment option for brain metastases [27], but it leads to significant cognitive side effects such as neurocognitive decline or radiation encephalopathy, dementia, brain atrophy, and coma [28]. SRS can deliver radiation to a focal tissue with better accuracy and shorter treatment duration but is limited beyond certain numbers of BM [29]. Systemic therapy, particularly chemotherapy, provides simultaneous treatment for both primary cancer and brain metastasis, but BM that arise from a subpopulation of the primary tumor or have acquired new mutations may exhibit drug resistance [30]. BBB

permeability is another potential obstacle for BM treatment. Around 98% of the CNS cancer drugs fail to enter clinical trials due to insufficient drug penetration of the BBB [31]. In order to tackle brain metastases, efforts should concentrate on identifying novel targets to prevent and treat BM and drug design to improve CNS penetration and balance between treatment efficacy and neurotoxicity.

1.2   Microtubules as targets for cancer treatment

1.2.1   Why target Microtubules?

Microtubules (MTs) play very important roles in cells. They are the major components of the mitotic spindle, which separates two sets of duplicated chromosomes into two daughter cells. Disruption of microtubule function induces defects in spindle assembly or spindle-kinetochore attachment, which the activates the spindle assembly checkpoint (SAC) and prevents cells from entering metaphase-anaphase transition [32]. Prolonged cell cycle arrest eventually will lead to cell death. Tumor cells have uncontrolled mitosis compared to normal cells. The rapid progression of cancer cells through mitosis makes them more vulnerable to anti-mitotic drugs [28]. Thus, microtubule targeting agents (MTAs) that disrupt microtubule functions are among the most successful anti-tumor strategies [29].

1.2.2   Microtubules and their complex dynamics

Microtubules are found in all eukaryotic cells and are one of the three major components of the cytoskeleton. They are crucial for many cellular functions including maintenance of cell shape, transportation of intracellular vesicles and organelles, cell motility, and

separation of chromosomes during cell division [33, 34]. MTs are tube-shaped polymers of α-tubulin and β-tubulin heterodimers. A microtubule has two ends, the plus (+) end and the minus end (-), where tubulin subunits are added or removed to accomplish the growth or shrinkage of MT. At the plus end (+), the addition or removal of subunits is faster, with β-tubulin facing out; while at the minus end (-), the addition or removal is relatively slow, with the α-tubulin facing out. Tubulin polymerizes to MTs using the energy provided by GTP (Fig. 1-1). Heterodimers slowly assemble to form a short MT nucleus, followed by rapid, reversible, noncovalent addition of tubulin for elongation to form a hollow cylinder [35]. The MT core is formed by tubulin-GDP, while stabilizing tubulin-GTP caps at the ends of the MT inhibit depolymerization [36, 37].

MTs are not simply equilibrium polymers. They have complex polymerization dynamics that are precisely controlled by numerous factors to regulate many cellular functions. Dynamic instability and treadmilling are two types of dynamics that MT use to accomplish movement. Dynamic instability is a process in which MT rapidly switch between phases of growth and shrinkage, altering the length of MT [38]. On the other hand, treadmilling, is a process by which MTs grow at one end while shortening on opposite end, so that the length of MT remains unchanged [36]. The shift between microtubule elongation and shortening is dynamic [39].

Stable or capped microtubule — Tubulin-bound GDP — Tubulin-bound GTP
Tubulin-bound GTP or GDP–Pi
Cap

Cap loss

Depolymerizing microtubule

Tubulin-bound GDP
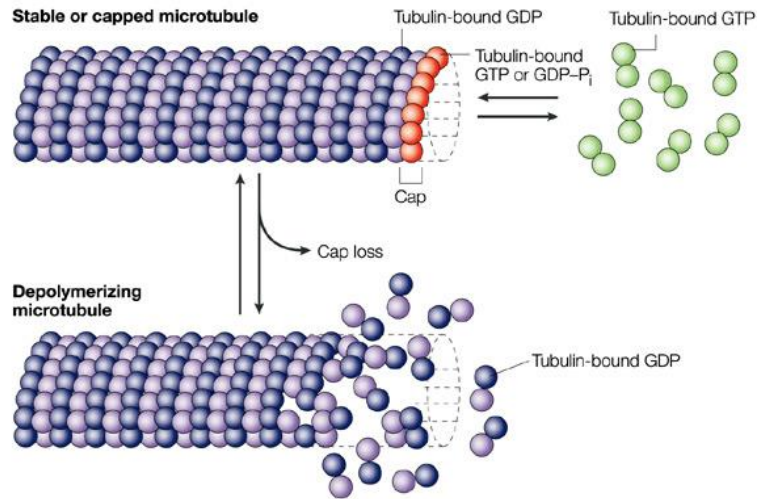
Nature Reviews | Cancer

Figure 1-1. Polymerization dynamics of microtubules and the GTP cap. (Jordan, Mary Ann, and Leslie Wilson. "Microtubules as a target for anti-cancer drugs." Nature Reviews Cancer 4.4 (2004): 253-265.[40]) [Reprinted with permission of Nature Reviews Cancer].

MT dynamics in cells are relatively slow during interphase, but increase 20-100 fold during mitosis, as required for correct segregation of chromosomes [41, 42]. During prometaphase, the MT in spindle poles grow and shorten rapidly to probe the three-dimensional space facilitating chromosome capture and attachment to kinetochores. In metaphase, microtubules oscillate back and forth under high tension with attached chromosomes to align them at the metaphase plate [43]. During anaphase, microtubules shorten at the same time to separate the chromosomes synchronously into two daughter cells [44]. The importance of MT during mitosis and cell division makes them one of the

most successful anti-cancer drug targets. In general, cancer cells that divide rapidly and undergo mitosis frequently are more vulnerable to mitotic poisons than normal cells.

MT dynamics can be affected by the expression and phosphorylation of the microtubule associated proteins (MAPs), which include microtubule stabilizing proteins (e.g. cyclin-dependent kinase 1, tau), microtubule destabilizing proteins (e.g. oncoprotein 18, katanin, XKCM1) [32] and microtubule regulatory proteins (e.g. motor proteins kinesins, dyneins) [39]. In addition, many natural or synthesized compounds such as taxols, *Vinca* alkaloids and combretastatin, which are referred to as microtubule-targeting agents (MTAs), can also affect the dynamics of MTs.

1.2.3   Microtubule targeting agents

In the past decades, a large number of compounds that bind to and act on tubulin or microtubules have been successfully used in the treatment of cancer. MTAs interfere with highly dynamic mitotic spindle microtubules, disrupt spindle assembly or spindle-kinetochore attachment, and inhibit mitotic progression [45]. Based on the mechanism of action, MTAs can be classified into two major groups: microtubule stabilizing agents (MSAs) and microtubule destabilizing agents (MDAs). MSAs, such as paclitaxel and docetaxel, stabilize microtubule polymers and inhibit microtubule depolymerization. MDAs, such as *Vinca* alkaloids (vinblastine, vincristine) and colchicine, prevent polymerization of tubulin subunits and destabilize the microtubules. Despite the difference in mechanisms of action between MSAs and MDAs , the general anti-mitotic outcome is similar: at high concentrations, those drugs block the dividing cells in mitosis by increasing or decreasing the microtubule polymer mass; at low concentrations, they

block the mitosis by suppressing the dynamics of spindle microtubules without changing the microtubule organization [46]. It is estimated that 1-2% binding can reduce microtubule mass by 50%, which makes MTAs potent in killing cancer cells [47].

Different types of MTA bind to different sites on the tubulin heterodimer or at different positions within the microtubules. There are generally three binding sites on tubulin: the taxol binding site, the colchicine binding site, and the *Vinca* alkaloid binding site (Fig. 1-2, Fig. 1-3). *Vinca* alkaloids (e.g. vinblastine, vincristine) bind to the plus end of MT (Fig. 1-2A, Fig. 1-3) to suppress microtubule dynamics. Colchicine binds to soluble tubulin dimers to form complexes, and then copolymerizes into the microtubule lattice, suppressing microtubule dynamics. This process is slow and quasi-irreversible (Fig. 1-2B, Fig. 1-3). Paclitaxel binds to the β-tubulin subunit along the microtubule surface (Fig. 1-2C, Fig. 1-3), which promotes assembly and inhibits disassembly of microtubules, thus stabilizing microtubule dynamics [48, 49].
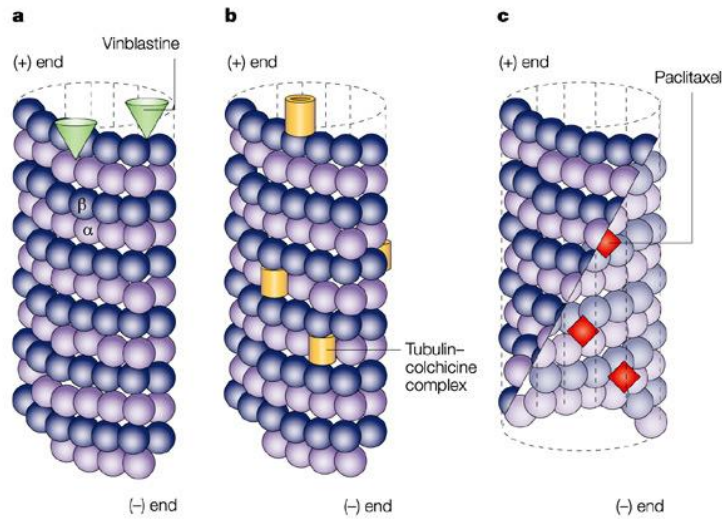
Figure 1-2. Three binding sites on microtubules. A. Vinblastine bound to high-affinity sites at the microtubule plus end. B. Colchicine bound to soluble tubulin and suppressing microtubule dynamics. C. Paclitaxel suppresses microtubules' dynamics by binding along the interior surface of the microtubule.

(Jordan, Mary Ann, and Leslie Wilson. "Microtubules as a target for anticancer drugs." Nature Reviews Cancer 4.4 (2004): 253-265.[40]) [Reprinted with permission of Nature Reviews Cancer].
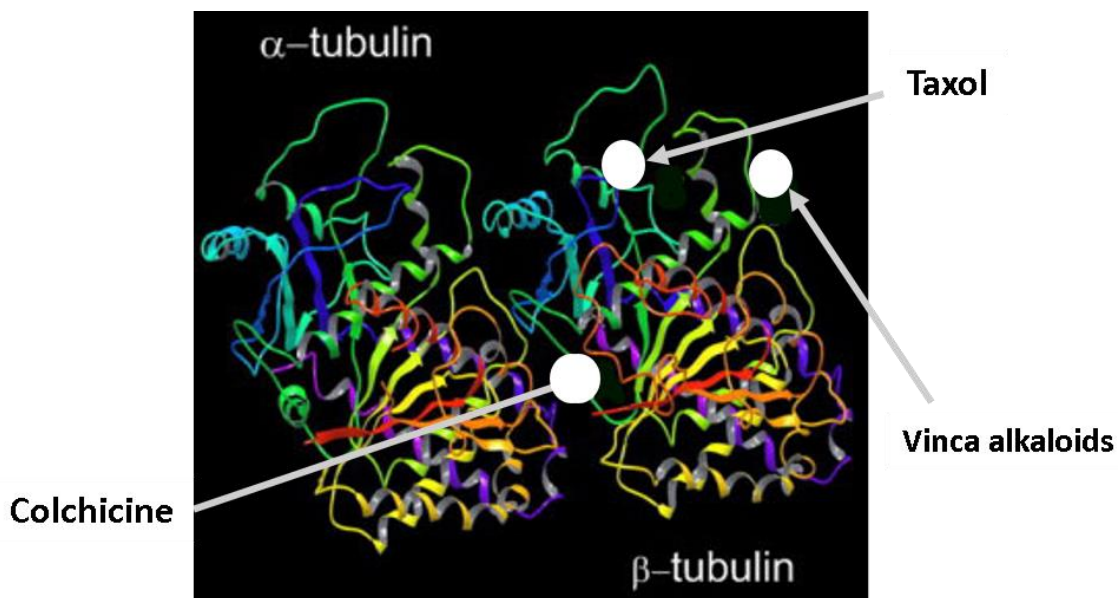
Figure 1-3. 3D structure of tubulin heterodimer with three binding sites.

MTAs are unique compared to other types of anti-cancer agents due to their extreme diversity and structural complexity. Drugs that bind to the *Vinca* alkaloid site, including vinblastine, vincristine, vinorelbine, vindesine, vinflunine, dolastatins, are effective in treating lymphomas, leukemias, bladder cancers, and breast cancers, but they typically require intravenous (IV) administration and generally are associated with neurotoxicity and myelosuppression [50, 51]. Drugs that bind to the taxol site, including paclitaxel and docetaxel, are used to treat solid tumor malignancies [52, 53]. Epothilone and its derivatives are taxol domain binding agents with increased water solubility and improved penetration of the BBB [54]. Colchicine is not used as an anti-tumor drug because of its severe toxicities. However, some drugs that bind to the colchicine site, such as combretastatins, podophyllotoxin, and BNC105, are used as anti-angiogenesis agents for cancer treatment [55]. Several other colchicine site-binding MTAs including

11

plinabulin, ombrabulin and verubulin are currently under clinical investigation as anti-cancer agents [56]. Currently, several microtubule destabilizing agents which bind to novel sites on tubulin are under investigation as cancer therapeutics. These include hemiasterlin, estramustine, noscapine, and herbicides [57].

Although MTAs are widely used as chemotherapeutic agents, a major limitation is their high toxicity. Disrupting microtubule dynamics in non-dividing cells, such as peripheral neurons, can lead to neuropathy. Disrupting microtubules in hematologic cells can induce myelosuppression. Neurotoxicity may be the result of inhibition of vesicle trafficking along nerve fibers and disruption of the normal cytoskeleton of neurons. The resulting morbidity, such as constipation or intestinal paralysis, is usually permanent [58]. Another drawback of using MTAs clinically for cancer treatment is that many cancers acquire resistance to those drugs over time. Development of resistance to MTAs has several potential mechanisms. First, increased P-glycoprotein (P-gp, the product of the multi-drug resistance gene) may accelerate drug efflux [59]. Second, mutation and/or post-translational modification of tubulin may prevent drug binding. Third, changes in expression of the 13 isotypes of α- and β-tubulin can alter microtubule dynamics and response to MTAs. For example, increased level of βIII-tubulin is associated with resistance to taxanes in lung, breast and ovarian cancers [60, 61]. Fourth, alterations in the expression, intracellular localization, or post-translational modification of microtubule-regulatory proteins can influence the sensitivity of microtubules to MTAs. Last, but not least, cancer cells typically possess lesions in genes that mediate apoptosis, which can reduce sensitivity to MTA-induced cell death.

To overcome challenges like multidrug resistance and high toxicity, efforts should be made in the following aspects of MTA development. Structure-activity relationship studies can improve on existing compounds by selecting agents that are insensitive to resistance mechanisms, with increased tumor selectivity, and reduced side effects. Discovery of novel MTAs that are insensitive to active efflux can help to overcome multidrug resistance. Discovery of new agents that disrupt mitosis without interfering with microtubule dynamics in non-dividing cells can help to overcome high toxicity. In addition, novel microtubule-interacting drugs with different binding sites might have synergistic effects with current MTAs [62], which may help to widen the therapeutic window, avoiding toxicity as well as cross-resistance. Besides multidrug resistance and high toxicity, challenges such as low bioavailability, poor solubility, and low penetrance through the BBB should also be considered when it comes to new drug development. New formulations and different analogues can help to improve the MTA's pharmaceutical properties.

1.2.4 Chalcones as novel microtubule targeting agents

Although paclitaxel and *Vinca* alkaloids are widely used clinically for cancer treatment, due to the limitations of those drugs, new MTAs with higher therapeutic index and better biopharmaceutical properties are highly desired. Natural products are an excellent resource for drug discovery; most MTAs were discovered from the large-scale screening of natural products. Chalcones are widely distributed natural precursors of flavonoids, and their derivatives (compounds with a 1, 3-diphenyl-2-3propen-1-one scaffold) have been found to exhibit a variety of pharmacological properties, including broad spectrum

anti-tumor activity [63]. In recent years, many chalcone-inspired compounds have been designed and synthesized with the purpose of enhancing their anti-tumor activity. Some studies have reported that microtubule destabilization is the major mechanism by which chalcone derivatives exert their anti-tumor activity [64-70]. A recent study revealed that chalcones with a methoxy group on the aromatic ring have selective anti-proliferative activity in cancer cells compared to normal cells [71]. In addition, indole-based chalcones with improved translational potential as anti-tumor drugs have been shown to destabilize microtubules [64, 65, 72]. Thus, the above findings suggest that chalcone synthesis and molecular modification is a promising strategy to gain better anti-tumor agents.
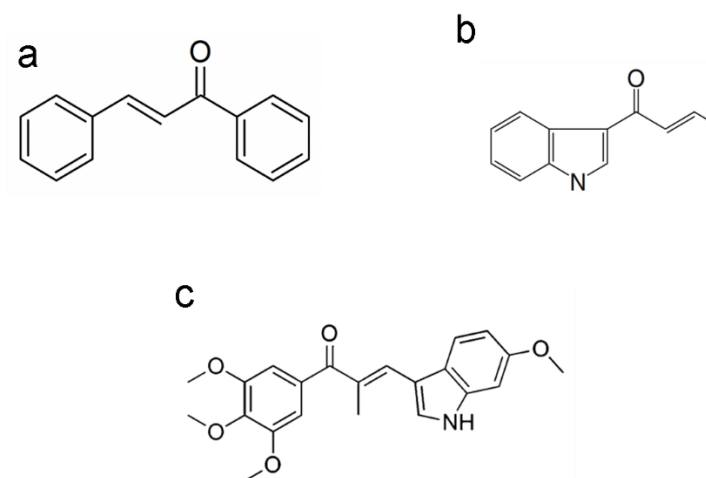
Figure 1-4. Microtubule targeting indole-chalcone analogs. A. structure of chalcone. Compounds B-C, which share the indole-chalcone scaffold, are reported as novel microtubule disrupting compounds [64, 65].

1.3   MTA-induced cell death mechanism

1.3.1 Spindle assembly checkpoint
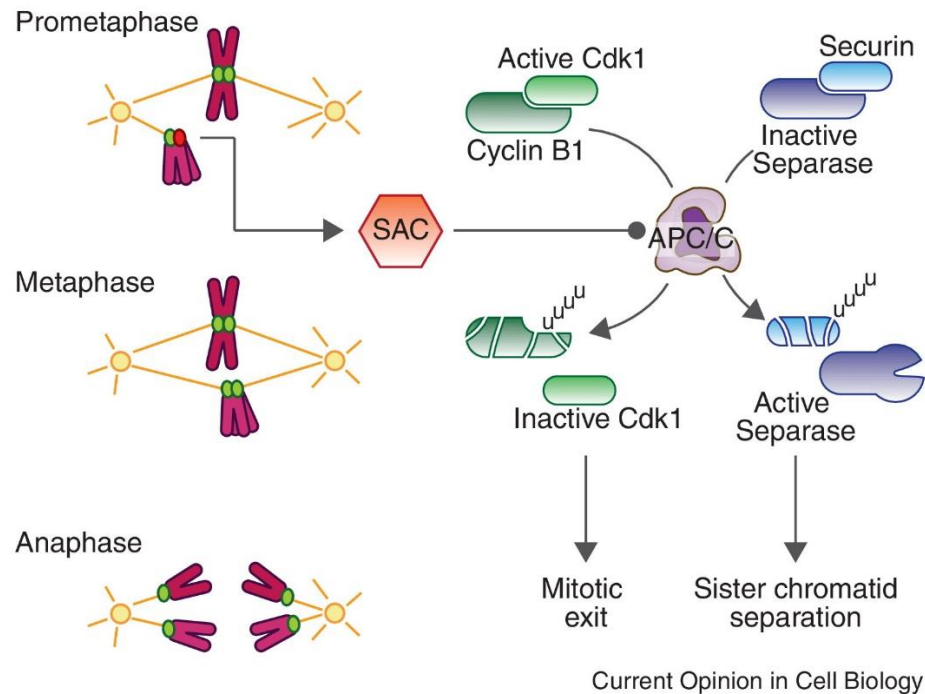
Figure 1-5. The function of the spindle assembly checkpoint during mitosis.

In prometaphase, unattached kinetochores activate the spindle assembly checkpoint, which can inhibit the anaphase-promoting complex (also called APC/C or cyclosome) from signaling mitotic exit. Once all the chromosomes are stably attached to kinetochore spindle microtubules, APC/C will degrade cyclin B1 and securin. The degradation of these two proteins signals chromatid separation and mitotic exit. (Topham, Caroline H., and Stephen S. Taylor. "Mitosis and apoptosis: how is the balance set?" Current Opinion in Cell Biology 25.6 (2013): 780-785. [73]) [Reprinted with permission of Current Opinion in Cell Biology].

Non-replicating mammalian cells are in the G_0 (quiescence) phase. Replicating cells undergo a classical "cell cycle" consisting of interphase and the mitotic phase.

Interphase is typically divided into the G_1 phase (first growth phase), S phase (DNA replication), and G_2 phase (second growth phase). The mitotic or M phase (also known as chromosome separation phase) can be divided into 6 subphases: prophase, prometaphase, metaphase, anaphase, telophase, and cytokinesis. Cell cycle progression is monitored by three checkpoints to ensure the fidelity of chromosome replication and segregation. These checkpoints include the G_1 checkpoint at the end of the G_1 phase, the G_2 checkpoint during G_2/M transition, and the spindle assembly checkpoint (SAC) during mitosis. The SAC keeps the fidelity of mitosis progression by transiently blocking the metaphase-anaphase transition until all chromosomes obtain bipolar attachment to kinetochore microtubules [32]. Upon proper attachment of chromosomes, the SAC is switched off to allow APC/C to degrade cyclin B and securin, which signals chromosome separation and mitosis exit. MTAs disrupt assembly of spindle microtubules, reduce the tension at chromosomal kinetochores, and prevent chromosomes from obtaining correct bipolar attachment. The presence of a single chromosome that is unable to achieve correct attachment is sufficient to sustain the activity of SAC. Prolonged activation of SAC blocks mitotic progression and triggers cell death machinery [74]. More frequent cell division and a high frequency of cell-cycle checkpoint deficiencies in cancer cells can make them more sensitive to MTA-induced mitotic cell death.

1.3.2 Cyclin-dependent kinases

Cyclin-dependent kinases (Cdks) are a family of serine/threonine protein kinases comprised of three cell-cycle-related subfamilies (e.g. Cdk1, Cdk4, and Cdk5), whose activities depend on formation of regulatory complexes with one of 29 noncatalytic

regulatory cyclins (e.g. cyclin B, cyclin Y, and cyclin C) [75, 76]. Progression of the cell

cycle is precisely controlled by the complexes of Cdks and cyclins [77]. Cyclin B is a

pivotal activator of Cdk1 in mitosis. The Cdk1/cyclin B1 complex regulates cell cycle

progression in mitosis. The activity of Cdk1/cyclin B1 must be sustained from prophase

to metaphase (Fig. 1-6). Otherwise, cells stay at G_2 phase without entering mitosis [78].

The activity of Cdk1 is controlled by the following mechanisms: 1) Cyclin B1

distribution and degradation is tightly associated with Cdk1 activity. During early

mitosis, the Cdk1/cyclin B1 complex translocates from the cytosol to the nucleus to

phosphorylate and activate mitotic substrate proteins. By the end of metaphase, cyclin

B1 is degraded by the ubiquitin-proteasome pathway, which turns off Cdk1 and signals

mitotic exit [79-81]. Premature entry of the complex into the nucleus leads to premature

chromatin condensation and apoptosis [82]. 2) Phosphorylation of Cdk1 inhibits its

activity during the G2 phase, while dephosphorylation of Cdk1 during early mitosis

activates Cdk1 [83]. 3) Intracellular Cdc25 phosphatases activate Cdk1 by

dephosphorylating Cdk 1 on Thr 14 and Tyr15 sites [84]. Cdk 1 is maintained in an

inactive state through the phosphorylation of these two sites by members of the

Wee1/Mik1/Myt1 protein kinase family [84, 85]. Checkpoint kinases (Chk1, Chk2)

inhibit Cdk1 activity at G2/M phase [86].

MTAs lead to prolonged SAC activation and APC/C inhibition. Without APC/C-

mediated degradation of cyclin B1, Cdk1 maintains its activity, which blocks the cell

cycle at the metaphase-anaphase transition phase. Prolonged activation of Cdk1 can also

stimulate p53 to upregulate the expression of pro-apoptotic Bcl-2 proteins, and Cdk1 can

directly phosphorylate Bcl-2, leading to mitochondrial membrane permeabilization (MMP) and apoptosis [87, 88].
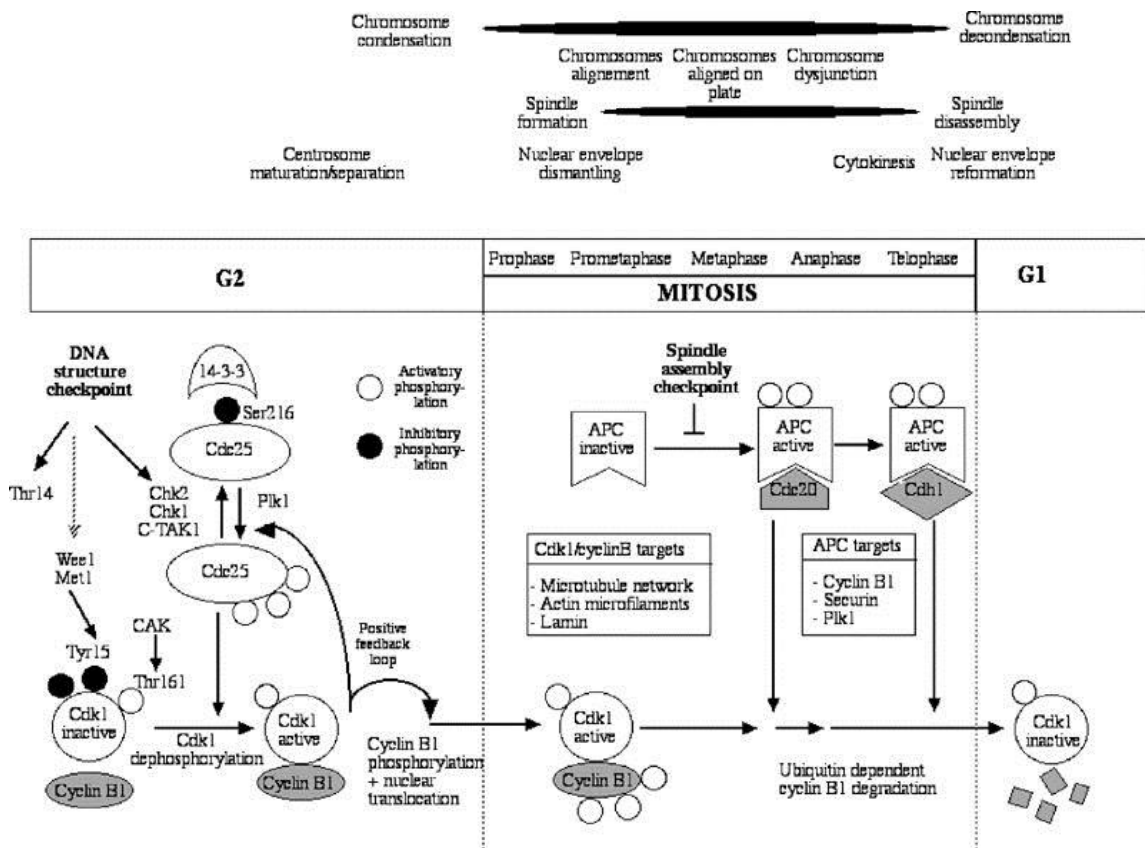
Figure 1-6. Involvement of Cdk1/cyclin B1 complex in cell cycle control.

During G$_2$-M transition, cdc25 dephosphorylates Cdk1 on Thr-14 and Tyr-15, thereby promoting the assembly of an activeCdk1/cyclin B1 complex. Upon activation, Cdk1/cyclin B1 complex translocate to the nucleus and triggers the phosphorylation of mitotic substrate proteins. Once all chromosomes have obtained the bipolar attachment, APC/C induces the ubiquitination of cyclin B1, triggering entry into anaphase. (Castedo, Maria, et al. "Cell death by mitotic catastrophe: a molecular definition." Oncogene 23.16 (2004): 2825. [79]) [Reprinted with permission of Oncogene].

1.3.3 Mitotic catastrophe
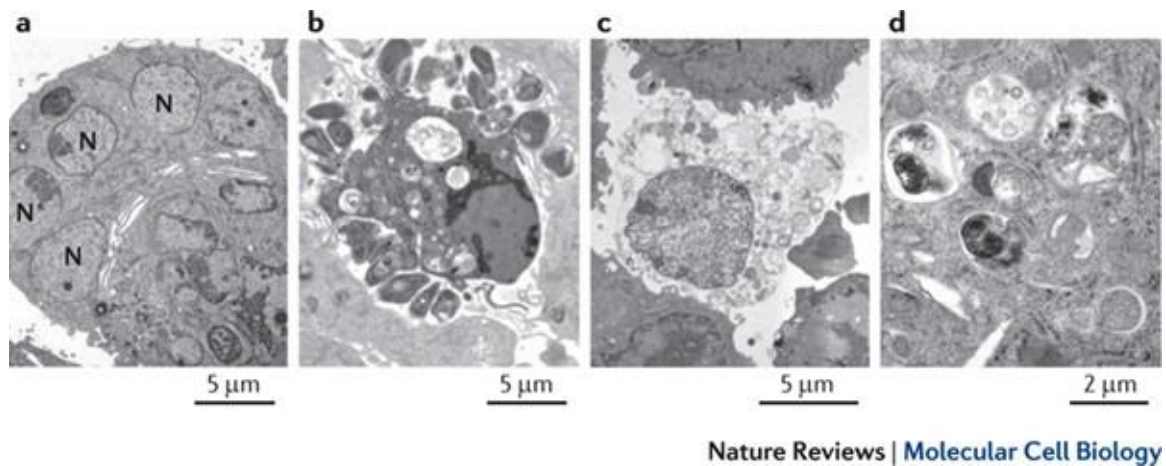
Figure 1-7. Electron microscopy images of different cell death processes.

a: HCT-116 cells undergo mitotic catastrophe showing the accumulation of multiple micronuclei (N, nucleus). b: HeLa cells undergoing apoptosis with chromatin condensation and plasma membrane blebbing. c: CT26 cells undergoing necrosis show nuclear membrane dilatation, circumscribed chromatin condensation, and cytoplasm swelling. d: Murine striatal cells exhibiting autophagic vacuolization. (Vitale, Ilio, et al. "Mitotic catastrophe: a mechanism for avoiding genomic instability." Nature reviews. Molecular cell biology 12.6 (2011): 385.[89]) [Reprinted with permission of Nature reviews].

Mitotic catastrophe (MC) is a cell death process that occurs as a result of failure to complete mitosis [90]. It is an oncosuppressive mechanism used by the cell to drive itself to an irreversible fate when it senses mitotic failure. The concept of MC was first used in 1986 to describe cells that prematurely entered mitosis [91]. It has been a controversial concept because some considered it as a cause of cell death rather than a mode of cell

death [92]. Nevertheless, definitions of MC that cover both morphological and biochemical aspects have been widely used. MC can be triggered by DNA damage, microtubule disruption, or dysfunctional cell cycle checkpoints [89, 92]. Formation of multiple spindle poles due to centrosome overduplication can also trigger MC [17]. MC is always accompanied by mitotic arrest, and the most prominent morphological characteristic is the formation of giant cells with multiple micronuclei that originate from aberrant chromosome segregation [92].
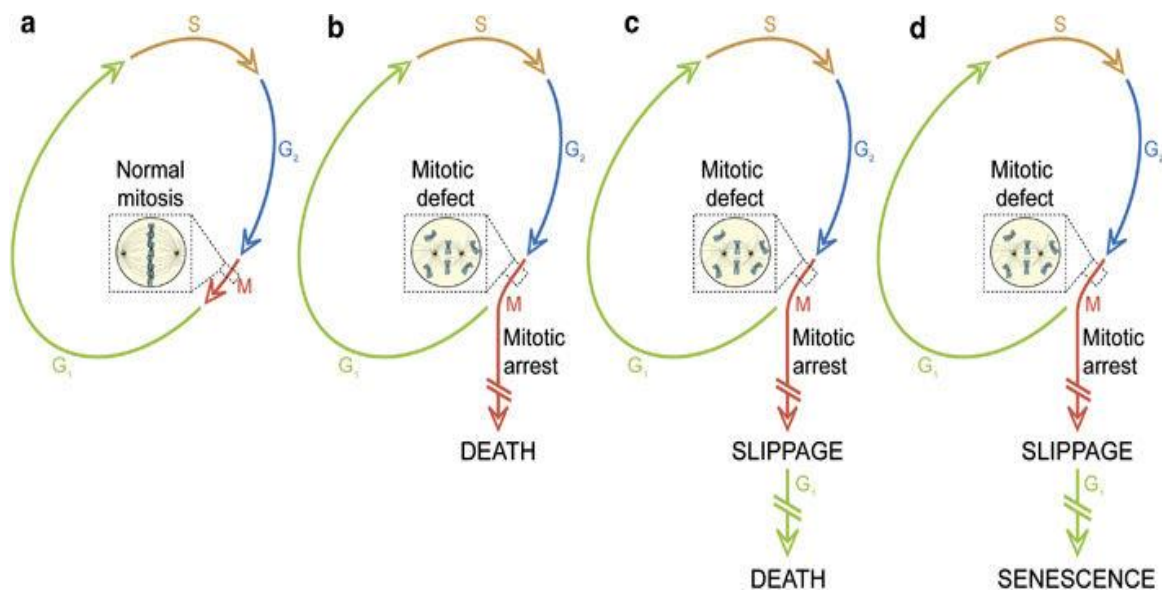
Figure 1-8. Outcomes of mitotic catastrophe. a. A healthy cell progress through the G_1, S, G_2 and M phases to complete a normal cell cycle. During mitotic catastrophe, mitotic arrest can trigger different fates: b. Cells die during mitosis arrest. c. Cells die in the G_1 phase of the subsequent cell cycle after mitotic slippage, d. Cells exit mitosis and undergo senescence. (Galluzzi, Lorenzo, et al. "Molecular definitions of cell death subroutines: recommendations of the Nomenclature Committee on Cell Death 2012."

Cell death and differentiation 19.1 (2012): 107. [90]) [Reprinted with permission of Cell death and differentiation].

Cell death through MC is not homogeneous because different initiating stimuli or genetic backgrounds can lead to different outcomes. Currently, there are three major outcomes of mitotic catastrophe that have been well addressed [89, 90].

    The first possible outcome is mitotic cell death, during which cells die without exiting mitosis after a prolonged mitotic arrest (Fig. 1-8 b). During 'mitotic death', mitotic derangement activates SAC that arrests cells in the mitotic phase. Cell death machinery will be triggered in the presence of accumulated cyclin B1 [93]. Cell death occurring at this phase is characterized by caspase-2 activation and mitochondrial membrane permeabilization, with release of cell death effectors such as cytochrome c [79]. The second possible outcome is mitotic slippage. In this case, some cells can escape SAC after extended mitosis to get into the G_1 phase of the subsequent cell cycle without dividing (Fig. 1-8c) [94]. Cells that have gone through mitotic slippage cannot avoid the fate of death. In the normal cell cycle, Cdk1/cyclin B1 activation drives cells into mitosis and degradation of cyclin B1 allows cells to exit mitosis. During MC, cyclin B1 degradation is prevented by SAC, but cyclin B1 cannot escape unspecific slow degradation during sustained mitotic arrest [95]. Once the checkpoint loses its activity due to cyclin B1 degradation, cells with deranged chromosomes will exit mitosis without cell division, with nuclear envelopes reformed around random groups of chromosomes to form multinucleated cells [95]. Mitotic cell death and mitotic slippage are two

independent and competing mechanisms, the final fate of the cell is decided by which branch occurs first [58, 73]. A third possible outcome is senescence, a process associated with the cell being trapped in a state of irreversible cell cycle arrest (Fig. 1-8d). This only happens in a limited number of cells. Senescent cells are generally characterized by enlarged cell morphology and increased senescence-associated β-galactosidase activity (SA-β-gal). The crosstalk between TP53 and mTOR may determine whether or not a cell undergoes senescence [96]. Some consider this permanent growth arrest state as a type of cell death [97, 98].

Mitotic catastrophe can eliminate cells with defects in mitosis through apoptosis, necrosis, or senescence [89, 90]. Therefore, cell death during mitosis often occurs in conjunction with apoptosis and necrosis [99]. MC shares some biochemical hallmarks with apoptosis such as mitochondrial membrane permeabilization and caspase activation [100]. In cells competent to undergo apoptosis, mitotic catastrophe is always followed by apoptosis. But mitotic catastrophe is fundamentally different from apoptosis, as cells that die through mitotic catastrophe usually do not show DNA fragmentation or cytoplasm shrinkage that are observed in apoptotic cells [79]. Blocking apoptosis by treatment with caspase inhibitors cannot prevent the formation of giant multinucleated cells induced by spindle poisons [101]. Although commonly, apoptosis is not absolutely required for the lethal effect of mitotic catastrophe [102, 103]. In the absence of apoptosis, MC is sufficient to induce cell death by other mechanisms [104].
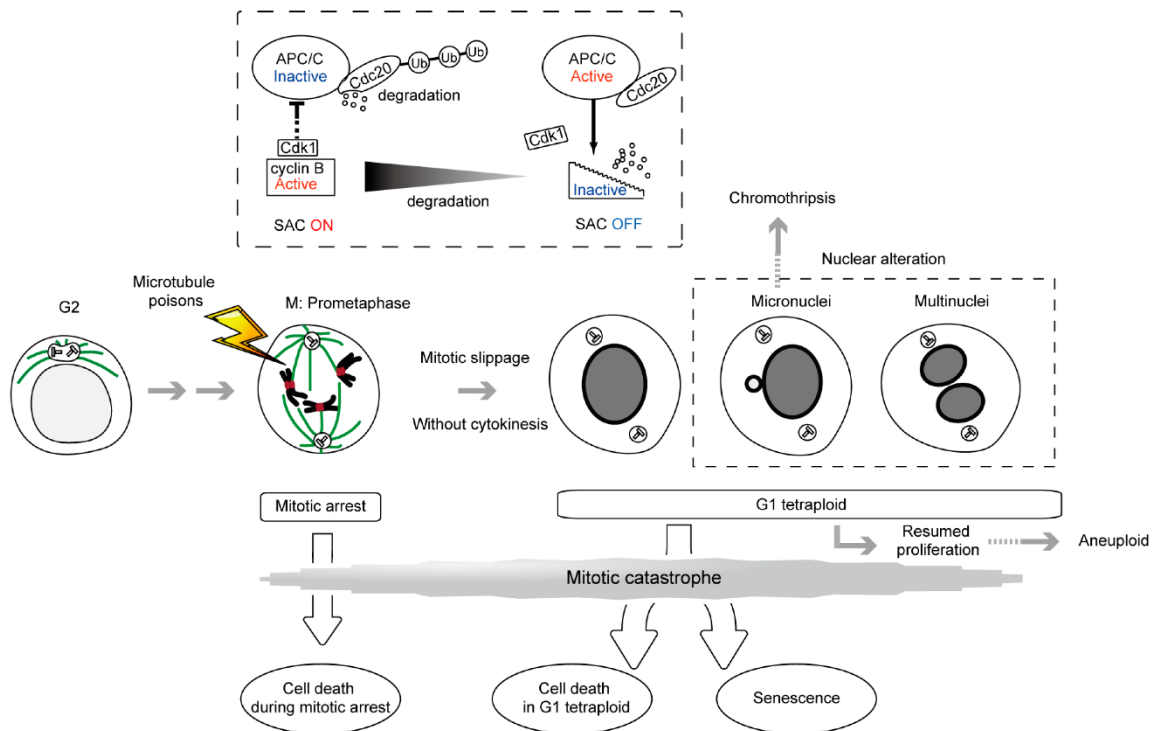
Figure 1-9. Mitotic catastrophe induced by microtubule targeting agents. (Nakayama, Yuji, and Toshiaki Inoue. "Antiproliferative fate of the tetraploid formed after mitotic slippage and its promotion; a novel target for cancer therapy based on microtubule poisons." Molecules 21.5 (2016): 663. [105]) [Reprinted with permission of Molecules].

1.3.4 Apoptosis

Apoptosis, also known as type I programmed cell death, is a highly regulated and controlled cell death mechanism in eliminating cells. It is the most important and well-studied programmed cell death mechanism. Apoptosis plays very important roles in many physiological processes including execution of immune effector functions, embryonic development, and chemical-induced cell death [106]. Apoptosis can be triggered by a wide variety of stimuli such as radiation, oxidative stress, ER stress, and some drugs [106]. As shown in Fig. 1-7, the morphology of apoptosis is distinct from

MC, with cytoplasm shrinkage, chromatin condensation, nucleosome fragmentation and plasma membrane blebbing in apoptotic cells, as compared to the formation of nuclear envelopes around individual clusters of missegregated, uncondensed chromosome in giant cells undergoing MC [106, 107]. Cysteine-aspartic proteases (caspase) are the executioners of apoptosis and they are essential for the morphological and biochemical changes of apoptosis [108]. The caspase family is comprised of initiator caspases, including caspase-2, -8, -9, -10, and executioner caspases, including caspases-3, -6 and -7 [109]. All are synthesized as inactive pro-caspase precursors and are activated by proteolytic cleavage. Exposure of phosphatidylserine on the surface of the cell membrane (detected by annexin-V binding) is another hallmark of apoptosis.

There are two main apoptotic pathways: the extrinsic or death receptor pathway and the intrinsic or mitochondrial pathway (Fig. 1-10). Both intrinsic and extrinsic pathways can trigger the activation of caspases, which play the major role in executing apoptosis [110-112]. The extrinsic or death receptor apoptotic pathway requires external stimulation by ligands such as TNF-related apoptosis-inducing ligand (TRAIL) or FAS to activate the plasma membrane death receptors, The activated death receptors recruit adaptor proteins, such as TRAILR or FAS-associated death domain protein (FADD) to activate initiator caspases [113]. Initiator caspases cleave and activate the executioner caspase-3 and -7, ultimately lead to subsequent cleavage of various cellular proteins and cell death [106, 111, 113]. The intrinsic or mitochondrial pathway of apoptosis is triggered by stimuli such as DNA damage, ER stress, and cytokine deprivation. In response to different stimuli, pro-apoptotic BH3-only proteins become activated. For

instance, BID is activated by death receptor stimulation, cytotoxic T-lymphocyte killing and heat shock induced caspase-8 activation; BAD is activated by phosphorylation; and PUMA, Noxa are upregulated by p53 [114]. The BH3-only proteins facilitate the Bax and Bak to form dimers and oligomers on the outer mitochondrial membrane (OMM) and subsequently lead to mitochondrial outer membrane permeabilization (MOMP) [114, 115]. Upon MOMP, mitochondrial intermembrane space proteins like cytochrome c and SMAC are released from mitochondria [109, 110, 116]. Cytochrome c promotes assembly of Apaf-1 to form the apoptosome, which then activates the initiator caspase-9. The latter cleaves and activates the executioner caspases -3 and -7 [111, 116]. Initiator and executioner caspases play distinct roles during intrinsic apoptosis, with the initiator caspase responsible for mitochondrial morphological changes and ROS production, and the executioner caspases promoting DNA fragmentation, membrane blebbing, chromatin condensation, and cell shrinkage [117].
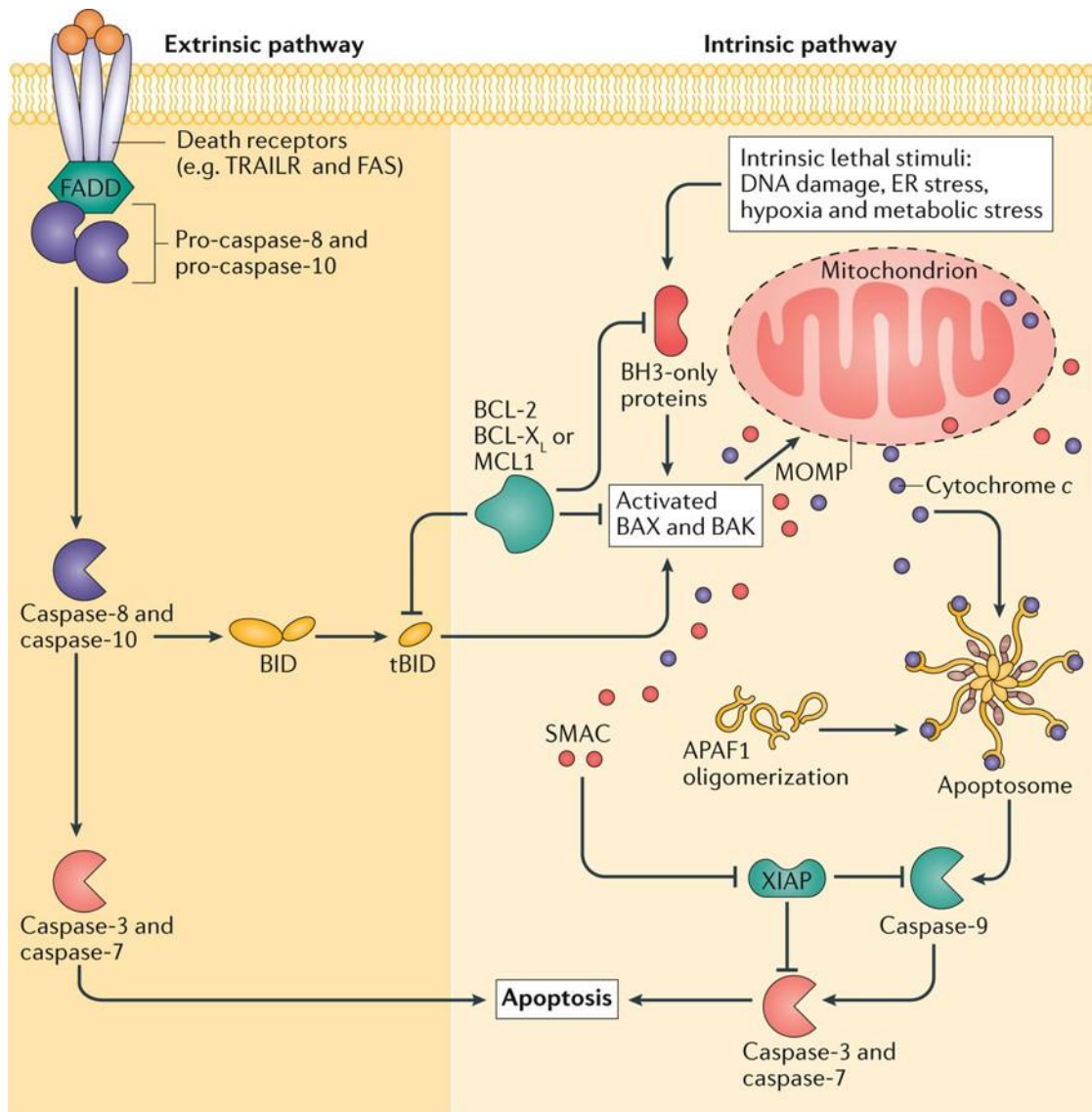
Figure 1-10. Overview of intrinsic and extrinsic pathways of apoptosis. (Ichim, Gabriel, and Stephen WG Tait. "A fate worse than death: apoptosis as an oncogenic process." Nature Reviews Cancer 16 (2016): 539-548. [116]) [Reprinted with permission of Nature Reviews Cancer].

1.3.5 Necrosis

Necrosis has traditionally been regarded as a form of unregulated cell death, in which there is an unordered response to damage such as infection, ischemia, or toxins. Necrotic cell death is characterized by organelle swelling, loss of cell membrane integrity, nuclear distension, and cell lysis, typically followed by an inflammatory response to cell debris [118]. Recently, a regulated and programmed mode of necrosis has been found, which is termed necroptosis [107]. Necroptosis plays an important role in some pathologies and normal embryonic development. Necroptosis is characterized by cellular swelling and leakage, cytoplasmic granulation, organelle dysfunction, and cell lysis [119]. Necroptosis can be triggered by stimuli such as TNF (tumor necrosis factor), CD95L, TRAIL, and TWEAK (TNF-related weak inducer of apoptosis). Death receptors that are involved in initiating apoptosis will induce necroptosis if caspases are inhibited or if ATP levels are low [120-122]. Fig. 1-11 illustrates cell death signaling pathways induced by TNF via the TNFR. When caspase-8 functions normally, upon stimulation, TNFR1 recruits caspase 8, FADD and TRADD to form death-inducing signaling complex (DISC, also called complex II) and initiate pro-apoptotic caspase activation [119, 123]. However, when caspase is inhibited, DISC cannot induce apoptosis, and a complex named the necrosome, (composed of RIPK1, RIPK3 and FADD) will form and trigger necrosis [107, 118].
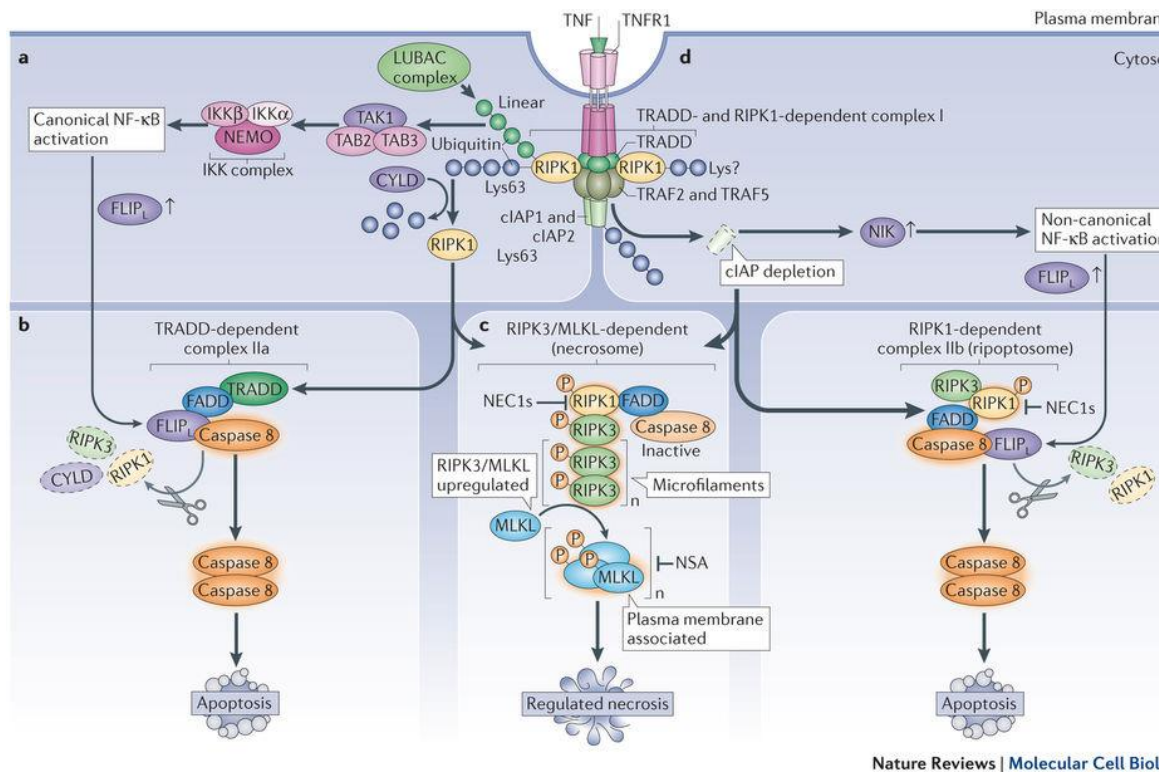
Figure 1-11. TNFR1 can induce either apoptosis or necroptosis via different signaling pathways. (Berghe, Tom Vanden, et al. "Regulated necrosis: the expanding network of non-apoptotic cell death pathways." Nature reviews. Molecular Cell Biology 15.2 (2014): 135. [119]) [Reprinted with permission of Nature Reviews. Molecular Cell Biology].

1.3.6 Bcl-2 anti-apoptotic family

The B cell leukemia/lymphoma gene 2 (Bcl-2) family proteins are predominantly localized to perinuclear endoplasmic reticulum or to mitochondrial membranes. Bcl-2 family members play important roles in cell death process by regulating the MOMP and the release of death effector molecules. There are three subfamilies of Bcl-2 proteins: the pro-apoptotic effector proteins,(e.g. Bax, Bak, Bad), the anti-apoptotic members (e.g.

Bcl-2, Bcl-xL, and Mcl-1), and the pro-apoptotic BH3-only proteins(e.g. PUMA, BID and BIM) [116]. The pro-apoptotic proteins trigger MOMP by forming dimers and oligomers on the mitochondrial membrane following the apoptotic stimuli. The anti-apoptotic proteins inhibit the permeabilization of mitochondria by binding to pro-apoptotic Bcl-2 proteins to prevent formation of pores on mitochondria. BH3-only proteins sensitiz to apoptosis by antagonizing the anti-apoptotic members or promoting the Bax or Bak oligomerize insert into the OMM to induce MOMP. For a long time, the anti-apoptotic members of the Bcl-2 family have been closely associated with protection from apoptosis, and the phosphorylation of these proteins can increase the sensitivity of tumor cells to anti-cancer drugs by facilitating apoptosis [124]. However, recent studies showed that Bcl-2 is not always associated with the sensitivity of cells to death-promoting stimuli, it is also involved in the cell cycle progression [125, 126]. In one study Bcl-2 was detected within the nucleus and its expression is upregulated during prophase and metaphase, decreased in telophase, and lost after the cell division [126]. MTAs induce phosphorylation of Bcl-2 on T69, S70 and S87 sites and Bcl-xL on T47 and S62 sites. It remains unclear whether the phosphorylation of Bcl-2 is simply a consequence of G_2/M arrest or a determinant of apoptosis [124, 127-131]. In addition, it has been suggested that Bcl-2 family members are critical in the execution of mitotic catastrophe and the determination of cell fate following mitotic catastrophe [132, 133]. Bcl-2 overexpression enhances the frequency of catastrophic mitoses [134].

Bcl-2 family members can be phosphorylated and regulated by numerous kinases such as JNK, c-Raf, protein kinase A, p38, protein kinase C, mTOR, Cdk1, and GSK3

[129]. MTA- induced phosphorylation of Bcl-2 and Bcl-xL during mitosis is mediated by Cdk1 and the phosphorylation is the link coupling mitotic arrest to cell death [133, 135, 136]. Other studies have shown that activation of the JNK pathway is responsible for MTA-induced Bcl-2 phosphorylation [137, 138]. The conflict between these studies may be due to the use of cancer cell lines with different genetic backgrounds. In addition, cell death phenotypes occurring after treatment with MTAs often are not well characterized to distinguish between apoptosis, mitotic catastrophe, and necrosis, which makes it difficult to draw a conclusion or compare results from different studies.

1.3.7 Involvement of JNK in cell cycle and cell death

C-Jun NH_2-terminal kinases (JNKs) also known as stress-activated protein kinases (SAPKs), are essential in cellular responses to stress factors and cytotoxic agents. The JNK signaling pathway can be activated by a wide range of stimuli such as irradiation, anti-tumor agents, inflammatory cytokines, and oxidative stress [139, 140]. There are three isoforms of JNK: JNK 1 and 2 are ubiquitously expressed, JNK 3 is found mainly in the nervous system [141]. JNKs inhibit cells growth and mediate apoptosis through the following mechanisms; 1) Activation of downstream transcription factor substrates like c-Jun, ATF2, p53 and c-Myc, 2) inhibition of anti-apoptotic Bcl-2 family members such as Bcl-2 and Bcl-xL via phosphorylation, and 3) induction of the release of apoptotic factors such as cytochrome c from mitochondria [142-145].

Recent studies have suggested that JNKs may also play complex and controversial roles in cell cycle progression [146]. JNKs localize to centromeres to phosphorylate c-Jun during mitosis and the early G_1 phase. But JNK activity also appears

to be sustained from S phase to anaphase with peak activity in metaphase [147]. JNK induces cdc25c phosphorylation during the G_2 phase, which has the effect of inhibiting Cdk1. On the other hand, inhibition of JNK has also been reported to delay activation of Cdk1 and prevent cyclin B1 degradation [148]. Finally, JNKs have been reported to promote Aurora B expression and Histone-H3 phosphorylation [148, 149] as well as Gadd45α and Gadd45γ induced G_2/M phase arrest [150].

Many studies support the correlations between MTA-induced cell cycle arrest, JNK activation, phosphorylation of Bcl-2 during G_2/M phase and cell death [146, 149, 151-153]. MTAs induce early activation of JNKs and subsequent activation of their downstream targets, c-Jun, JunD, and ATF2 [154]. Activation of JNK by MTAs inhibits the anti-apoptotic proteins of Bcl-2 and Bcl-xL by inducing phosphorylation [137, 151, 153, 155]. Paclitaxel-induced apoptosis is JNK-dependent, corresponding with cytochrome c release and caspase-3 activation in ovarian cancer cells, but inhibition of JNK does not interfere with paclitaxel-induced mitotic arrest [156].

Chapter 2

Evaluation of Novel Indole-Based Chalcones as Microtubule-Targeted Agents for Brain Cancer Therapy

2.1 Abstract

We have developed a series of small molecules that induce a novel, non-apoptotic cell death mechanism, methuosis, in cancer cells. During structure-activity relationship studies of methuosis-inducing compounds, we designed and synthesized a group of unique chalcone derivatives with improved anti-tumor activity and a different mechanism of action. Our lead compound in this class is 3-(6-methoxy-2-methyl-1H-indol-3-yl)-1-(4-pyridinyl)-2-propene-1-one (6-MOMIPP). 6-MOMIPP exhibits potent anti-proliferative and cytotoxic activity in glioblastoma and other cancer cell lines, with GI_{50} in the nanomolar range. However, 6-MOMIPP does not induce methuosis. Instead, by 24 h, 6-MOMIPP causes the majority of cells to round up from the culture dish and arrest in mitosis. By 48 h, cell viability is greatly reduced, correlating with activation of caspases 9, 7, and 3. Caspase inhibitors block cell death induced by 6-MOMIPP, suggesting that cell death is caspase-dependent. Phase-contrast images show that the few

remaining live cells are enlarged, flattened, and contain multiple micronuclei. 6-MOMIPP significantly decreases the amount of polymerized microtubules in the cells, supporting a role for 6-MOMIPP in microtubule depolymerization. Immunofluorescence staining of tubulin reveals general disruption of the microtubule network in U251 cells after treatment with 6-MOMIPP at 250 nM and above. *In vitro* drug-binding competition and cross-linking studies with β-tubulin suggest that 6-MOMIPP binds directly to tubulin at the colchicine binding site. Inhibiting Cdk1 activity with BMS-265246 greatly reduces cell death induced by 6-MOMIPP, indicating that prolonged Cdk1 activation may cause a blockage of the metaphase-anaphase transition, and leading to cell death. 6-MOMIPP-induced cell death is also accompanied by activation of the JNK signaling pathway, and a JNK inhibitor, SP600125, provides modest protection. Cell viability studies have shown that toxicity of 6-MOMIPP is substantially reduced in quiescent human fibroblasts, HUVEC (human umbilical vein endothelial cells), and rat neuronal progenitor cells. These results suggest that 6-MOMIPP represents a group of new tubulin binding agents with promising potential as anti-cancer agents.

2.2 Introduction

The standard of chemotherapy for GBM is temozolomide (TMZ), which works by damaging DNA and triggering the intrinsic apoptotic pathway. However, glioblastoma cells harbor a series of mutations, enabling them to easily develop resistance to TMZ and other alkylating agents by increasing their capacity to repair DNA lesions [157]. In order to improve the treatment for GBM and other drug-resistant cancers, approaches that trigger cell death through non-apoptotic cell death mechanisms need to be developed.

We have defined a novel non-apoptotic form of cell death termed as 'methuosis' [158]. Methuosis was initially described in GBM cells that ectopically expressed active Ras or Rac1 [159]. It is a form of caspase-independent cell death that involves massive vacuolization of macropinosomes and endosome compartments [160, 161]. To explore this type of cell death, we have designed and synthesized indolyl-pyridinyl-propenones (IPP, a subclass of synthetic indole-based chalcones) that induce methuosis in glioblastoma and other tumor cell lines [158, 162, 163]. In the course of performing structure-activity relationship studies, our group identified a lead compound, 3-(5-methoxy-2-methyl-1H-indol-3-yl)-1-(4-pyridinyl)-2-propene-1-one (MOMIPP) that effectively induces methuosis at micromolar concentrations. Continuing in the effort to discover small molecules that induce methuosis, the scaffold of MOMIPP was modified to generate a series of indole-chalcone derivatives. Some of these revamped indolyl-pyridinyl-propenones (IPPs) exhibited potent anti-proliferative and cytotoxic activity in glioblastoma and other cancer cell lines, with GI_{50} in the nanomolar level. However, during the biological activity studies of these new compounds, we found that the cell death mechanism did not correspond to the features of methuosis. Rather, preliminary studies suggested that the more potent compounds might represent a distinct class of microtubule-targeted agents (MTAs) [164].

MTAs are among the most widely used chemotherapeutic agents [45]. By interfering with highly dynamic mitotic spindle microtubules, MTAs activate the spindle assembly checkpoint (SAC) to arrest mitotic progression and trigger cell death [46]. Generally, MTAs are divided into three subgroups according to their binding sites on

tubulin and modes of activity: *Vinca* alkaloids [50], taxanes [54], and drugs that bind to the colchicine site, such as combrestatine and podophyllotoxin [165]. Although MTAs are among the most successful chemotherapeutic agents, their utility is limited by myelosuppression and neurotoxicity [58] and acquired chemoresistance, [59-61]. New agents with better tumor selectivity, fewer side effects, and resistance to active efflux are needed. In addition, challenges such as low bioavailability, poor solubility, and low passage through the BBB must be overcome.

In order to rationally guide chemotherapeutic development, it is important to understand the precise mechanisms of action of the new group of microtubule-targeted IPPs we have discovered. In the present studies, the most stable and potent compound, 6-MOMIPP, was selected to be our prototype to carry out mechanistic studies.

2.3 Materials and Methods

2.3.1   Cell Culture

U251 human glioblastoma cells were obtained from the Development Therapeutics Program (DTP), NCI Division of Cancer Treatment and Diagnosis (DCTD) (operated by Charles River Laboratories for the National Cancer Institute). TMZ-resistant U251 cells were generated in our lab as described previously [158]. A172 (CRL-1620), LN229 (CRL-2611), T98G (CRL-1690), and U87MG (HTB-14) cell lines were obtained from the American Type Culture Collection. SNB75 (503406), SNB19 (502596), and SF295 (503169) cell lines were purchased from the DCTD Tumor Repository. Unless stated otherwise, cell lines were maintained in Dulbecco's modified Eagle medium (DMEM),

supplemented with 10% (v/v) fetal bovine serum (FBS) (JR Scientific) at 37 °C with 5% CO_2/95% air.

Melanoma cell lines: SK-MEL-5, M238 parental, M238 B-RAF inhibitor resistant, M249 parental, M249 B-RAF inhibitor resistant, SK-MEL-28, SK-MEL-5 human melanoma cell line and B16F10 mouse melanoma cell line were provided by Dr. Kam C. Yeung (University of Toledo, Toledo, OH). A375, WM2664, SK-MEL-2, UACC-62, M14, and LOX-IMVI human melanoma cell lines were obtained from Dr. Ivana de la Serna (University of Toledo, Toledo, OH). SK-MEL-2, M238 parental, M249 parental, UACC-62, M14, and LOX-IMVI cell lines were maintained in Roswell Park Memorial Institute (RPMI) 1640 medium supplemented with 10% (v/v) FBS at 37 °C with 5% CO_2/95% air. M238 B-RAF inhibitor-resistant cells and M249 B-RAF inhibitor-resistant cells were maintained in RPMI 1640 medium containing 3µM PLX4032 (dissolved in DMSO). SK-MEL-5 and SK-MEL-28 cells were maintained in Minimum Essential Medium (MEM) supplemented with 10% (v/v) FBS and 10% (v/v) Non-Essential Amino Acid at 37 °C with 5% CO_2/95% air.

Lung cancer cell lines: The H460 large cell lung cancer cell line was provided by Dr. James C. Willey (University of Toledo, Toledo, OH). A549 human lung carcinoma cells, H292 human mucoepidermoid pulmonary carcinoma cells, H125 adenocarcinoma cells and H125 cisplatin-resistant (CPT-R) cells were generously provided by Dr. Randall J. Ruch (University of Toledo, Toledo, OH). H460, A549, H292, and H125 were maintained in RPMI supplemented with 10% (v/v) FBS at 37 °C with 5% CO_2/95% air. H125 CPT-R cells were maintained in RPMI containing 1µM cisplatin.

The RN46A-B14 cell line was a gift from Dr. Bryan Yamamoto (Indiana University, Indianapolis, IN). The parental RN46A cell line is immortalized with SV40 large T antigen and transfected with human brain-derived neurotrophic factor which is required for serotonergic differentiation [166]. RN46A-B14 cells were maintained in DMEM/F12 1:1 Media, supplemented with 100 μg/ml hygromycin, 250 μg/ml G418, and 10% (v/v) FBS at 33°C with 5% CO_2 /95% air. Cells were differentiated by maintaining at 39°C in DMEM/F12 1:1 medium containing 100 μg/ml hygromycin, 250 μg/ml G418, and 1 mM cAMP (Fisher Cat. No. AC22580-0010) for 10 days, with replenishment of fresh medium and drug every day.

Human Umbilical Vein Endothelial Cells (HUVEC) were purchased from Thermo Fisher Scientific (Cat. No.C0035C). Cells were maintained in Medium 200PRF (Thermo Fisher Scientific Cat. No. M200PRF) supplemented with Low Serum Growth Supplement (Thermo Fisher Scientific Cat. No. S00310) at 37°C with 5% CO_2/95% air. Normal human skin fibroblast cells were derived from a skin biopsy as described previously [167]. Cells were maintained in DMEM supplemented with 10% (v/v) FBS at 37 °C with 5% CO_2/95% air.

2.3.2 Chemicals

The indole-based chalcones, MOMIPP, MOFLIPP (2j), CT-1-125 (2l), CT-2-36 (2m), 6-MOMIPP (9b) were synthesized as described previously [162, 164, 168]. Compounds, unless indicated otherwise, were stored at -20 °C as 20 mM stock solutions in DMSO, and then serially diluted in DMSO so that the desired final drug concentrations could be achieved by making a 1/1000 dilution into the culture medium. Caspase-9 inhibitor Z-

LEHD-FMK was obtained from R&D Systems, Inc. (Cat. No. FMK008). Pan-caspase inhibitor PRO-VAD-FMK was purchased from Vergent Bioscience (Cat. No. 90101). JNK inhibitor SP600125 was obtained from Cayman Chemical (Cat. No. 10010466) and stored at -20^0C as a 15 mM stock in DMSO. Roscovitine was purchased from Santa Cruz Biotechnology (Cat. No. sc-24002A) and stored at -20^0C as a 10 mM stock in DMSO. BMS-265246 was obtained from Selleckchem (Cat. No. S2014) and was stored at -20^0C as a 5 mM stock in DMSO. N, N'-Ethylenebis iodoacetamide (EBI) was purchased from Toronto Research Chemicals (Cat. No. E917500) and was stored at -20^0C as a 100 mM stock in DMSO.

2.3.3   Live-cell Imaging

For acquisition of phase-contrast images of live cells, 100,000 U251 cells were seeded in 35 mm culture dishes and allowed to attach for 24 h. Thereafter, cells were incubated in medium with the compounds at the indicated concentrations or the equivalent volume of vehicle (DMSO). Phase-contrast images were obtained at the indicated time intervals after treatment, using an Olympus IX70 inverted microscope equipped with a heated stage, a DP80 digital camera, and cellSens™ imaging software (Diagnostic Instruments, Inc.). The seeding densities of different cell lines for live-cell imaging studies were: melanoma cancer cell lines, 200,000 cells/dish; lung cancer cell lines, 100,000 cells/dish; HUVEC, high/low density, 400,000/100,000 cells/dish; fibroblasts, high/low density, 400,000/100,000 cells/dish. RN46A-B14 cells were seed at a density of 100,000 cells/dish and allowed to differentiate for10 days. Thereafter, cells were incubated with

the indicated concentrations of compounds and phase-contrast images were taken at indicated time intervals after treatment.

2.3.4 SRB Assay

Sulforhodamine B (SRB) colorimetric assay was used to assess effects of compounds on cell proliferation after two-days of treatment [169]. Cells were seeded into 96-well plates with four replicate wells for each culture condition. One day later, four wells in a separate plate were assayed to establish a pre-drug (time-0) baseline, which indicates the cell density at the beginning of the drug treatment. At the same time, the rest of cells were exposed to compounds at indicated concentrations for 48 h. At the endpoint of the assay, cells were fixed with 10% trichloroacetic acid (TCA) and stained with SRB (Sigma Aldrich. Cat. No. S9012-5G). After extensive washing, the SRB in the cells was dissolved in 10 mM Tris-HCl and absorbance at 515 nm was quantified on SpectraMax Plus plate reader (Molecular Devices). The concentration of compound producing fifty-percent growth inhibition (GI_{50}) relative to the control without drug was calculated as described in the NCI-60 human cell line screening protocol (http://dtp.nci.nih.gov/branches/btb/ivclsp.html). The density of individual cell lines seeded for SRB assay in 96-well plates was: U251, 2000 cells/well; SNB75, 6000 cells/well; U87, 5500 cells/well; SNB19, 5000 cells/well; SFB295, 5500 cells/well; LN229, 5500 cells/well; A-172, 3500 cells/well; T89G, 3500 cells/well; A375, 2000 cells/well; WM2664, 4000 cells/well; SK-MEL-2, 5000 cells/well; SK-MEL-5, 4000 cells/well; SK-MEL-28, 4000 cells/well;   M238 parental, 4000 cells/well; M238 resistant, 5000 cells/well; M249 parental,   4000 cells/well; M249 resistant, 5000

cells/well; UACC-62, 2000 cells/well; M14, 2000 cells/well; LOX-IMVI, 3000 cells/well.

2.3.5 ATP Cell Viability Assay

Cell viability was assessed by measuring cellular ATP, using the CellTiter-Glo® luminescence assay kit according to the manufacturer's protocol (Promega Corp. Cat: No. PR-G7571). Cells were seeded in white-walled opaque 96-well plates with four replicate wells for each culture condition. On the second day, compounds at the indicated concentrations were added and cell viability was assayed after 48 h. Luminescence was read by using a Berthold Tech Centro XS3 LB 960 luminometer and data were acquired with the MikroWin software. The seeding density for each cell line was: U251, 2000 cells/well; U251 TMZ-R, 2000 cells/well; U87MG, 5500 cells/well; LN229, 5500 cells/well; T98G, 3500 cells/well; A172, 3500 cells/well; H460, 5000 cells/well; H125, 4000 cells/well; H125 CPT-R, 4000 cells/well; H292, 5000 cells/well; A549, 5000 cells/well; A375, 2000 cells/well; SK-MEL-2, 5000 cells/well; SK-MEL-5, 4000 cells/well; UACC-62, 2000 cells/well; B16F10, 4000 cells/well; HUVEC 12000, cells/well; fibroblasts, 12000 cell/well. RN46A-B14 cells were seeded at a density of 5000 cells/well and allowed to differentiate for 10 days. Thereafter the cells were treated with compounds and cell viability was assayed at a 48 h end-point.

2.3.6 Whole Cell Tubulin Polymerization Assay

Microtubules in whole cells were analyzed by flow cytometry as described previously [170]. U251 cells were plated in 60 mm dishes at a density of 300,000 cells/dish with

three replicate wells for each culture condition. After one day, cells were treated with the indicated concentrations of 6-MOMIPP, colchicine, paclitaxel or an equivalent volume of DMSO for 24 h. Thereafter, cells were harvested by trypsinization and pelleted (600 x g, 5 min), and cell pellets were resuspended and fixed in 1 ml of 0.5% glutaraldehyde (Ted Pella Cat. No. 18420) in microtubule-stabilizing buffer (80 mM PIPES, pH 6.8, 1 mM $MgCl_2$, 5 mM EDTA, and 0.5% Triton X-100) for 10 min at room temperature. Then glutaraldehyde was quenched by adding 0.7 ml of 1 mg/ml NaBH4 in PBS. After that, cells were pelleted (1000 x g, 5 min) and resuspended in 100 µl of 50 µg/ml RNase (Qiagen, Cat. No. 19101) in antibody diluting solution (AbDil: PBS, pH 7.4, 0.2% Triton X-100, 2% bovine serum albumin, and 0.1% NaN3) for an overnight incubation at 4^0C. Finally, 25 µl of anti-α-tubulin–FITC antibody (1:50 dilution in AbDil) (Sigma Aldrich, Cat. No. F2168, Lot 026M4824V) was added to each sample to incubate in the dark for 3 h. Then cells were incubated with 1 ml of 50 µg/ml propidium iodide in PBS for 10 min before being analyzed with a Becton-Dickinson FACS-Calibur flow cytometer.

2.3.7 Immunofluorescence

U251 cells were seeded on glass coverslips in 60 mm dishes at a density of 350,000 per dish. One day after plating, fresh medium was added with DMSO or 6-MOMIPP at the indicated concentration. After 24 h, cells were fixed with ice-cold methanol for 10 min and blocked with 10% goat serum (Gibco, Cat. No. 16210-064) in PBS for 20 min. α-tubulin was detected by immunofluorescence microscopy, using a primary mouse monoclonal antibody (1:100, 1 h) (Sigma Aldrich, Cat. No.T5168, Lot 016K4886), followed by Alexa Fluor 568-labeled goat anti-mouse IgG (1:600, 1h) (Life

Technologies, Cat. No. A11031, Lot 482209A). Nuclear DNA was stained with 300 nM 4', 6-diamidino-2-phenyl-indole (DAPI) (Sigma Chemical Co.) for 5 min and cells were washed with deionized water. Images were obtained with an Olympus IX70 inverted microscope.

2.3.8 Cell Cycle Analysis

U251 cells were seeded in 60 mm dishes at a density of 350,000 cells/dish, with triplicates for each culture condition. On the second day after plating, the cells were treated with 6-MOMIPP at indicated concentrations for 24 h or 48 h. Then the cells were harvested by trypsinization, fixed with ice-cold 70% ethanol, washed twice by centrifugation/resuspension in PBS, and finally resuspended in 900 μL PBS containing 6.25 mM $MgSO_4$ and 1 mM $CaCl_2$. 2μL of a 100 mg/mL RNase A solution was added and the cells were incubated at 37 °C for 15 min. DNA was stained by adding 100 μL of a 500 mg/mL aqueous solution of propidium iodide (PI) and cells were analyzed with a Becton-Dickinson FACS-Calibur flow cytometer. Whole cells were identified based on their forward scatter (FSC) and side scatter (SSC) traces. DNA histograms were generated with CellQuest Pro software.

2.3.9 Cell Synchronization

350,000 U251 cells were seeded in 60 mm dishes. One day after plating, cells were washed twice with PBS and then switched to DMEM without serum or leucine for 24 h to induce cell cycle arrest (Crystalgen. Cat. No. 226-024) before further analysis.

2.3.10 Immunoblot Analysis

U251 cells were seeded at density of 1,000,000 cells per 10 cm dish and allowed to attach for 24 h. Thereafter, cells were treated with compounds at the indicated concentrations or an equivalent volume of DMSO for 24 h or 48 h. In studies employing inhibitors (e.g. caspase inhibitors, Cdk1 inhibitor BMS-265246 or JNK inhibitor SP600125), cells were treated with inhibitors 2 h before adding the 6-MOMIPP. Then, both floating and attached cells were harvested by trypsinization and lysed in SDS sample buffer (65 mM Tris-HCl, 10% glycerol, 0.5% β-mercaptoethanol, 2% SDS, pH 6.8). The protein concentration in each sample was determined by colorimetric assay using Bio-Rad reagent (Bio-Rad, Cat. No. 5000006). Equal amounts of protein (generally 80 μg) were subjected to SDS-PAGE in 12.5% polyacrylamide gels, and the proteins were electroblotted on to PVDF membrane. The membranes were blocked by incubation with 5% nonfat milk in Tris-buffered saline-Tween buffer (TBST, 20mM Tris, 137mM NaCl, 0.2% Tween 20) at room temperature for 1 h. Primary antibody was then added and incubation was continued overnight at 4^0C followed by 1 h secondary antibody incubation. Proteins were detected by enhanced chemiluminescne (ECL) using the ECL detection kit obtained from Alkali Scientific Inc. (Cat. No. XR96) and an Alpha Innotech Fluor Chem HD2 imaging system. Chemiluminescent signals were quantified by using Alpha View software.

Primary antibodies used for immunoblot analysis were as follows: Rabbit anti-Caspase-9 (Cat. No. 9502S); rabbit anti-Cleaved Caspase-3 (Asp175) (Cat. No. 9661S); rabbit anti-Caspase-7 (Cat. No. 9492S); rabbit anti-phospho-SAPK/JNK (Thr183/Tyr185) (Cat. No. 9251S); rabbit anti-SAPK/JNK antibody (Cat. No. 9252s); rabbit anti-Bcl-xL

(54H6) (Cat. No. 2764s); rabbit anti- Phospho-Bcl-2 (Ser70) (5H2) (Cat. No. 2827s); rabbit anti-phospho-c-Jun (Ser63) (Cat. No. 9261S); rabbit anti-c-Jun (60A8) (Cat. No. 9165s); rabbit anti- PP1α (Cat. No. 2582S); rabbit anti- Phospho-PP1α (Thr320) (Cat. No. 2581S), all purchased from Cell Signaling Technology. Rabbit anti-phospho-Bcl-xL (Ser62) (Cat. No. PA535496) was obtained from Thermo Fisher Scientific. Mouse monoclonal anti-phospho-Histone H3 (Ser10) antibody (Cat. No. 05-806) was purchased from Sigma-Aldrich. Mouse monoclonal antibody against α-tubulin (Invitrogen/Life Technologies Cat. No. T5168). Secondary antibodies used in the experiments were HRP-coupled goat anti-mouse (Cat. No. 554002) and goat anti-rabbit (Cat. No. 554021) antibodies that were obtained from BD Biosciences.

2.3.11 Scintillation Proximity Assay

The colchicine and vinblastine competition-binding SPAs were conducted as described previously [171]. 6-MOMIPP was stored at -20^0C as a 1.3 mM stock in vehicle consisting of DMSO, Solutol-HS15, and water (1:2:11v/v/v), and then serially diluted in DI water so that the desired final drug concentrations could be achieved by making a 1/1000 dilution into the reaction mixture. Vinblastine and colchicine were dissolved in the same solvent as 6-MOMIPP. [^{3}H]-colchicine (1 mCi/ml, specific activity 60-87 Ci/mM; Cat. No. NET189250UC), [^{3}H]-vinblastine (0.25 mCi/ml, specific activity 20.8 Ci/mM; Cat. No. NET1176050UC), and Streptavidin-yttrium silicate (YSI) beads (Cat. No. RPNQ0015) were purchased from Perkin Elmer, Inc. Long-chain biotin-labeled tubulin (Cat. No. T333P) and guanosine 5'-triphosphate sodium salt (GTP, Cat. No. BST06-010) were obtained from Cytoskeleton Inc.

[^{3}H]-colchicine competition assay: 0.5µCi [^{3}H]-colchicine (diluted with ethanol to a final volume of 10 µl) was added to individual wells in white-walled 96-well plate (Perkin Elmer Cat. No.6005290) and allowed to air dry for 1 h. Then 90 µl of ice-cold binding buffer (80 mM PIPES pH 6.8, 1 mM Mgcl2, 1 mM EGTA and 1 mM GTP) containing 50 µg long-chain biotin-labeled tubulin and unlabeled vinblastine, colchicine or 6-MOMIPP (final concentrations 10 nM, 50 nM, 1 µM, 2.5 µM, 5 µM, 10 µM), were added to each well. The reaction mixtures were incubated at 37^{0}C for 2 hours, with 4 replicates for each condition. At the end of the incubation, Streptavidin-YSI beads (0.08 mg suspended in 20µl binding buffer) were added to each reaction well for 15 min and the signal emitted from YSI in proximity to the tubulin-bound [^{3}H]-colchicine was quantified with a Packard TopCount®NXT^{TM} Microplate Scintillation & Luminescence Counter. Results were plotted by using GraphPad Prism 7.

 [^{3}H]-vinblastine competition assay: 0.5 µCi [^{3}H]-vinblastine (diluted into to a final volume of 10 µl ethanol) was added to the wells of a white-walled 96-well plate to air dry for 1 h. Then unlabeled vinblastine, colchicine, or 6-MOMIPP (final concentrations 0.24 µM or 2.4 µM) was added along with 1 µg long-chain biotin-labeled tubulin in a total of 80 µl ice-cold binding buffer. Reaction mixtures were incubated at 37^{0}C for 2 h, with 4 replicates for each condition. Streptavidin-YSI beads (0.4 mg suspended in 50µl binding buffer) were added to each reaction mixture and scintillation signals were quantified after 15 min as described above.

2.3.12 EBI Cross-linking and Drug Binding Assay

The ability of 6-MOMIPP to protect key residues in the colchicine binding site of β-tubulin from cross-linking by N,N'-ethylene-bis (iodoacetamide) (EBI) was assayed as described previously [172]. U251 cells were seeded at the density of 1,000,000 cells per 10 cm dish and allowed to attach for 24 h. Thereafter, cells were treated for 4 h with 6-MOMIPP, paclitaxel, colchicine or an equivalent volume of DMSO at indicated concentrations, EBI was then added to the medium at a final concentration of 100 µM, and incubation was continued for 1.5 h. Floating cells were combined with attached cells (harvested by trypsinization) and cells were lysed in SDS sample buffer. The protein concentration were determined by colorimetric assay using Bio-Rad reagent (Bio-Rad). For each sample 80 µg protein was subjected to SDS-PAGE and transferred to PVDF membrane. Immunoblot assays were performed as described earlier, using a mouse monoclonal antibody against β-tubulin (Santa Cruz Biotechnology, Cat. No. sc-5274).

2.3.13 Annexin V live-dead Cell Assay

The Muse® Annexin V and Dead Cell Assay Kit (EMD Millipore Corporation, Cat. No. MCH100105) was used to assess the extent of apoptosis in cells treated with test compounds. 100,000 U251 cells were seeded in 35 mm dishes. On the second day, the cells were treated with 6-MOMIPP at the indicated concentrations for 24 h or 48 h. Floating and attaching cells were combined, and pelleted by centrifugation (1000 x g, 5 min). Cells were resuspended in PBS to a final concentration of 300,000 cells/ml and incubated for 10 min with Annexin V and 7-ADD at room temperature. Finally, cells were analyzed by using a Muse® Cell Analyzer to quantify the Annexin-positive (early

apoptosis) and Annexin + 7-ADD positive (dead) populations. The total apoptosis cell population was the summary of early apoptotic and dead cell populations.

2.3.14 Statistical Analysis

GraphPad Prism 7 was used for statistical analysis. For replicate experiments, data are presented as the mean $\pm$ S.D.. Statistical significance between control and treated groups was determined by Student's unpaired T test. * $p<0.05$, ** $p<0.005$, *** $p<0.001$, **** $p<0.0001$.

2.4 Results
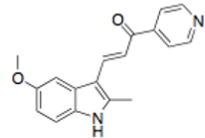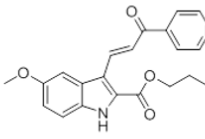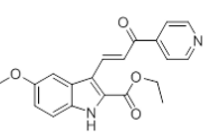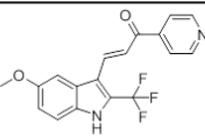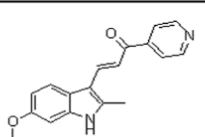
2.4.1 Indole-based chalcones inhibit proliferation of U251 cells

Newly synthesized indole-based chalcones were originally designed to improve the efficacy of existing methuosis-inducing drugs [162, 164]. To evaluate the anti-proliferative activities of these new derivatives, SRB assays against U251 cells, a standard glioblastoma cell line, were performed. Our lead methuosis-inducing compound, MOMIPP, was chosen for reference. Cells were treated with various concentrations of compounds for 48 h and optical density, which reflects cell density, was measured. As Fig. 2-1 shows, the four of the newly designed indole-based chalcones are more potent in inhibiting the proliferation of U251 cells compared to MOMIPP. GI_{50} is the dose able to achieve 50% growth inhibition, compared to control treated only with vehicle. As the results in Table 2-1 show, the GI_{50}'s of the newly synthesized compounds are in the nanomolar range, which are much lower than the GI_{50} for MOMIPP. Among all the compounds, CT-2-36 exhibited the best anti-tumor activity, suggesting the

47

introduction of a propyl carboxylate group on the indole ring is beneficial to the anti-tumor activity. In addition, moving the methoxy group from the 5-position (MOMIPP) on the indole ring to the 6-position (6-MOMIPP) decreased the GI_{50} from 2.32μM to 0.054μM, suggesting that the location of methoxy group is essential for anti-tumor activity. Addition comparisons of the anti-proliferative activities of MOMIPP and CT-2-36 in the NCI-60 cancer cell lines were done by NCI, with compounds we submitted to their Chemotherapeutic Agents Repository. Results showed that CT-2-36 has much lower GI_{50} than MOMIPP in a broad spectrum of cancer cell lines, data are not shown here.

Table 2-1.

Chemical structure, structure name and GI$_{50}$ of indole-based chalcones used in the study.

Compound	Structure Name	Structure	GI$_{50}$ (µM)
MOMIPP	3-(5-Methoxy-2-methyl-1H-indole-3-yl)-1-(4-pyridinyl)-2-propen-1-one		2.32
CT-2-36	Propyl trans-3-(5-Methoxy-1H-indol-2-carboxylate-3-yl)-1-(4-pyridinyl)-2-propen-1-one		0.008
CT-1-125	Ethyl trans-3-(5-Methoxy-1H-indol-2-carboxylate-3-yl)-1-(4-pyridinyl)-2-propen-1-one		0.014
MOFLIPP	trans-3-(5-Methoxy-2-trifluoromethyl-1H-indol-3-yl)-1-(4-pyridinyl)-2-propen-1-one		0.118
6-MOMIPP	trans-3-(6-Methoxy-2-methyl-1H-indole-3-yl)-1-(4-pyridinyl)-2-propen-1-one		0.054
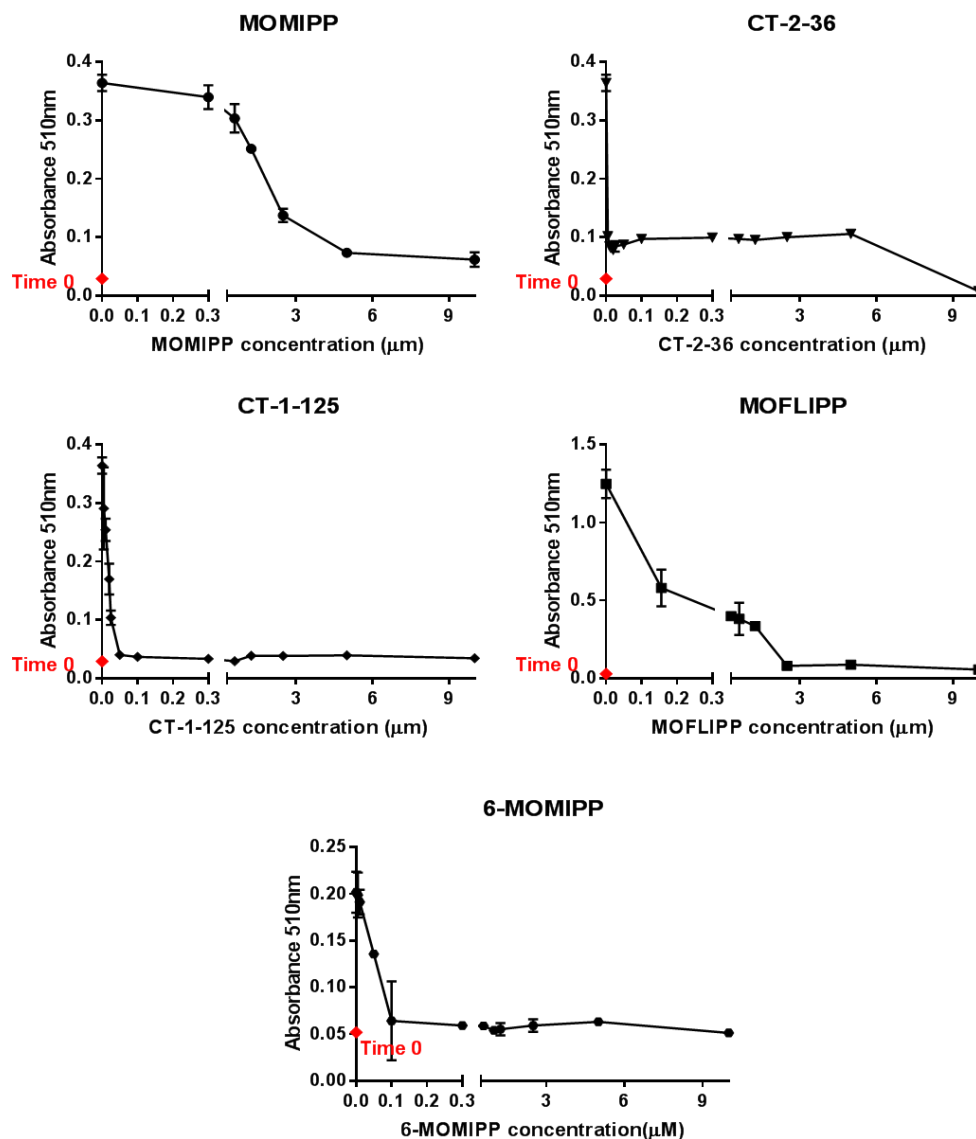
Figure 2-1. Newly synthesized indole-based chalcones exhibit potent anti-proliferation activity against U251 glioblastoma cells. U251 cells were treated with different compounds at the indicated concentrations for 48 h. Cell mass remaining attached to the wells was assessed by SRB colorimetric assay. The value at Time 0 reflects the cell density at the beginning of treatment. Each point represents the mean ± S.D. of 4 replicates.

2.4.2 Indole-based chalcones induce accumulation of multinucleated cells

These newly designed compounds had much more potent anti-proliferation activity compared to MOMIPP, so the next step was to evaluate their effect on cell morphology. U251 cell morphology was examined by phase-contrast microscopy after treatment with the new compounds. Two compounds, CT-2-36 and 6-MOMIPP, were selected to conduct future experiments, given that CT-2-36 is the analog with the most potent anti-proliferative activity and 6-MOMIPP has the structure that most highly resembles MOMIPP. Phase contrast images of U251 cells treated with CT-1-125 and MOFLIPP were published previously [162], and those cells died without the cytoplasmic vacuolization typical of methuosis. In Fig. 2-2, U251 cells were treated with DMSO, 10 μM MOMIPP, 0.6 μM CT-2-36 or 1 μM 6-MOMIPP and phase-contrast images were obtained at 4 h, 24 h, 48 h, and 72 h. Instead of the characteristic vacuoles seen in cells undergoing methuosis, cells treated with CT-2-36 and 6-MOMIPP exhibited extensive blebbing of plasma membrane at the early time points and detached from the culture dish. At the later time points, the majority of cells lost viability, and the few remaining attaching cells contained multiple micronuclei. These distinct morphological changes suggested that the increased cytotoxicity of the new indolyl chalcones derivatives may be attributed to their having different biological activity from our previous methuosis-inducing compounds.
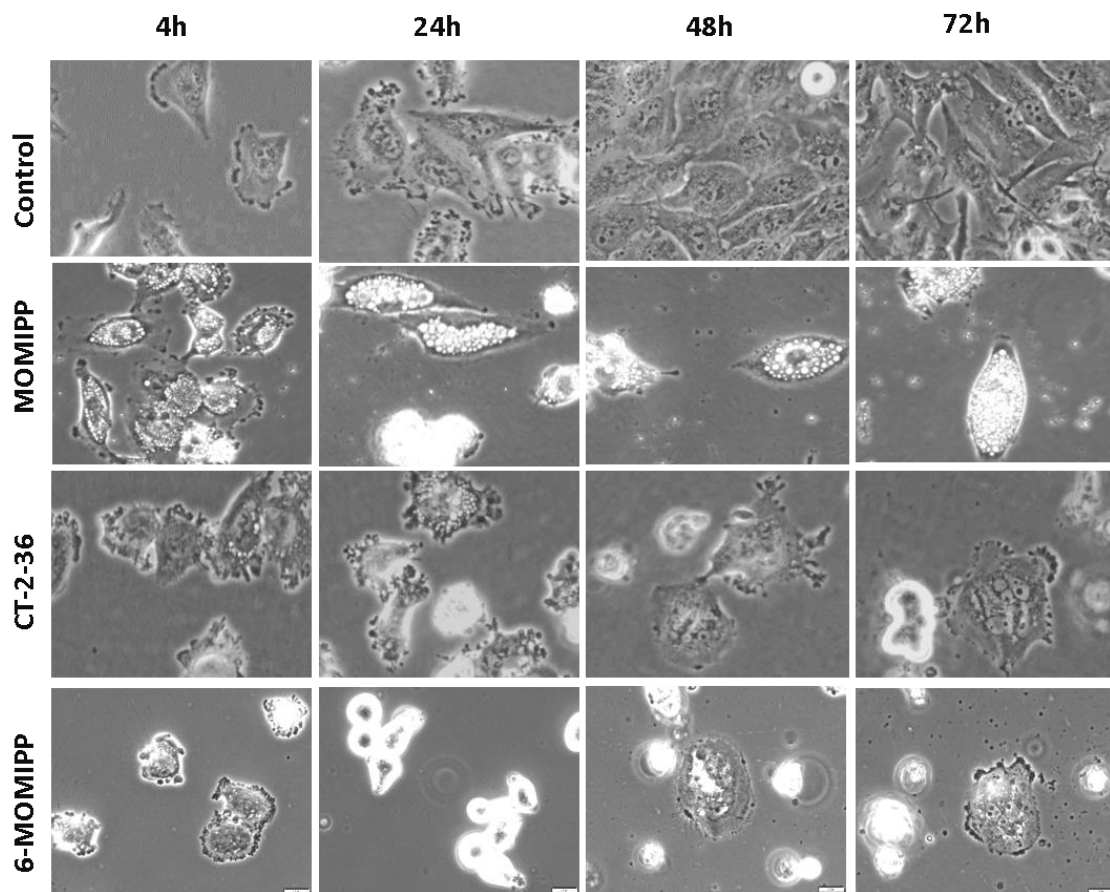
Figure 2-2. Comparison of the effects of MOMIPP, CT-2-36, and 6-MOMIPP in U251 cells. 100,000 U251 cells were seeded in 35mm dishes and treated with DMSO, 10 μM MOMIPP, 0.6 μM CT-2-36 or 1 μM 6-MOMIPP. Phase-contrast images were taken after 4 h, 24 h, 48 h, or 72 h.

2.4.3 6-MOMIPP induces G_2/M arrest in glioblastoma cell lines

The increased cytotoxicity and distinct morphological effects of the new compounds suggest that they might be affecting cell growth and viability through a mechanism other than methuosis. Cell rounding and detachment from substratum is frequently observed in the cells treated with mitotic inhibitors. To determine if these new compounds have an influence on the mitotic process, cell cycle analysis was performed. Cell cycle

progression was analyzed by quantifying DNA content by flow cytometry following drug treatment. 6-MOMIPP was chosen as our prototype to carry out further studies due to it is more stable in the culture medium compare to CT-2-36. U251 cells were treated with concentrations of 6-MOMIPP ranging from 0.1 μM to 5 μM for 24 h, 48 h, or 72 h. Then both attached and detached U251 cells were collected and subjected to flow cytometry after staining the DNA with PI. As DNA histograms show in Fig. 2-3, treatment with 6-MOMIPP resulted in substantial accumulation of cells in G_2/M (4N) at 24 h, with a concomitant decrease in G_1 and S phase. A sub G_0 population increased when the incubation time was extended to 48 h or longer, indicating that majority of cells underwent death after 48 h (Fig. 2-3). Fig. 2-4 A-C depicts the quantified cell cycle distribution, in each phase, after treatment with 6-MOMIPP for 24 h, 48 h, or 72 h. The results demonstrate that 6-MOMIPP induces cell cycle arrest in a concentration-dependent manner. The majority of U251 cells were arrested in G_2/M by 24 h at concentrations above 250 nM. The G_2/M phase population decreased and the sub-G_0 population increased between 48 h and 72 h, suggesting that 6-MOMIPP- induced G_2/M arrest is followed by extensive cell death. The effects of the other three new compounds (CT-2-36, CT-1-125, MOFLIPP) on cell cycle distribution were previously described [162], and are consistent with 6-MOMIPP. These results were confirmed in another glioblastoma cell line, T98G, as shown in Appendix A Fig. 1- Fig. 2.
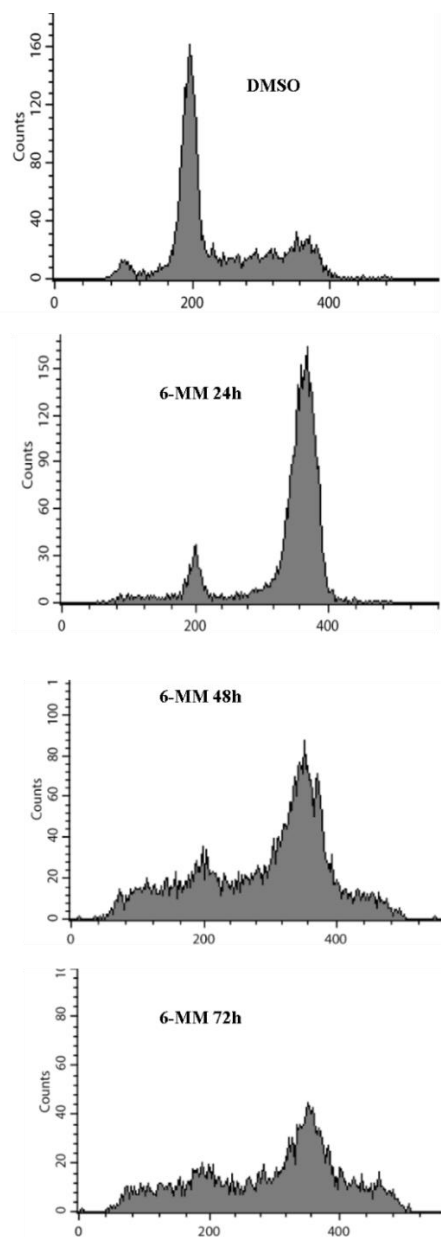
Figure 2-3. Effect of 6-MOMIPP on cell cycle distribution in U251 cells. DNA histograms of cells treated with 6-MOMIPP at 1 µM for 24 h, 48 h or 72 h were generated by flow cytometry as described in the Material and Methods section. The results shown are representative of three separate replicates.

54

A

B

C
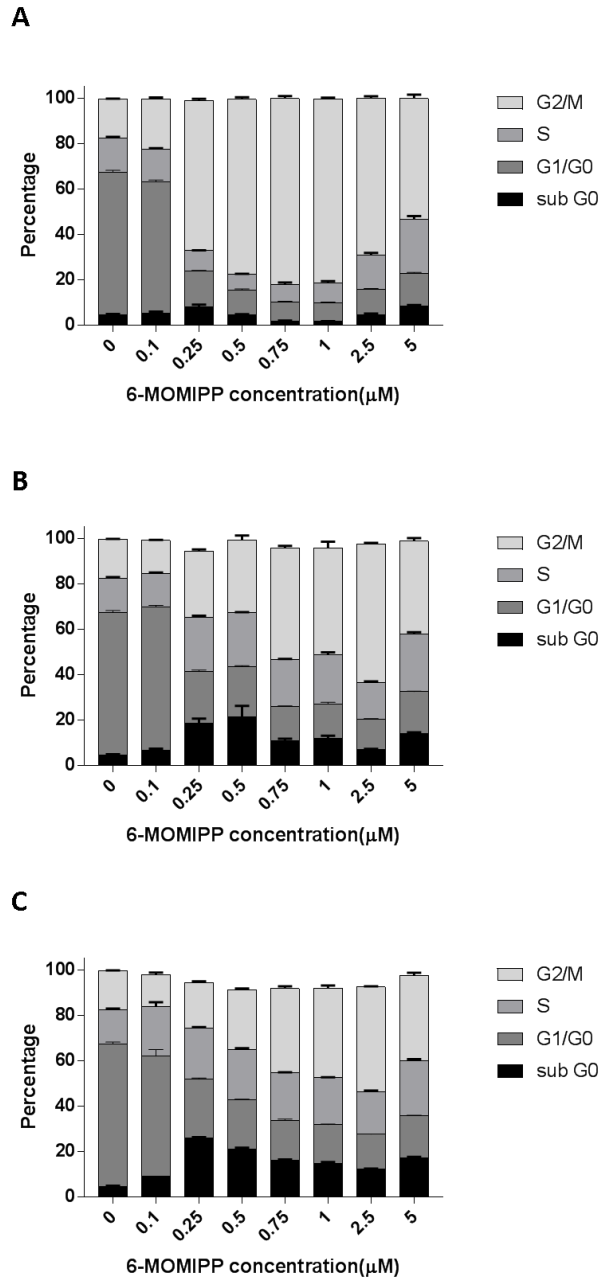
Figure 2-4. Quantification of cell cycle distribution in U251 cells treated with 1 µM 6-MOMIPP for 24 h (A), 48 h (B) or 72 h (C). CellQuest Pro software was used to determine cells in G_1, S and G_2/M compartments based on DNA content. At each time

55

point the results from three separate experiments were analyzed and the results (percentage of cells in each phase of the cell cycle) represent the mean ± S.D.

2.4.4   6-MOMIPP induces caspase-dependent cell death in U251 cells

The preceding cell cycle analysis revealed that 6-MOMIPP induced substantial cell death by 48 h, as indicated by an increase in the sub-G_0 population. To evaluate and quantify the cytotoxicity of 6-MOMIPP in more detail, ATP assays and Annexin V live-dead cell assays were performed. The ATP assay determines the number of viable cells in culture based on the amount of ATP present, which reflects the metabolically active cells. The annexin V live-dead cell assay can distinguish between healthy cells, early apoptotic cells, and late apoptotic/dead cells by Annexin V (stains phosphatidylserine on the membrane of apoptotic cells) and 7-AAD (a membrane permeable dye that stains nuclear DNA in cells that have lost membrane integrity). ATP assays were performed in U251 cells, after a 48 h treatment with 6-MOMIPP. The results in Fig. 2-5A show that 6-MOMIPP inhibited U251 cell viability with an IC_{50} of 0.358 μM after 48 h. The viability of cells dramatically decreased at concentrations above 0.5 μM. The live-dead cell assays revealed that the proportions of early apoptotic, late apoptotic, and dead cells increased after 48 h treatment with 6-MOMIPP at concentrations ranging from 0.5 μM to 5 μM (Fig. 2-5B), which is consistent with the ATP assay results.
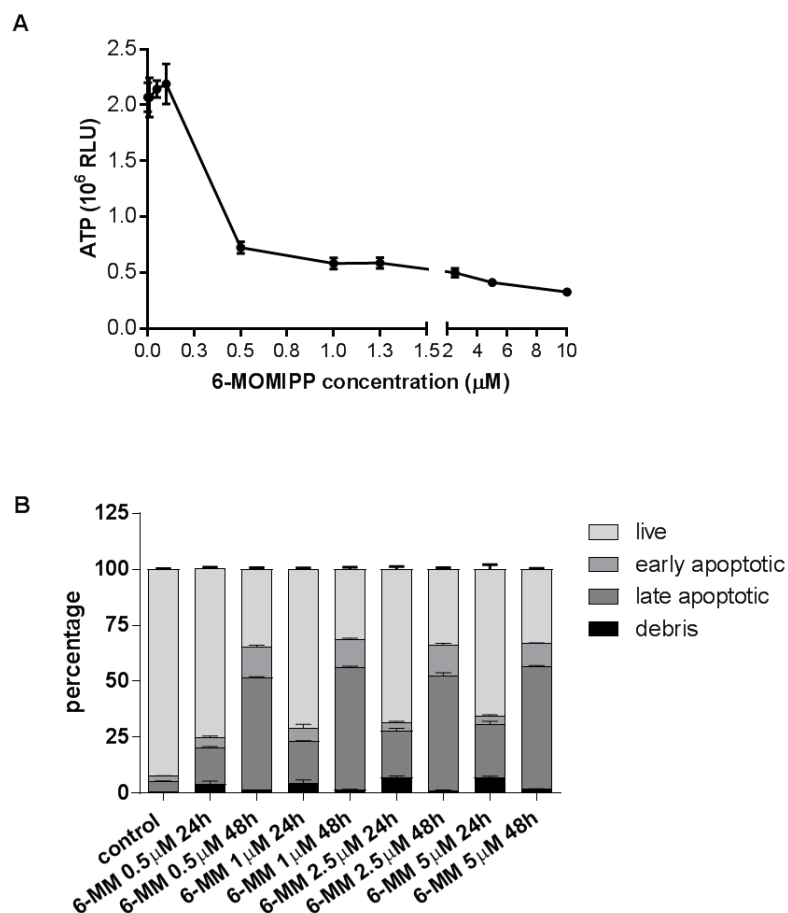
Figure 2-5. 6-MOMIPP-induces cell death in U251 cells. A. Cells were seeded in white-walled opaque 96-well plates at a density of 2000 cells/well. On the second day, cells were treated with 6-MOMIPP at the indicated concentrations for 48 h. ATP was measured by CellTiter-Glo® luminescence assay as described in the Methods. Values represent the mean ± S.D. of four replicates. B. 100,000 U251 cells were seeded in 35 mm dishes. On the second day, the cells were treated with 6-MOMIPP at the indicated concentrations for 24 h or 48 h. Cells were harvested and stained with annexin-V and 7-ADD and the percentages of live, early apoptotic and late apoptotic/dead cells were

determined with the Muse® system, as described in the Methods. The values on the bar graphs represent the mean ± S.D. derived from three replicate cultures.

Caspase activation, detected by cleavage of procaspases to lower molecular weight active caspases, is a major indicator of apoptosis. It is essential for the morphological and biochemical changes that accompany this form of cell death. To determine whether the cell death induced by 6-MOMIPP is associated with caspase activation, the status of several caspases was measured by immunoblot analysis. U251 cells were treated with 1 μM of 6-MOMIPP for 24 h or 48 h and then both attached and floating cells were subjected to SDS-PAGE. Immunoblot results show that 6-MOMIPP caused time-dependent cleavage of caspase-9, caspase-7, and caspase-3 (Fig. 2-6A). Caspase activation was detected after 48 h incubation with 6-MOMIPP, which is consistent with the cell cycle analysis showing that sub-G_0 (dead) cells accumulate at that time. It is also consistent with the cell viability assays showing extensive cell death by 48 h. To evaluate whether 6-MOMIPP-induced caspase activation is required for cell death, two caspase inhibitors were used to block caspase activation. As illustrated in Fig. 2-6A, Pro-VAD-FMK (a pan-caspase inhibitor) and Z-LEHD-FMK (caspase- 9 specific inhibitor) combined together effectively blocked caspase activation induced by 6-MOMIPP at 48 h. ATP assays showed that by blocking caspase activation, the number of viable cells was significantly increased after 6-MOMIPP treatment (Fig. 2-6B). Annexin-V live-dead cell assay was also performed to assess the dead cell percentage after caspase inhibition. (Appendix A Fig. 3). These results agree with the ATP assay. Taken together,

the data demonstrate that 6-MOMIPP induces caspase activation by 48 h, and that caspase activation is required for 6-MOMIPP-induced cell death in U251 cells.
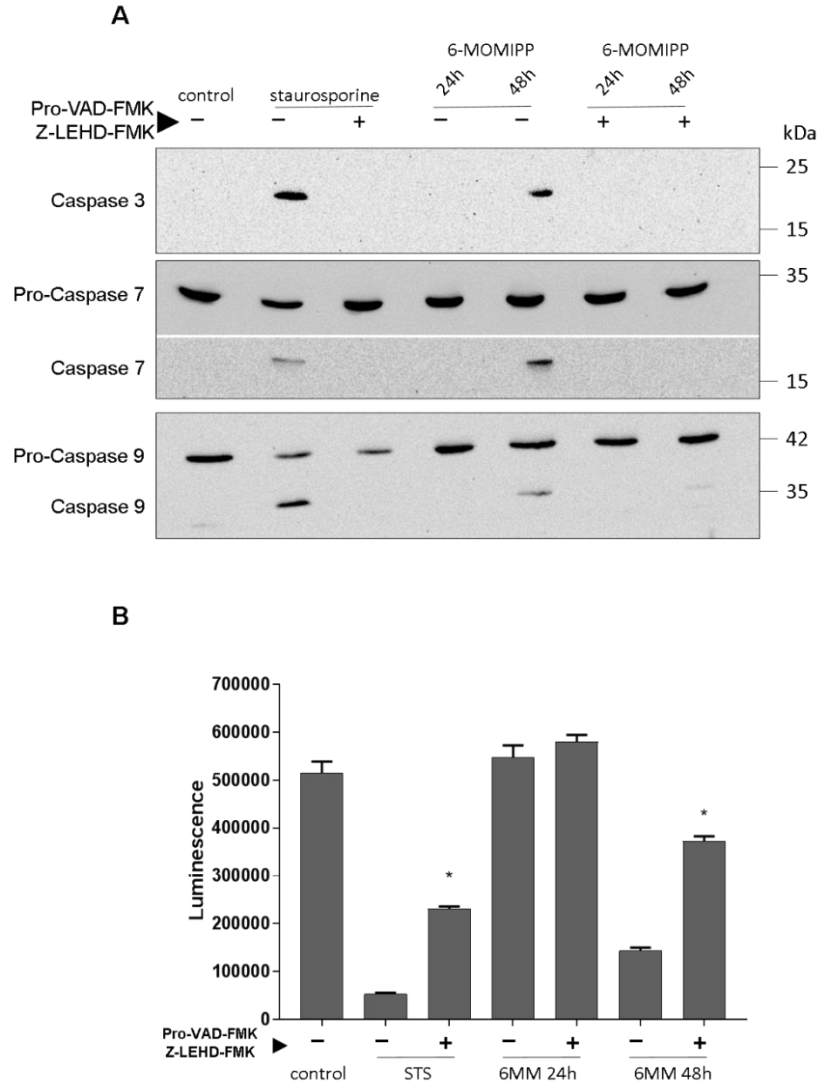
Figure 2-6. 6-MOMIPP induces caspase-dependent cell death in U251 cells. A. U251 cells were treated with 1 µM 6-MOMIPP or the equivalent volume of DMSO for 24 h or 48 h. For the inhibitor study, cells were pretreated with Pro-VAD-FMK and Z-LEHD-FMK for 2 h before 6-MOMIPP treatment. The cells (attached and detached) were

harvested and lysed in SDS sample buffer and subsequently subjected to immunoblot analysis as described in the Methods. The results shown are representative of three separate experiments. B. U251 cells were seeded in a white-walled opaque 96-well plate at a density of 2,000 cells/well and treated with 1μM 6-MOMIPP or the equivalent volume of DMSO for 48 h. Caspase inhibitors were added 2 h before 6-MOMIPP treatment. Cell Titre Glo® viability assays were performed and luminescence was determined as described in the Methods. Values represent the mean ± S.D. of four replicates. *Increases in viability observed with addition of caspases inhibitors were significant at p<0.05.

2.4.5   6-MOMIPP inhibits polymerization of cellular microtubules

6-MOMIPP induces mitotic arrest and causes accumulation of micronuclei in U251 cell, similar to the effects typical of MTAs. To investigate the underlying mechanism of 6-MOMIPP, the effects of compound on tubulin polymerization were assessed in U251 cells. It is well-known there are two groups of MTAs: microtubule stabilizing agents, such as paclitaxel, and microtubule destabilizing agents, like vinblastine and colchicine [40]. In this study, paclitaxel and colchicine were chosen as reference drugs. Tubulin polymerization assays in U251 cells were based on whole cell microtubule analysis by flow cytometry [170]. U251 cells were exposed to 6-MOMIPP, paclitaxel, or colchicine for 24 h, then glutaraldehyde was used to fix the microtubule network after the soluble tubulin was washed out. FITC-conjugated antibody against α-tubulin was then used to stain the polymerized tubulin and flow cytometry was used to quantify the fluorescence signal in individual cells. As Fig. 2-7 shows, the microtubule destabilizer, colchicine,

60

significantly reduced median fluorescence signal of the treated cell population compared to DMSO control, indicating tubulin depolymerization. The microtubule stabilizer, paclitaxel, dramatically increased the median fluorescence, indicating that tubulin polymerization was enhanced. In 6-MOMIPP treated U251 cells, the median fluorescence of polymerized tubulin decreased in a concentration depended manner, suggesting that 6-MOMIPP acts in a manner similar to the microtubule destabilizer, colchicine.

A
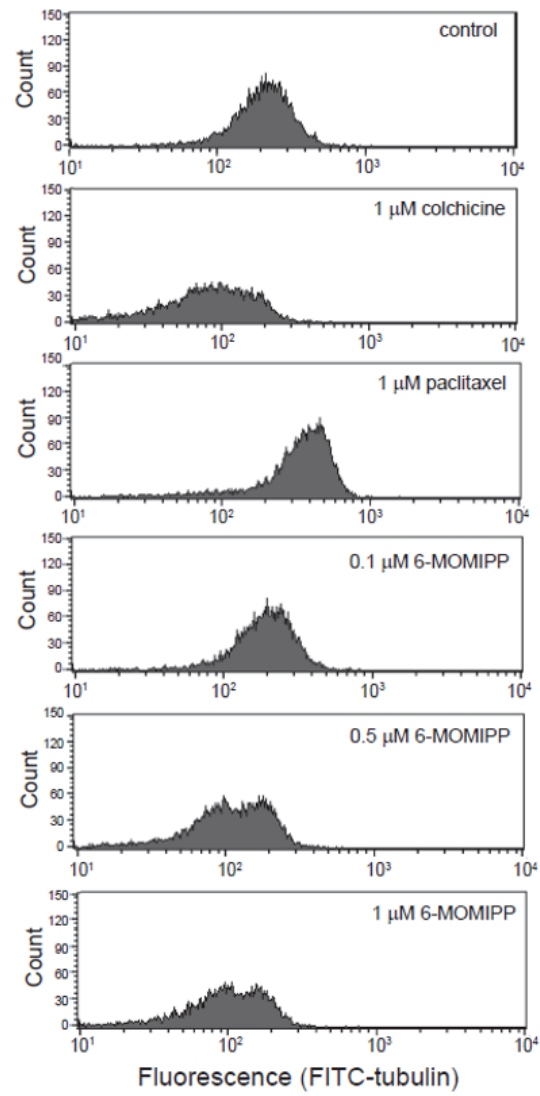
B
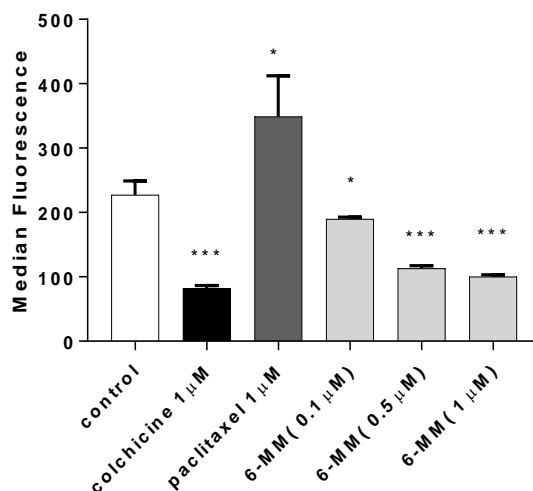
Figure 2-7. Effects of 6-MOMIPP on tubulin polymerization in cultured U251 cells.

Cells were treated with DMSO, colchicine (1 µM), paclitaxel (1 µM) or indicated concentrations of 6-MOMIPP for 24 h. Tubulin monomers were washed out of the cells and polymerized microtubules were fixed, immunostained and analyzed by flow cytometry as described in the Methods. The fluorescence intensity is depicted in histogram form in panel A, and as median fluorescence intensity in panel B. Each bar represents mean $\pm$ S.D. of three cultures. Significance of changes in median fluorescence relative to the control was: * $p < 0.05$, ** $p < 0.005$, *** $p < 0.001$.

To visualize the effects of 6-MOMIPP on microtubule organization in U251 cells, α-tubulin was immunostained and cells were subjected to fluorescence microscopy. As shown in Fig. 2-8, the vehicle-treated cells displayed an organized microtubule network, with distinct filamentous microtubules and surrounding an uncondensed cell nucleus. Cells treated with 0.1 µM 6-MOMIPP for 24 h also exhibited a dense network of

microtubules, similar to the DMSO control. However, in cells treated with higher concentrations of 6-MOMIPP, the microtubules were dispersed and disorganized. Some of the few cells that remained attached to the culture dish contained multiple micronuclei. This result confirms that 6-MOMIPP acts as a microtubule destabilizer.

Control

6-MM (0.1µM)

6-MM (0.25µM)

6-MM (0.5µM)

6-MM (0.75µM)

6-MM (1µM)
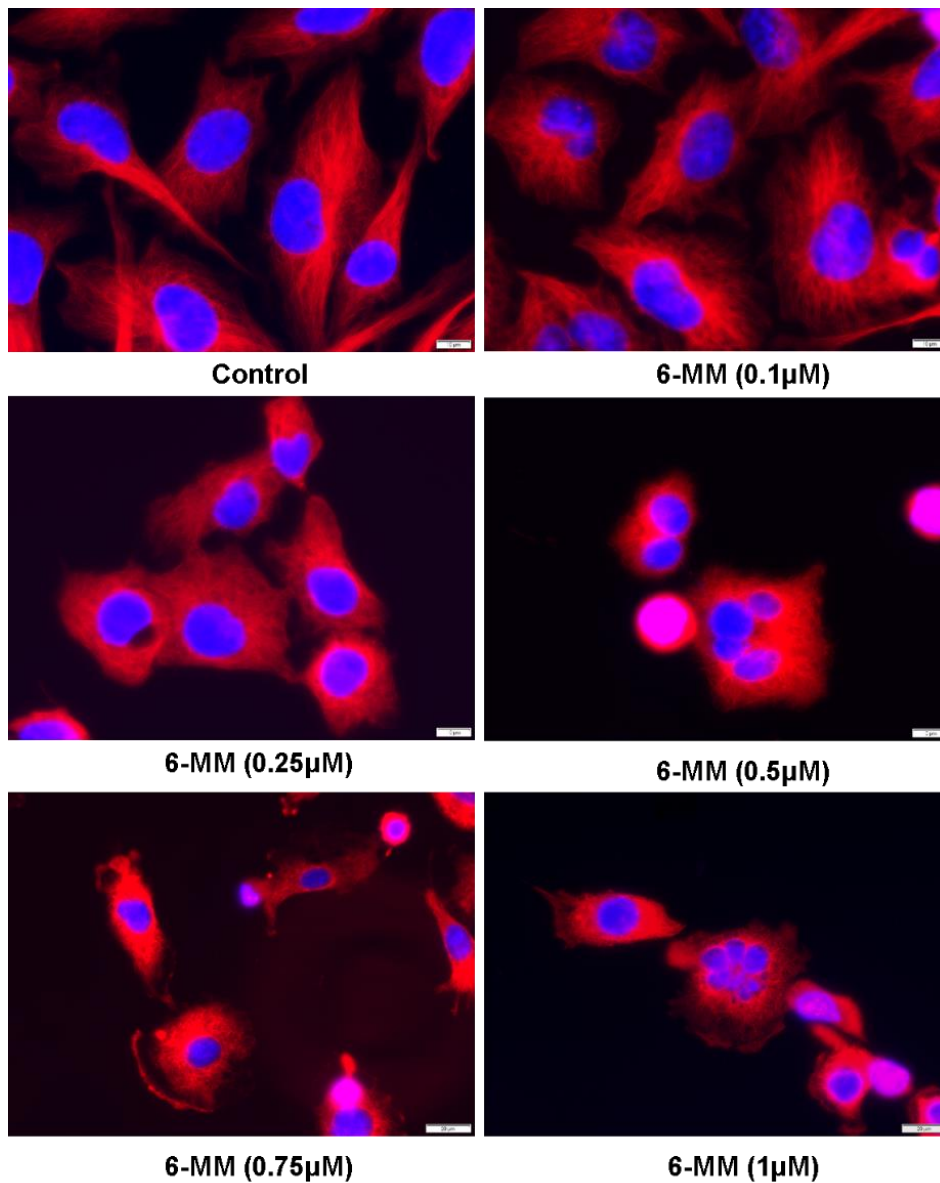
Figure 2-8. 6-MOMIPP disrupts microtubules and induces multiple-micronuclei in U251 cells. Cells were treated with DMSO (control) or 6-MOMIPP at the indicated concentrations for 24 h. Microtubules were stained with anti-α-tubulin primary antibody and Alexa Fluor 568-labeled goat anti-mouse secondary antibody (red fluorescence). Nuclei were stained with DAPI (blue fluorescence).

2.4.6 6-MOMIPP binds to tubulin on the colchicine binding site

To obtain information about how 6-MOMIPP interacts with tubulin, a competition-binding scintillation proximity assay (SPA) was performed [171]. The principle of this assay is that compounds that can bind to the colchicine site on tubulin can compete with [^{3}H] - colchicine. This will diminish the signal generated when biotinylated tubulin bearing [^{3}H]-colchicine interacts with streptavidin-coated yttrium sensor beads. As shown in Fig. 2-9A, 6-MOMIPP substantially inhibited the binding of [^{3}H]-colchicine to tubulin when added in a concentration range of 1–10μM. As expected, unlabeled colchicine also diminished the binding of [^{3}H]-colchicine, but vinblastine had no effect. In a converse experiment, the same set of MTAs was used to compete with [^{3}H]-vinblastine, in that case, only unlabeled vinblastine inhibited the binding of [^{3}H]-vinblastine to tubulin, whereas colchicine and 6-MOMIPP did not affect the bound radioactivity (Fig. 2-9B). This experiment strongly suggests that 6-MOMIPP binds to tubulin at or near the well-defined colchicine binding site.

To confirm the binding site of 6-MOMIPP on tubulin, we used an additional technique that is based on the principle that EBI (N, N'-ethylene-bis iodoacetamide) forms a crosslink between two cysteine residues (cys-239 and cys-354) on β-tubulin in

living cells. These two cysteine residues are involved in the colchicine-binding site. The covalent binding of EBI to β-tubulin generates a second band that migrates at a lower molecular weight than non-crosslinked β-tubulin on SDS gels [172]. When colchicine occupies its tubulin binding site, EBI access to the target cysteines will be blocked. U251 cells were treated with DMSO, 6-MOMIPP, colchicine, or vinblastine for 4 h followed by 1.5 h incubation with EBI. Then cells were harvested and subjected to SDS-PAGE and immunoblot analysis for β-tubulin. As shown in Fig. 2-10, incubation with colchicine, but not vinblastine, prevented the formation of the EBI crosslinked band. Similar to colchicine, 6-MOMIPP inhibited the formation of the EBI-crosslinked band at concentrations of 1 µM and above, suggesting that 6-MOMIPP occupies the colchicine binding site on β-tubulin.
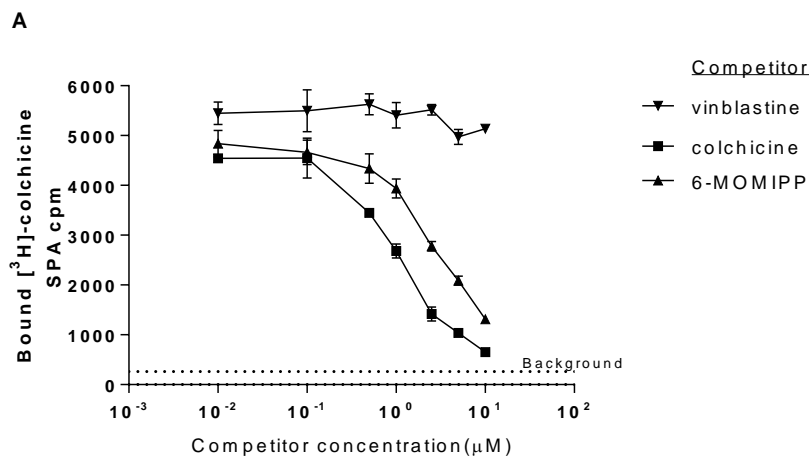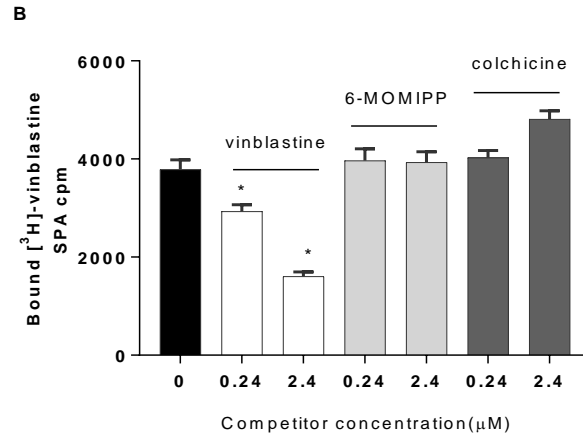
Figure 2-9. 6-MOMIPP competes with [³H]-colchicine but not [³H]-vinblastine binding to tubulin. A. 0.5 μCi [³H] colchicine, was incubated with unlabeled vinblastine, colchicine or 6-MOMIPP (final concentrations 10 nM, 50 nM, 1 μM, 2.5 μM, 5 μM, 10 μM), and 0.5 µg of long-chain biotin-labeled tubulin for 2 h. Then streptavidin SPA beads were added to each reaction mixture and scintillation signals were measured as described in the Methods. Each point represents the mean ± S.D. of 4 replicates. B. 0.5 μCi [³H]-vinblastine was incubated for 2 h with unlabeled vinblastine, colchicine or 6-MOMIPP (final concentrations 0.24 μM or 2.4 μM), and 1 µg of long-chain biotin-labeled tubulin. Then streptavidin SPA beads were added and scintillation signals were quantified. Each point represents the mean ± S.D. of 4 replicates. * p < 0.05, ** p < 0.005, *** p < 0.001.
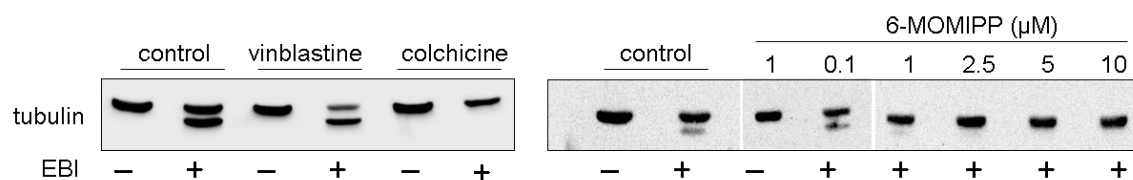
Figure 2-10. 6-MOMIPP behaves like colchicine in preventing EBI from forming crosslinks on β-tubulin. U251 cells were incubated for 4 h with 1 μM vinblastine, 1 μM colchicine, or 6-MOMIPP at indicated concentrations. Controls received an equivalent volume of DMSO. Cells were then harvested for SDS-PAGE and immunoblot analysis after a 1.5 h incubation with 100μM EBI. The results shown are representative of three separate experiments.

2.4.7 G_2/M arrest is required for 6-MOMIPP-induced cell death

It is clear that 6-MOMIPP destabilizes microtubules by binding to tubulin on the colchicine binding site. We also noted that the arrest at the G_2/M phase by 6-MOMIPP is followed by massive cell death, but the cell death mechanism and signaling pathways involved are not clear. Greater insight into this mechanism could help to better evaluate the translational potential of 6-MOMIPP. The relationship between 6-MOMIPP associated G_2/M arrest and cell death was assessed by arresting cells at the G_1/G_0 phase through serum and leucine starvation prior to addition of 6-MOMIPP. As shown previously, cells in normal medium underwent G_2/M arrest after 6-MOMIPP treatment (Fig. 2-3 and 2-4). In contrast, the cells maintained in serum/leucine-free medium stayed at the G_1/G_0 phase after addition of 6-MOMIPP for 24 h or 48 h (Fig. 2-11 A and B). The annexin V live-dead cell assay was used to evaluate the percentage of dead cells in

the same samples. As shown in Fig. 2-12, in normal medium, about 66% of cells died

after 48 h 6-MOMIPP treatment, which is a six-fold increase compared to control (11%

percent). In serum/leucine-free medium, the baseline of dead cells in vehicle-treated

controls was higher than in normal medium (36%). 6-MOMIPP treatment resulted in

62% dead cells, which is only 1.7-fold increase compared to control. This suggests that

preventing cells from undergoing G_2/M arrest has a protective effect (albeit, not

complete) on cell death induced by 6-MOMIPP (Fig. 2-12). Taken together, these results

suggest that mitotic arrest plays an important role in cell death induced by 6-MOMIPP.
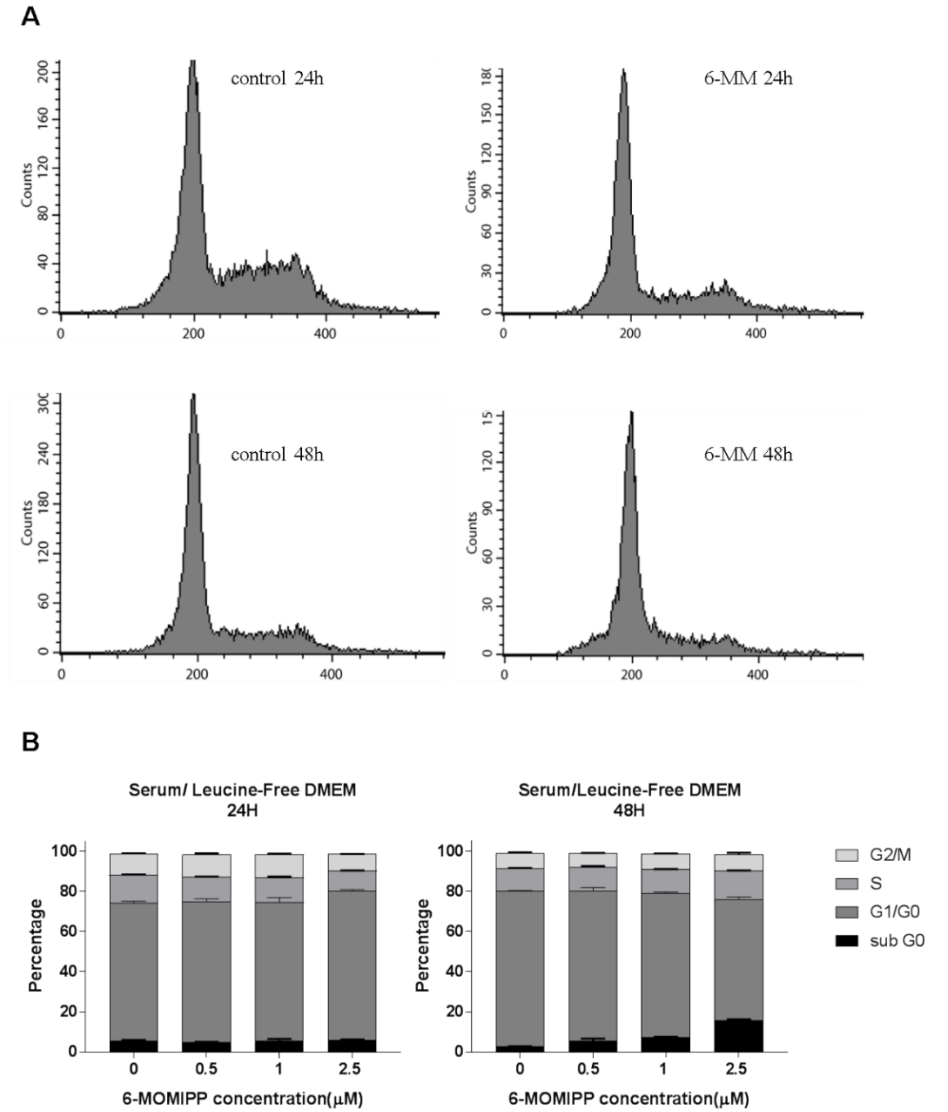
Figure 2-11. Serum/leucine starvation prevents G_2/M arrest induced by 6-MOMIPP in U251 cells. A. U251 cells were seeded at 350,000 cells in 60 mm dishes with DMEM medium supplemented with 10% FBS. On the next day, the medium was substituted with serum/leucine-free DMEM medium and incubation was continued for 24 h. Then the cells were treated with or without 1 μM 6-MOMIPP for 24 h or 48 h. Both attached and detached cells were harvested and processed for cell cycle analysis. B. Cell cycle

distribution after treatment of serum/leucine-starved cells with 6-MOMIPP for 24 h and

48 h. Bar graphs depict the results of three separate determinations (mean ± S.D.).
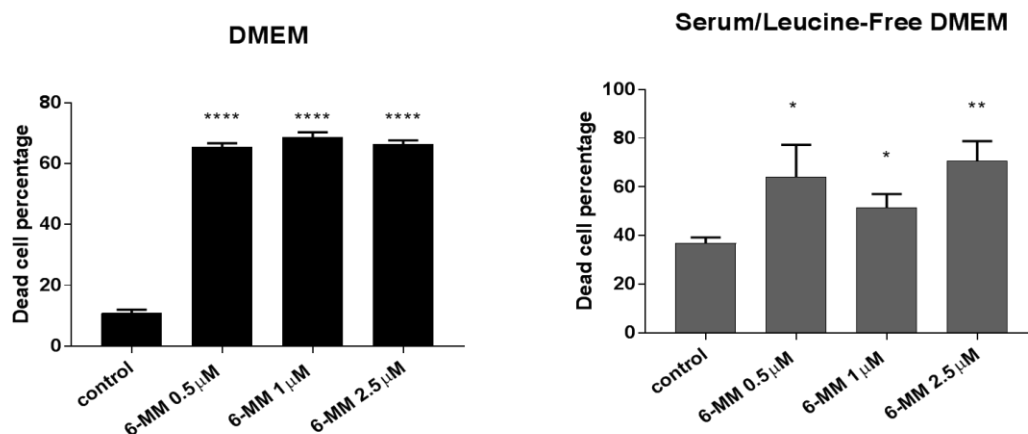
Figure 2-12. Serum/leucine starvation prevents cell death induced by 6-MOMIPP. U251

cells were seeded at 350,000 cells in 60 mm dishes with DMEM medium supplemented

with 10% FBS. On the next day, the medium was replaced with either regular medium

(left panel) or serum/leucine-free DMEM medium (right panel) for 24 h. Then the cells

were treated with or without 6-MOMIPP at indicated concentrations for 48 h. Both

attached and detached cells were harvested and processed for the live-dead cell assay as

described in the Methods. Each point represents mean ± S.D. of triplicate determinations.

Significance differences compared to the controls: * $p < 0.05$, ** $p < 0.005$, **** $p <$

0.0001.

2.4.8   Involvement of Cdk1 in regulating mitotic arrest and cell death induced by

6-MOMIPP

Mitotic arrest plays a key role in cell death induced by MTAs, but the signals that direct cells toward cell death after G_2/M arrest are only partly understood. To further investigate the connections between 6-MOMIPP-induced G_2/M arrest and cell death, some regulatory proteins involved in the G_2/M phase transition were analyzed. Cdk1 / cyclin B1 activity is required for cells to stay in mitosis until all chromosomes acquire bipolar attachment to kinetochore microtubules. MTA-induced mitotic arrest is associated with prolonged activation of the Cdk1/cyclin B1 complex. The phosphatase, PP1-α, is a direct substrate of the Cdk1/cyclin B1 complex in mitosis, with phosphorylation at Thr-320 during metaphase contributing to the activation of proteins critical to mitotic progression [173]. To determine the effects of 6-MOMIPP on Cdk1/cyclin B1 activity, the phosphorylation status of PP1-α was assessed after 6-MOMIPP treatment. Western blots (Fig. 2-13) showed that 6-MOMIPP induced phosphorylation of PP1-α on Thr-320 in a time-dependent manner, paralleling G_2/M arrest (Fig. 2-13). At 24 h, when the majority of cells were in mitosis, PP1-α was phosphorylated, whereas, at 48 h, when most cells underwent cell death, phosphorylated PP1-α was markedly decreased. A specific Cdk1 inhibitor, BMS-265246, was used to confirm that the phosphorylation of PP1-α induced by 6-MOMIPP at 24 h, is due to increased Cdk1/cyclin B1 activity in the mitotically arrested cells.

MTAs target the spindle microtubule dynamics and trigger SAC, which inhibits APC/C activity and prevents cyclin B1 degradation. As a result, Cdk1 maintains its activity and blocks metaphase-anaphase transition. To evaluate the metaphase/anaphase transition in cells treated with 6-MOMIPP, we evaluated the phosphorylation state of

histone-H3. The latter contributes to chromatin condensation during prophase, which is critical for the transition into metaphase [174]. Histone-H3 is phosphorylation on Ser-10 commences during late G_2 phase, is completed in prophase, and is maintained through metaphase. Ser-10 dephosphorylation begins at anaphase and ends at early telophase; it must be removed upon metaphase/anaphase transition [175-177]. Immunoblots (Fig. 2-13) show that 6-MOMIPP-induced cell cycle arrest was accompanied by robust histone-H3 Ser-10 phosphorylation at 24 h (Fig. 2-3). This indicates that the majority of cells were arrested in prophase and/or metaphase, consistent with the effects of MTAs on mitotic spindle assembly. At 48 h, histone-H3 Ser-10 protein was dephosphorylated, consistent with a high percentage of dead cells and the possibility of mitotic slippage, as described earlier. Blocking the activity of Cdk1 with BMS-265246 abolished histone-H3 phosphorylation in cells treated with 6-MOMIPP at 24 h, with no change in the total amount of histone-H3. Interestingly, DNA histograms of cells treated with BMS-265246 (with or without 6-MOMIPP) showed a prominent G_2/M peak (Fig. 2-14 A and B). When taken together with the lack of histone phosphorylation, this suggests that cells treated with the Cdk1 inhibitor were arrested at the G2 → prophase transition. Unlike cells treated with 6-MOMIPP alone, the cells treated with 6-MOMIPP plus the Cdk1 inhibitor did not have a large increase in the sub-G_0 population, (Fig. 2-14 A and B). This suggests that prolonged activation of Cdk1 during prophase/metaphase arrest may play an essential role in the 6-MOMIPP induced cell death mechanism. To explore this concept further, the effects of BMS-265246 on the viability and morphology of U251 cells treated with 6-MOMIPP were directly evaluated using ATP assays and phase contrast imaging.

73

As shown in Fig. 2-15 A and B, BMS-265246 by itself did not affect cell viability but induced flat, round cell morphology. Adding BMS-265246 to cells treated with 6-MOMIPP prevented the cells from rounding and detaching, and provided significant protection from loss of cell viability. In considering how abnormal activation of Cdk1/cyclin B1 may be linked to the initiation of apoptosis, one prominent possibility is that Cdk1 may inactivate anti-apoptotic Bcl-2 family proteins via phosphorylation [124]. Some groups have shown that Bcl-2 phosphorylation was closely associated in time with M phase arrest and activation of Cdk1. Therefore, the next series of studies was designed to examine the effects of 6-MOMIPP on the Bcl-2 anti-apoptotic family members and the relationship between Cdk1 activation and Bcl-2 phosphorylation. Western blot results (Fig. 2-13) revealed that at 24 h, by the time the majority of 6-MOMIPP-treated cells were arrested in mitosis, Bcl-2 was phosphorylated. The three mobility shifted bands most likely correspond to Ser70, Ser80, and Thr69 phosphorylation, respectively [138]. By 48 h, when most cells underwent cell death, Bcl-2 phosphorylation was lost. Essentially identical results were obtained when we examined the other abundant anti-apoptotic protein, Bcl-xL. The total amounts of the Bcl-2 and Bcl-xL proteins were not markedly reduced at 48 h, indicating that the loss of phosphorylation was not due to degradation of the proteins. Of particular note, the Cdk1 inhibitor, BMS-265246, blocked the phosphorylation of Bcl-2 and Bcl-xL. These experiments were confirmed by using another, less specific, but widely used, Cdk1 inhibitor, roscovitine, and results are shown in Appendix A Fig.4- Fig.6.

It remains unclear whether the effects of the Cdk1 inhibitors are direct (inhibiting Cdk1 phosphorylation of Bcl-2 proteins) or indirect (preventing transition to mitotic prophase/metaphase, where other kinases might phosphorylate Bcl-2/Bcl-xL) Nevertheless, these results strongly support the notion that increased Cdk1 activity plays a key role in promoting the phosphorylation and potential inactivation of anti-apoptotic Bcl-2 family members.
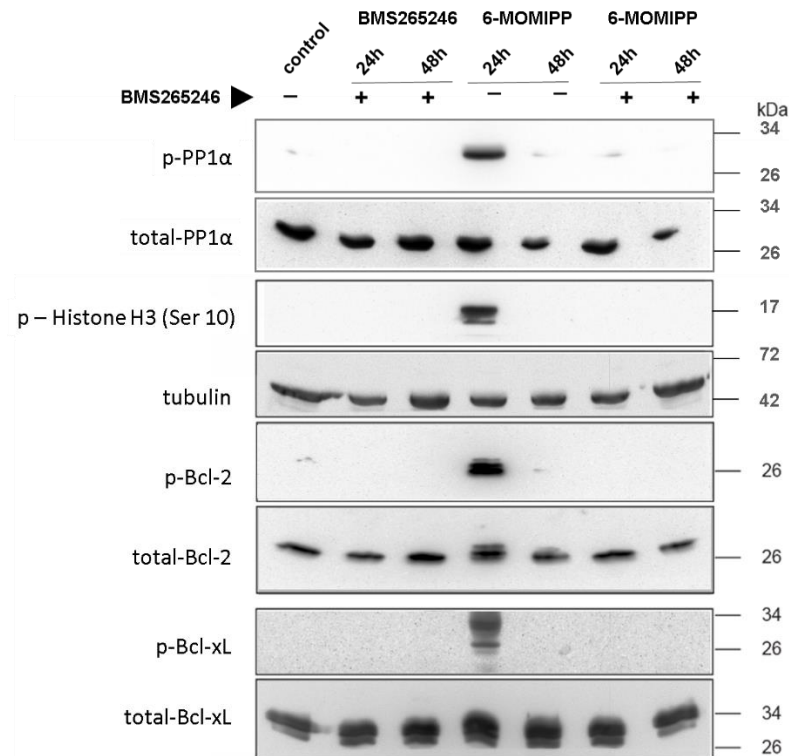
Figure 2-13. 6-MOMIPP-induced Cdk1 activation plays important role in mitotic arrest and Bcl-xL/Bcl-2 phosphorylation. 10^6 U251 cells were seeded in the 10 cm dishes and treated with 1 µM 6-MOMIPP, or an equivalent volume of DMSO. For the inhibitor study, 5 µM BMS-265246 was added to the cells 2 h before the addition of 6-MOMIPP. Detached and attached cells were harvested after 24 h or 48 h subjected to SDS-PAGE

and immunoblot analysis for the indicated proteins as described in the Methods. The results shown are representative of three replicate experiments.
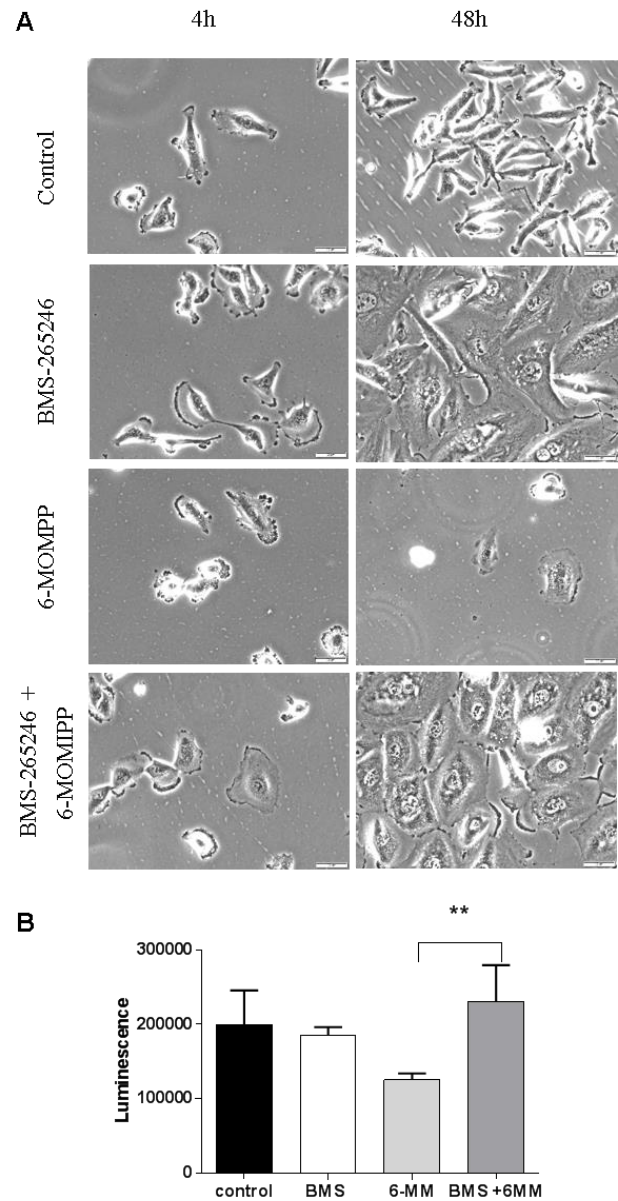
Figure 2-14. CDK1 inhibitor prevents cell death induced by 6-MOMIPP. A. 100,000 U251 cells were seeded in 35mm dishes. The next day, cells were treated with DMSO, 5 μM BMS-265246, 1 μM 6-MOMIPP or combination of both inhibitors, with   the

BMS-265246 added 2 h before the 6-MOMIPP. Phase-contrast images were acquired at 4 h and 48 h. B. U251 cells were seeded in white-walled opaque 96-well plates at a density of 2,000 cells/well. On the second day, 6-MOMIPP at the indicated concentrations was added and cell viability was assayed by Cell Titre Glo® after 48 h. For the inhibitor study, 5 μM of BMS-265246 was added 2 h before 6-MOMIPP treatment. Values represent the mean ± S.D. of four replicates. ** $p < 0.005$.
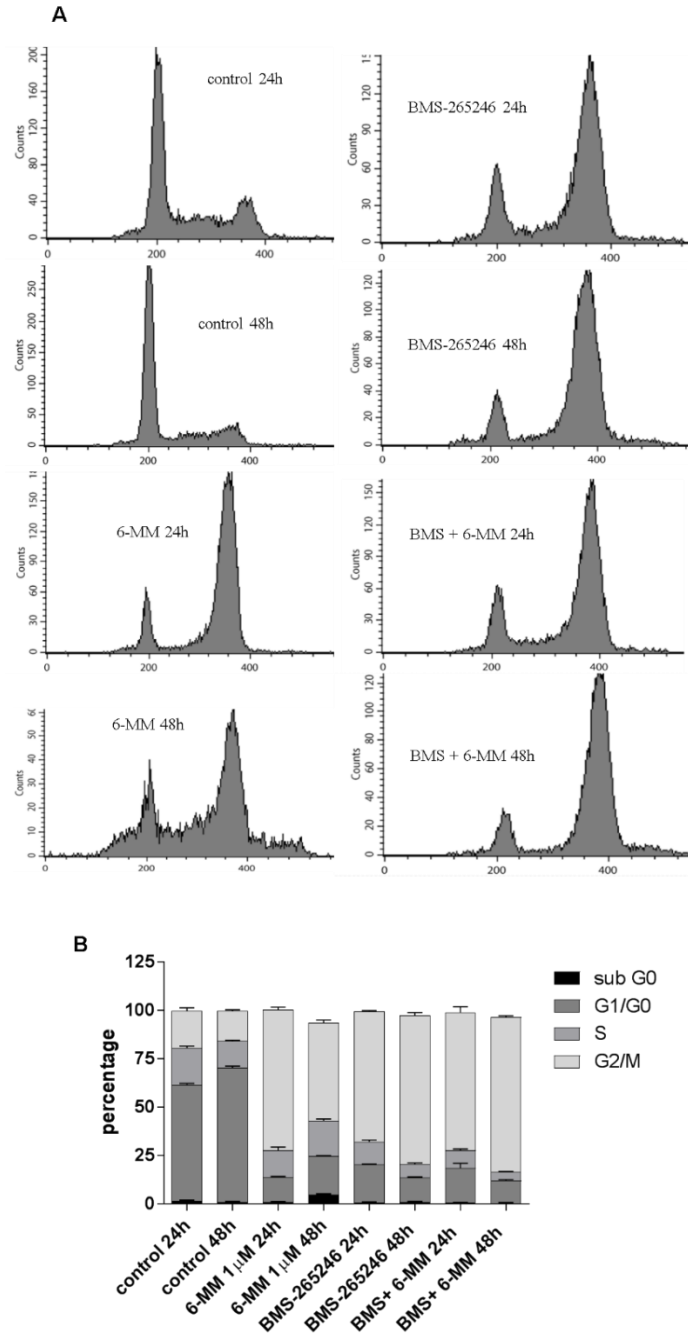
Figure 2-15. Effects of the Cdk1 inhibitor, BMS-265246, on the cell cycle. A. U251 cells were seeded at 350,000 cells in 60 mm dishes and treated with 1 μM 6-MOMIPP, 5 μM BMS-265246, or a combination of both compounds for 24 h or 48 h. For the

combination, the BMS-265246 was added 2 h before the 6-MOMPP. Attached and detached cells were harvested, fixed with 70% ethanol, stained with propidium iodide (PI) and subjected to flow cytometry to generate DNA histograms as described in the Methods. B. Data from triplicate cultures were used to determine the percentage of cells in each phase of the cell cycle (mean ± S.D.).

2.4.9   Involvement of JNK in regulating mitotic arrest and cell death induced by 6-MOMIPP

JNKs (JNK1/2) are essential in the cellular response to stress and cytotoxic agents, including MTAs [155, 178, 179]. MTA-induced G_2/M arrest and cell death have been correlated with activation of JNK and its downstream targets, c-Jun, JunD, and ATF2 [137, 151, 153-156]. To investigate whether or the JNK signaling pathway plays a role in 6-MOMIPP-induced cell death, western blots were performed against several proteins that are involved in JNK pathways. As shown in Fig. 2-16, 6-MOMIPP induced JNK phosphorylation in a time-dependent manner, and JNK phosphorylation was associated with the increase in mitotic cells. JNK phosphorylation/activation was highest after 24 h of 6-MOMIPP treatment, when the majority of cells were arrested in mitosis, whereas at 48 h, JNK phosphorylation was diminished as most cells underwent cell death. This suggested that JNK may be involved in the mitotic arrest induced by 6-MOMIPP. C-Jun, the main substrate of JNK and an important component of the AP-1 transcription factor, was also phosphorylated after 24 h of 6-MOMIPP treatment, matching the increase in JNK kinase activity. There was no detectable phosphorylated c-Jun after 48 h exposure to 6-MOMIPP. A specific mitogen-activated protein kinase inhibitor, SP600125, was

used to examine the role of JNK kinase in the cell death. As shown in Fig. 2-16, SP600125 significantly reduced the JNK phosphorylation at 24 h after 6-MOMIPP treatment. The phosphorylation of its direct downstream substrate, c-Jun, was also blocked by SP600125. JNK activation is known to be an upstream signal for Bcl-2 and Bcl-xL phosphorylation, so Bcl-2 and Bcl-xL were also evaluated in this study. The JNK inhibitor abolished the phosphorylation of Bcl-2 and Bcl-xL. In addition, inhibition of JNK by SP600125 also attenuated the activation of caspases 3, 7, and 9 at 48 h after 6-MOMIPP treatment (Fig. 2-16), suggesting that JNK may play a role in 6-MOMIPP-induced cell death. To confirm this, the effects of SP600125 on the viability and morphology of 6-MOMIPP treated U251 cells were investigated by using ATP assays and phase contrast imaging. As shown in Fig. 2-17 A and B, SP600125 induced a flattened morphology in U251 cells and caused a modest reduction in cell growth, reflected by decreased density compared to the control (Fig. 2-17 A) and a decreased signal in the CellTiter-Glo® ATP assay (Fig. 2-17 B). However, when the JNK inhibitor was added together with 6-MOMIPP, cell density (Fig. 2-17 A) and ATP levels (Fig. 2-17 B) were not reduced beyond what was seen with SP600125 alone. Thus, the JNK inhibitor appeared to provide some protection from 6-MOMIPP-induced cell death. As in the case of the Cdk1, it remains to be determined whether the role of JNK in 6-MOMIPP-induced cell death is related to its direct phosphorylation of Bcl-2/Bcl-xL, or its regulation of cell cycle transition between the G_2 and M phase. In this regard, recent studies have found that JNK can play a complex role in cell cycle progression [146]. For example, inhibition of JNK delays activation of Cdk1 and prevents cyclin B1

80

degradation [148]. In addition, JNK promotes Aurora B expression and Histone-H3 phosphorylation enabling timely control of the G_2/M transition [148, 149]. To check the role of JNK in cell cycle progression in our studies, an immunoblot analysis of Histone-H3 Ser-10 phosphorylation was performed. Inhibiting JNK activation with SP600125 abolished Histone-H3 Ser-10 phosphorylation at 24 h (Fig. 2-16), suggesting that the cells were unable to progress beyond the G_2 checkpoint to enter mitotic prophase and metaphase. This was consistent with the DNA histogram for cells treated with SP600125 alone, which revealed a prominent G_2/M peak (Fig. 2-18). Adding the SP600125 to cells treated with 6-MOMIPP did not change the shape of the DNA histogram, which remained indicative of G_2/M arrest (Fig. 2-18), but unlike cells treated with 6-MOMIPP alone, the cells treated with the combination of 6-MOMIPP and SP600125 did not show any Histone H3 phosphorylation (Fig. 2-16). This indicates that the JNK inhibitor prevented the 6-MOMIPP-treated cells from transitioning from G_2 into M phase, where Cdk1 activation, Bcl-2 phosphorylation and dysfunction of mitotic spindle assembly could trigger caspase activation and cell death.
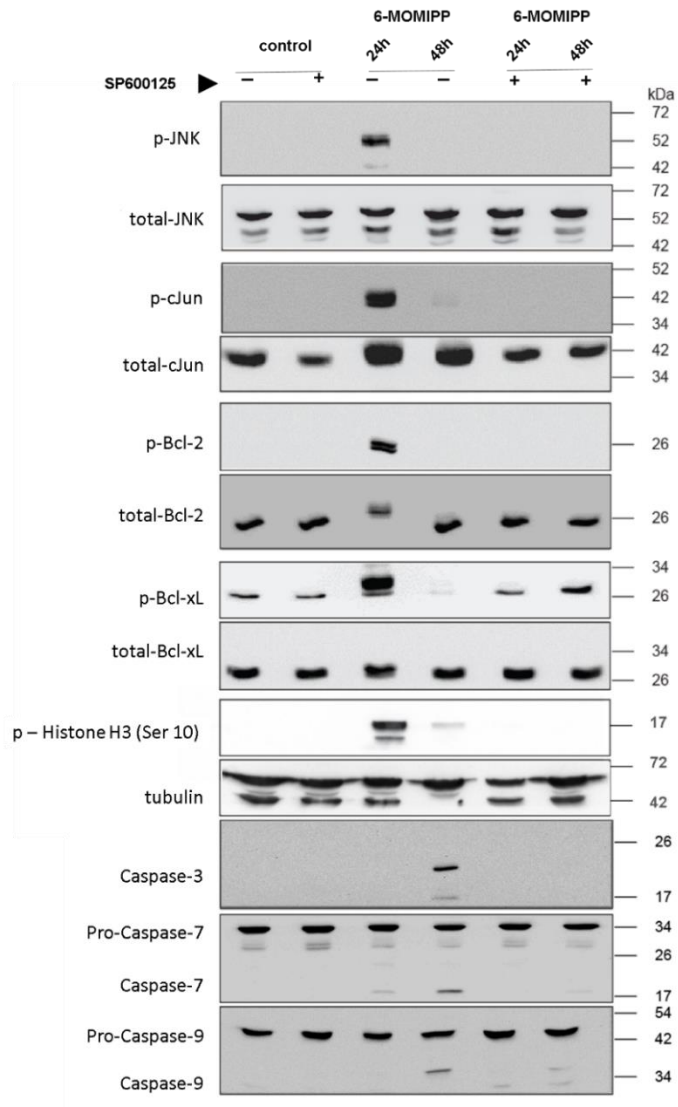
Figure 2-16. 6-MOMIPP activates JNK signaling pathway. 10^6 U251 cells were seeded in 10 cm dishes and treated with 1 µM 6-MOMIPP or an equivalent volume of DMSO for 24 h or 48 h. Where indicated, 75 µM SP600125 was incubated with the cells for 24 h or 48 h, either alone or together with 6-MOMIPP. The JNK inhibitor was added 2 h before the addition of 6-MOMIPP. Both detached and attached cells were harvested subjected to SDS-PAGE and immunoblot analysis, as described in the Methods. Similar results were obtained in three experiments.

A
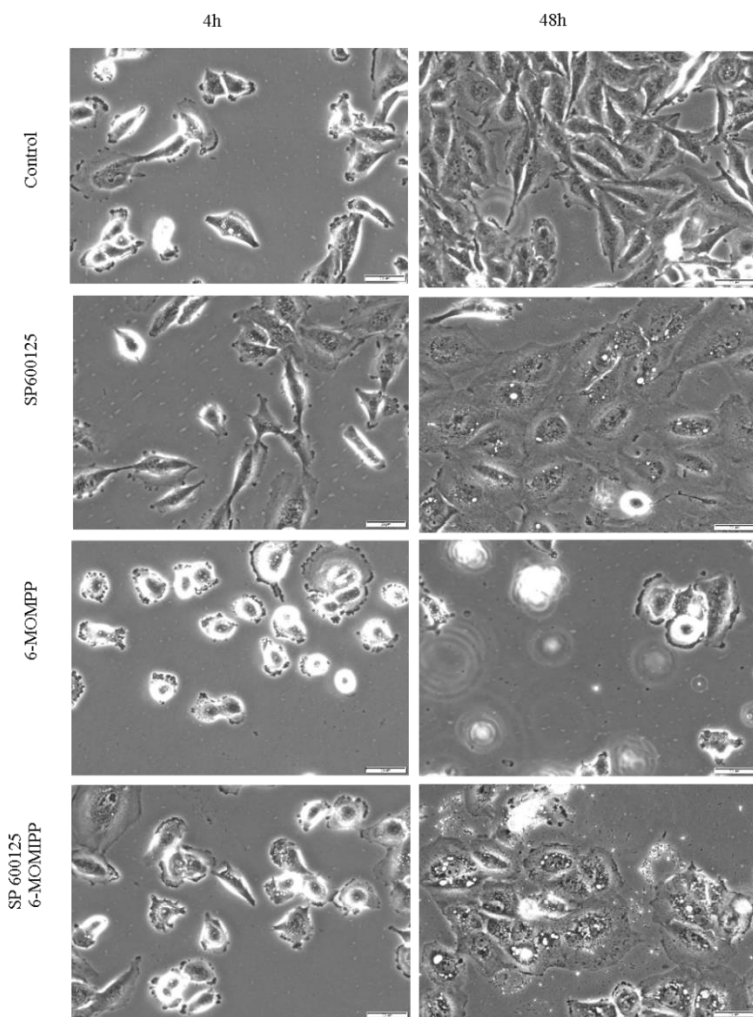
B
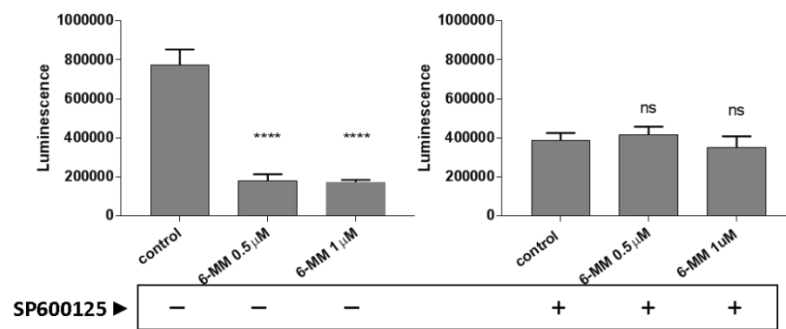
Figure 2-17. SP600125 blocks cell death induced by 6-MOMIPP. A. 100,000 U251 cells were seeded in 35 mm dishes. The next day, cells were treated with DMSO, 75 μM SP600125, 1 μM 6-MOMIPP or combination of both (with SP600125 added 2 h before 6-MOMIPP). . Phase-contrast images were acquired at 4 h and 48 h. B. U251 cells were seeded in white-walled opaque 96-well plates at a density of 2,000 cells/well. On the second day, 6-MOMIPP at the indicated concentrations was added and cells and viability was assayed by Cell Titre Glo® after 48 h. For the inhibitor study, 75 μM SP600125 was added 2 h before 6-MOMIPP and the two drugs were maintained for 48 h. Values represent the mean ± S.D. of four replicates. **** $p < 0.0001$.

85
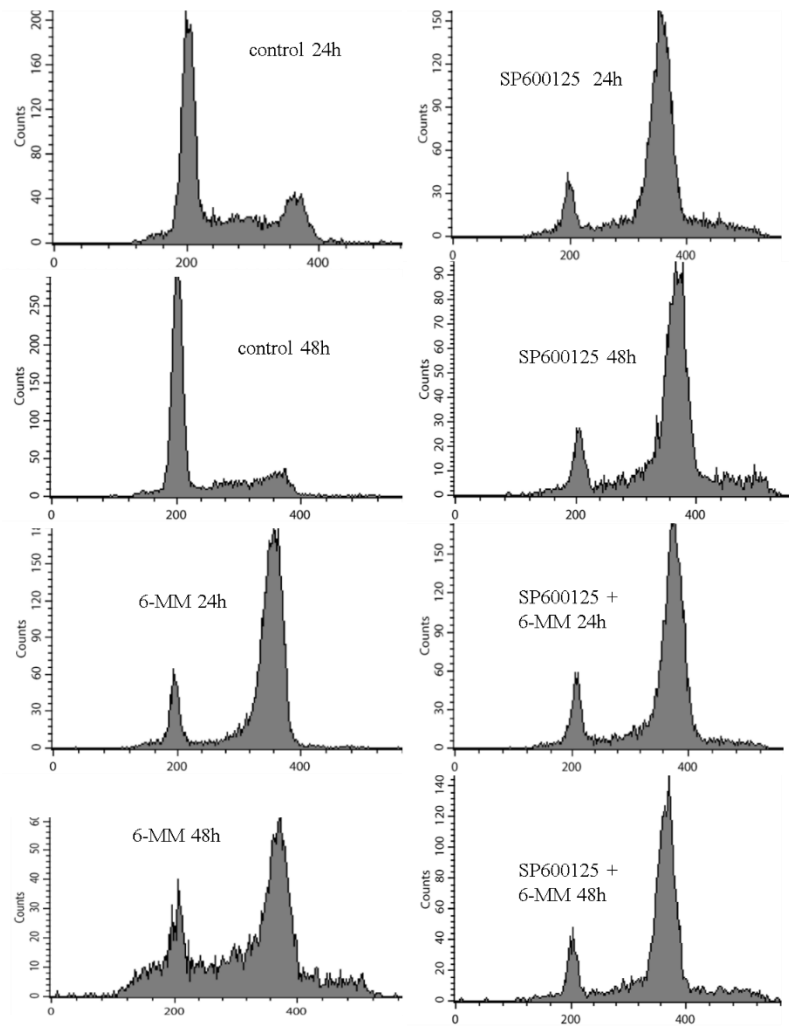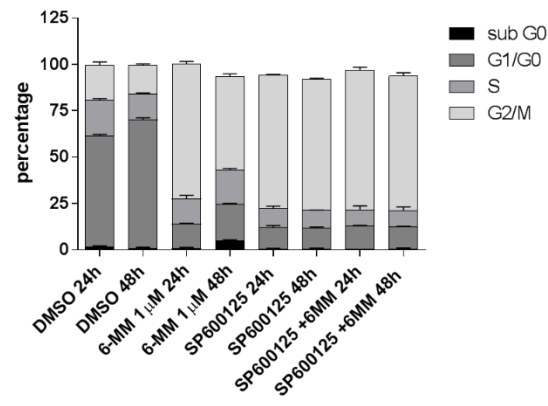
Figure 2-18. Effects of the JNK inhibitor, SP600125, on the cell cycle. A. U251 cells were seeded at 350,000 cells per 60 mm dish and treated with 1μM 6-MOMIPP for 24 h or 48 h. For the inhibitor study, 75 μM SP600125 was added 2 h before the 6-MOMPP and maintained throughout the time-course. Attached and detached cells were harvested, fixed with 70% ethanol and stained with propidium iodide (PI). The cellular DNA content in each sample was analyzed by flow cytometry as described in the Methods. The bar graphs show the cell cycle percentages based on the mean ± S.D. of determinations from three separate cultures.

2.4.10 Effects of 6-MOMIPP on viability of multiple cancer cell lines

Metastatic brain cancer is 10 times more common than primary brain tumors, given that 20-40% of patients with cancer develop brain metastases [23]. The majority of brain metastases come from lung cancer (50–60%), breast cancer (20–30%), and melanoma (5–10%) [180]. To better define 6-MOMIPP as a potential treatment for brain cancer and brain metastases, the cytotoxicity of 6-MOMIPP was evaluated in 16 cancer cell lines, derived from three different tumor types. These include 5 human glioblastoma cell lines: U251, U87MG, A172, LN229, T98G; 5 melanoma cell lines: A375, UACC62, B16F10, SK-MEL-2 and SK-MEL-5; and 4 lung cancer cell lines: H460, H292, A549, and H125. Acquired drug resistance often results in clinical chemotherapy failure, making the development of drugs that can kill drug-resistance cell lines a priority. Thus, this study also included two drug-resistant cell lines: U251 temozolomide resistant glioblastoma cells and H125 cisplatin-resistant lung cancer cells. As shown in Figs. 2-19 through 2-

21, 6-MOMIPP significantly reduced cell viability in multiple cancer cell lines, including drug-resistant cell lines. However, there were some major differences in sensitivity to 6-MOMIPP among the tumor cell lines within each class. For example, among the gliomas U87MG and A172 cells were much less sensitive than U251 or T98G. Similarly, among the melanoma lines, the SK-MEL-2 line stood out as being less sensitive than any of the other melanoma cells. The results also suggest that drug resistance mechanisms may influence sensitivity to 6-MOMIPP to some degree, as the TMZ-resistant variant of U251 and the cisplatin-resistant variant of H125 were both less sensitive to 6-MOMIPP than the corresponding parental cell lines. These results indicate that 6-MOMIPP could be used to treat brain metastases from lung and melanoma, in addition to primary brain tumors. This further confirms the translational potential of 6-MOMIPP as an anti-tumor agent.
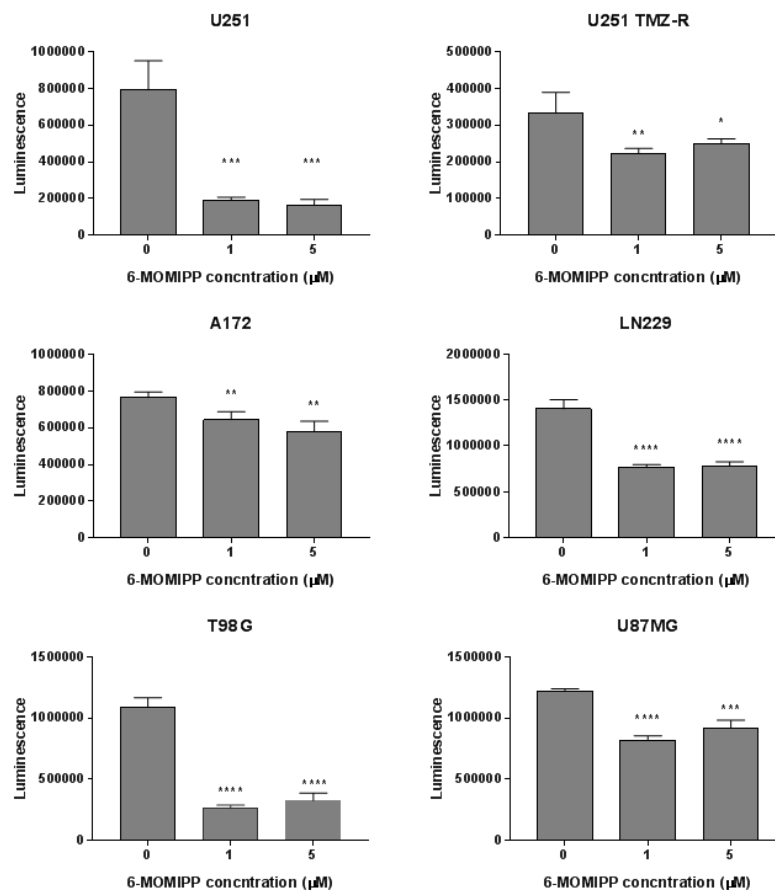
Figure 2-19. 6-MOMIPP inhibits the viability of glioblastoma cell lines. U251 Cells were seeded in white-walled opaque 96-well plates at a density of 2,000 cells/well with four replicate wells for each culture condition. The seeding densities for other cell lines were: U251 TMZ-R, 2,000 cells/well; U87MG, 5,500 cells/well; LN229, 5,500 cells/well; T98G, 3,500 cells/well; A172, 3,500 cells/ well. On the second day, 6-MOMIPP was added at the indicated concentrations and CellTiter-Glo® cell viability assays were performed after 48 h, as described in the Methods. . The results are the mean ± S.D. of four replicates. Significance of differences compared to the controls were: * p < 0.05, ** p < 0.005, *** p < 0.001, **** p < 0.0001.
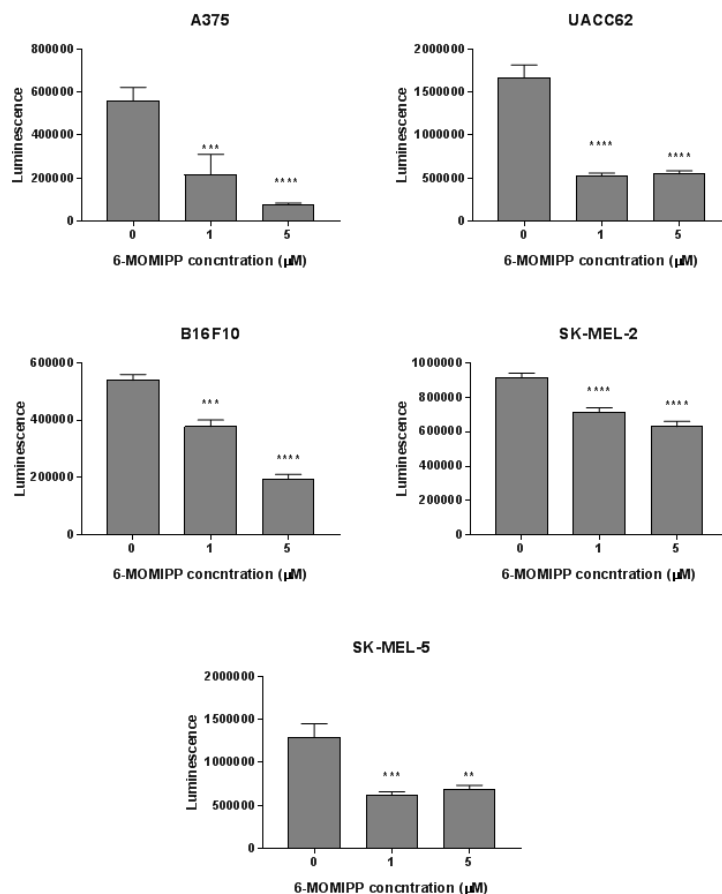
Figure 2-20. 6-MOMIPP inhibits the viability of melanoma cell lines. The seeding density for each cell line was: A375, 2,000 cells/well; SK-MEL-2, 5,000 cells/well; SK-MEL-5, 4,000 cells/well; UACC-62, 2,000 cells/well; B16F10, 4,000 cells/well in white-walled opaque 96-well plates, with four replicate wells for each culture condition. On the second day, 6-MOMIPP was added at the indicated concentrations and viability assays were performed after 48 h, as described previously. Values are the mean ± S.D. of four replicates. Significance of differences compared to the controls were: * $p < 0.05$, ** $p < 0.005$, *** $p < 0.001$, **** $p < 0.0001$.
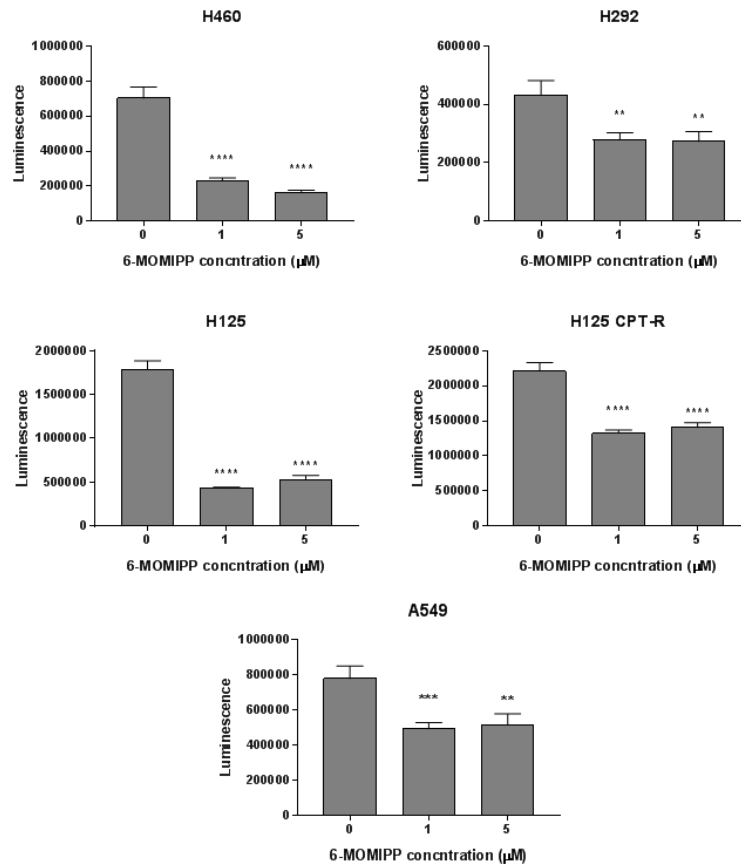
Figure 2-21. 6-MOMIPP inhibits the viability of lung cancer cell lines. The seeding density of each cell line was: H460, 5,000 cells/well; H125, 4,000 cells/well; H125 CPT-R, 4,000 cells/well; H292, 5,000 cells/ well; A549, 5,000 cells/well in white-walled opaque 96-well plates with four replicate wells for each culture condition. On the second day, 6-MOMIPP was added at the indicated concentrations and viability assays were carried out after 48 h. Values are the mean $\pm$ S.D. of four replicates. Significance of differences compared to the controls were: * $p < 0.05$, ** $p < 0.005$, *** $p < 0.001$, **** $p < 0.0001$.

2.4.11 6-MOMIPP has minimal effects on viability of non-transformed cell lines

The high toxicity of MTAs sometimes limits their use as anti-cancer agents, even if they excel in killing cancer cells. Disrupting microtubules and affecting the division of normal cells can induce myelosuppression, whereas disrupting microtubule dynamics in non-dividing cells such as peripheral neurons can lead to neuropathy. Myelosuppression is mainly due to the blockage of mitosis and proliferation of the rapidly cycling bone-marrow cells. Neuronal toxicity may be associated with the effects of these drugs on microtubules, which are key in carrying out many neuronal functions. To better evaluate 6-MOMIPP as an anti-tumor drug, cytotoxicity of 6-MOIMPP against 3 types of non-transformed cells was measured. Cell lines used in this study were: RN46A-B14, a SV40 large T antigen-immortalized rat neuron progenitor cell line [166], a human skin fibroblast cell line, and human umbilical vein endothelial cells (HUVEC). RN46A-B14 cells can be induced to differentiate into non-dividing cells with neuronal morphology (Fig. 2-22 A). HUVEC and fibroblast cells are dividing cells, so they were seeded at two different densities: confluent, which represents non-dividing status, and sub-confluent, representing the dividing status. As shown in Figs. 2-22 through 2-24, 6-MOMIPP did not have major effects on the viability of differentiated RN46A-B14 neurons, dividing and non-dividing fibroblasts, or HUVEC cells, although the cellular morphology of the latter exhibited a more flattened appearance. These findings suggests that 6-MOMIPP selectively kills cancer cells, with limited toxicity to non-malignant cells at the concentrations tested.
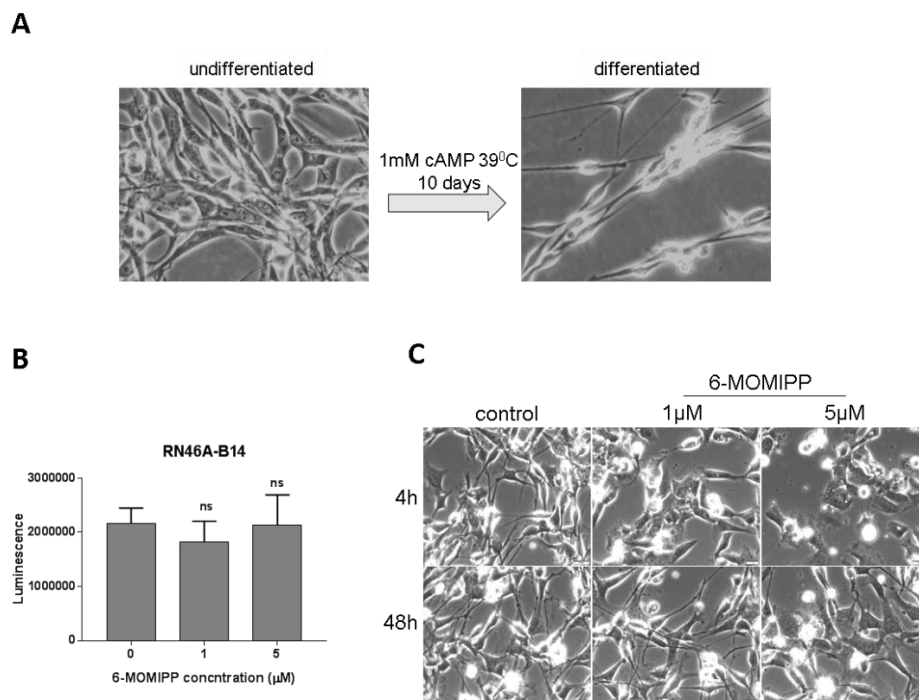
Figure 2-22. Effect of 6-MOMIPP on a rat neuron progenitor cell line. A. RN46A-B14 cells were maintained in DMEM/F12 1:1 media, supplemented with 100 μg/ml hygromycin, 250 μg/ml G418, 10% FBS at 33°C with 5% CO_2. Cells were differentiated to non-dividing neuronal cells at 39°C in DMEM/F12 1:1 medium containing 100 μg/ml hygromycin, 250 μg/ml G418, 10% FBS and 1 mM cAMP for 10 d. B. Undifferentiated RN46A-B14 cells were seeded at 5,000 cells/well in white-walled opaque 96-well plates with four replicate wells for each culture condition. On the second day, the cells switched to differentiation conditions for 10 d. Thereafter, cells were treated with DMSO or 6-MOMIPP at the indicated concentration for 48 h, and cell viability (ATP) was assayed as described previously. The bars depict the mean ± S.D. of four replicates. C. 100,000 cells were seeded in 35 mm dishes and induced to differentiate for 10 d. After

differentiation, cells were treated with DMSO or 6-MOMIPP at indicated concentrations

and phase contrast images were obtained after 4 h and 48 h.
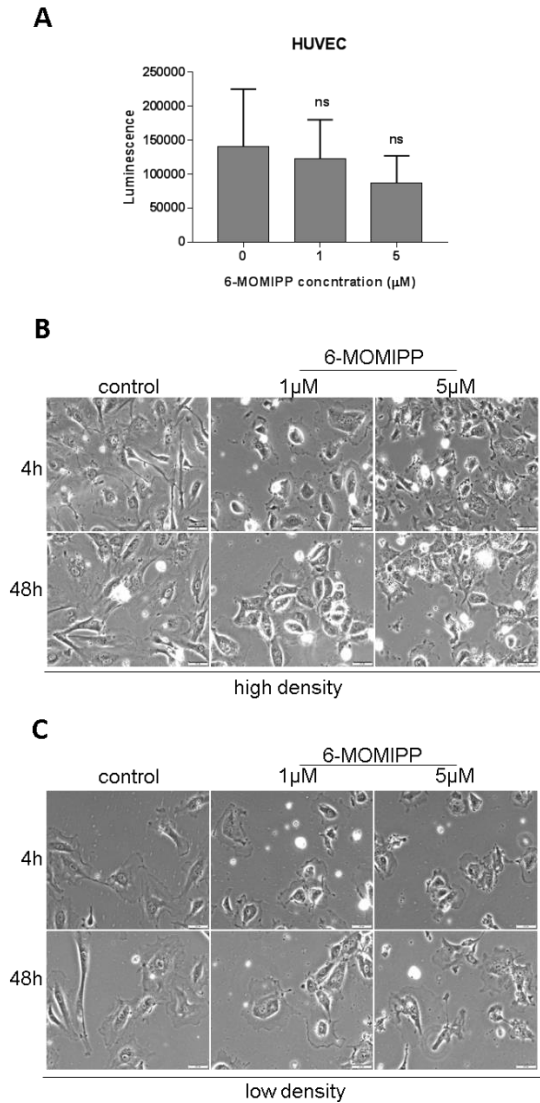
Figure 2-23. Effects of 6-MOMIPP on HUVEC cell line. A. Cells were seeded at 12,000

cells/well in 96-well plates, with four replicate wells for each condition. On the second

day, 6-MOMIPP was added at the indicated concentrations and cell viability (ATP) was

measured after 48 h. Values are the mean ± S.D. B. HUVEC cells were seeded in 35 mm

dishes at 400,000 cells/dish (B) or 100,000 cells per dish (C). On the second day after

plating, 6-MOMIPP was added at the indicated concentrations and phase contrast images were acquired after 4 h and 48 h.
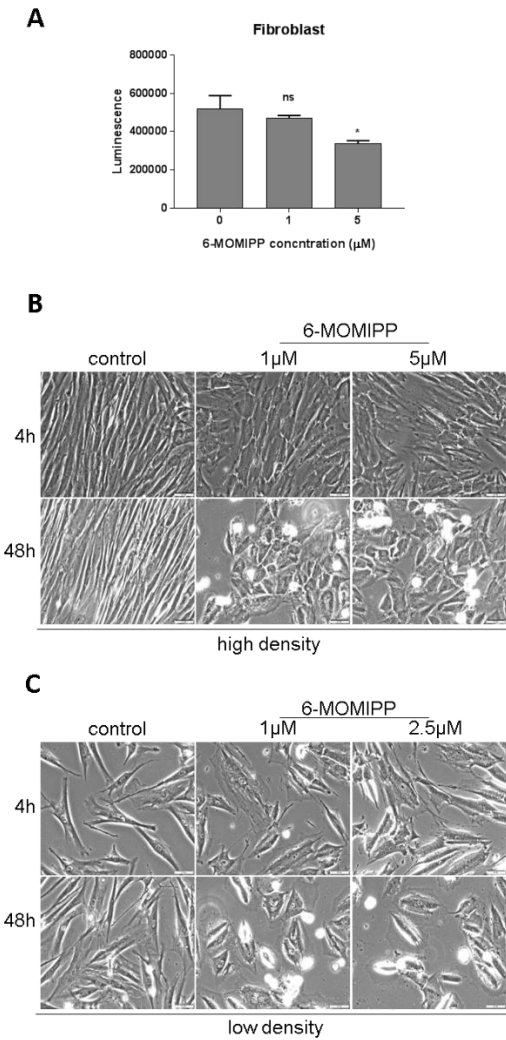
Figure 2-24. Effects of 6-MOMIPP on normal human fibroblasts. A. Cells were seeded at 12,000 cells/well in 96-well plates, with four replicate wells for each condition. On the second day after plating, 6-MOMIPP was added at the indicated concentrations and cell viability (ATP) was determined after 48 h. Values are the mean ± S.D. of four replicates. * $p < 0.05$, relative to the DMSO control. B. Fibroblasts were seeded in 35mm

dishes at 400,000 cells/dish (B) or 100,000 cells per dish (C). On the second day after plating, cells were treated with DMSO or 6-MOMIPP at indicated concentration and phase contrast images were acquired after 4 h and 48 h.

2.5 Discussion

Methuosis is a form of non-apoptotic cell death, which can be used as a new approach to treat GBM and apoptotic-resistant cancers [160, 161]. Indole-based chalcones were designed and synthesized in our laboratory to help explore the mechanism behind methuosis [158, 162, 163]. Our previous studies have established MOMIPP, our lead compound, which can effectively induce methuosis in glioblastoma and other cancer cell lines at micromolar concentrations [168]. During the SAR studies, a series of indole-chalcone derivatives with improved anti-tumor activity was developed [164]. However, biological activity studies showed that the morphology of cells treated with these new indolyl-pyridinyl-propenones (IPPs) did not resemble cells undergoing methuosis. Preliminary studies suggested that they are a group of new MTAs [164].

Based on preliminary studies evaluating the solubility and potency of this new class of IPPs, 6-MOMIPP, with a GI_{50} of 0.054 μM and IC_{50} of 0.358 μM, was selected as the lead compound to conduct detailed mechanistic studies. The results presented here demonstrate that 6-MOMIPP binds to tubulin on the colchicine binding site (Fig 2-9 and Fig 2-10) and causes depolymerization of the microtubule network in U251 glioblastoma cells (Fig 2-7 and Fig 2-8). Microtubule stabilizing agents and microtubule destabilizing agents have a similar effects on mitotic progression, involving the inhibition of microtubule dynamics. Thus, MTAs with different binding sites can act synergistically

95

as anti-tumor agents [181]. Furthermore, colchicine domain binding agents are not widely used as anti-tumor agents because of their potent toxicity [182]. Thus, 6-MOMIPP is particularly interesting as a novel colchicine domain binding molecule that could potentially be used as an anti-tumor agent. Cellular microtubule dynamics are precisely regulated to guarantee the correct division of cells. MTAs alter the dynamics of microtubules and disrupt the spindle-kinetochore attachment, interrupting cell cycle progression. Our studies reveal that 6-MOMIPP blocks U251 cells in the M phase after 24 h exposure (Fig 2-4), and the mitotic arrest is closely followed by extensive cell death (Fig 2-5). Blocking caspase activation with caspase inhibitors can partially prevent cell death induced by 6-MOMIPP (Fig 2-6), suggesting that the cell death is caspase-dependent.

Most MTA-arrested cells are actually retained in mitotic prometaphase rather than the G_2 phase [183]. Some studies have shown that preventing cells from entering mitosis by inducing G_2 arrest can significantly reduce the cytotoxicity of MTAs [184-186], suggesting that mitotic entry is a prerequisite for MTA-induced cell death. Our studies employing the Cdk1 and JNK inhibitors support this conclusion, since cells treated with those compounds were blocked at the transition from G_2 into M, and were protected from cell death (Figs. 2-13 through 2-18). We also found that by arresting U251 cells in the G_1/G_0 phase, the cytotoxicity of 6-MOMIPP was greatly reduced (Fig. 2-11, Fig. 2-12). Taken together, these observations indicate that mitotic entry is required for cell death after microtubule disruption by 6-MOMIPP.

In actively cycling cells or cells arrested in G_1/G_0, cellular insults are known to trigger apoptosis mediated by p53 and the activation of caspases [104, 187]. By comparison, the mechanisms linking G_2/M arrest with nuclear abnormalities with induction of caspase-dependent cell death are not well defined. Some studies have shown that inhibition of Cdk1 blocks apoptosis induced by taxol in MDA-MB-435 cells and MCF-7 cells [188, 189]. Knockdown of Cdk1 with siRNA, or by inhibiting its activity, increases the cell population at the G_2 phase with reduction of the M phase population [190], indicating that Cdk1 activation or mitotic entry is a prerequisite for taxol-induced apoptosis. High Cdk1/cyclin B1 activity is required for cells to stay in mitosis until all the chromosomes acquire bipolar attachment to kinetochore microtubules. MTA-induced mitotic arrest is associated with Cdk1/cyclin B1 complex upregulation, and the increase is closely matched in timing with mitotic arrest [191]. We found that exposure of U251 cells to 6-MOMIPP resulted in histone-H3 Ser-10 phosphorylation and Cdk1 downstream substrate PP1-α activation, with a timeline parallel to that of M-phase arrest (Fig. 2-13). This suggests that 6-MOMIPP triggers the Cdk1 activation and prolongs the metaphase-anaphase transition. Choi et al, proved that Cdk1 contributes to MTA-induced accumulation of prometaphase arrested cells by showing that the Cdk1 inhibitor, roscovitine, can abrogate nocodazole-induced prometaphase arrest [191]. In our study, we observed that blocking Cdk1 activation with BMS-265246 could prevent the majority of cells from undergoing cell death (Fig. 2-14), demonstrating that Cdk1 activation plays an important role in 6-MOMIPP-induced cell death. Cell cycle analysis showed that BMS-265246 did not change the percentage of cells detained at the G_2/M phase after 6-

97

MOMIPP treatment. However, cell cycle analysis distinguishes cell cycle phase based on DNA content, preventing it from delineating between populations in G_2 and M phase. Western blot results revealed that BMS-265246 diminishes Histone-H3 Ser-10 and PP1-α phosphorylation induced by 6-MOMIPP, suggesting BMS-265246 might arrest cells at G_2 phase or prometaphase, and that this could prevent cell death induced by 6-MOMIPP. In summary, 6-MOMIPP leads to the accumulation of cells in M phase and upregulates the expression of major proteins involved in mitosis progression, suggesting that cell death induced by 6-MOMIPP occurs after the prolonged metaphase-anaphase transition, which may be triggered by Cdk1.

A common feature observed in cells treated with microtubule inhibitors is an increase in Bcl-2 phosphorylation. The anti-apoptotic relative, Bcl-xL, also undergoes phosphorylation in response to microtubule disruption. We found that Bcl-xL and Bcl-2 phosphorylation occurs after 24 h exposure to 6-MOMIPP, while dephosphorylation takes place before extensive cell death occurs (Fig. 2-13). This is consistent with some studies that show Bcl-2 and Bcl-xL undergo dephosphorylation before apoptosis ensues [124, 192]. There is some evidence that abnormal accumulation of Cdk1/cyclin B1 is associated with inactivation of anti-apoptotic Bcl-2 family proteins and that this accounts for the initiation of apoptosis during mitotic arrest [135]. However, other groups suggest that Bcl-2 phosphorylation is tightly associated with mitotic arrest but is not necessarily a determinant of progression into apoptosis [124]. Our observation that Bcl-2/Bcl-xL phosphorylation decreases as the number of apoptotic cells increases after 48 h of 6-MOMIPP treatment argues against the idea that Bcl-2 phosphorylation needs to be

maintained throughout the time course of mitotic cell death. However, it is possible that transient phosphorylation of the anti-apoptotic Bcl-2/Bcl-xL triggers early changes that shift cells into an irreversible cell death cascade that continues even when the phosphorylation is reversed. We noted that the Cdk1 inhibitor, BMS-265246, could prevent phosphorylation of Bcl-2 and Bcl-xL (Fig. 2-13), signifying that Cdk1 may be responsible for the extensive phosphorylation of Bcl-2 and Bcl-xL that occurs in mitotically arrested cells. Signals generated in response to prolonged mitotic arrest are eventually transduced to the cell death machinery. Therefore, the molecular and functional correlation between mitotic arrest and cell death induced by 6-MOMIPP was studied. JNK1/2 (collectively referred to as JNK) are stress- activated kinases that can propagate pro-apoptotic signals. JNK was phosphorylated after U251 cells were exposed to 6-MOMIPP for 24 h, and cell death was attenuated by the JNK inhibitor, SP600125 (Fig. 2-16, Fig. 2-17). This demonstrates that JNK may be the primary stress signal resulting from microtubule disruption and that the cell death is mediated by JNK activation. JNK regulates the proliferation of cells largely by phosphorylation of c-Jun and activation of the AP-1 transcription complex. Our results also showed that JNK phosphorylates its downstream substrate, c-Jun, and that the JNK inhibitor could block c-Jun phosphorylation (Fig. 2-16). It has been reported that vinblastine-induced phosphorylation of Bcl-2 and Bcl-xL is mediated by JNK [137]. In our study, we found that SP600125 could block phosphorylation of Bcl-2 and Bcl-xL just as well as the Cdk1 inhibitor. There are several possible interpretations of this observation. One possibility is that both Cdk1 and JNK contribute to the phosphorylation of Bcl-2 proteins. This

seems unlikely, since there is essentially no residual phosphorylation when either inhibitor is used. A second possibility is that inhibitors used in this study are not entirely specific. BMS-265246 and roscovitine have been reported to have high specificity for Cdks [193, 194], but some non-specific inhibition of kinases other than JNK has been reported with SP600125 [195]. Finally, the effect of SP600125 may not reflect direct inhibition of JNK-mediated phosphorylation of Bcl-2/Bcl-xL, but rather, the inhibition of G2 → M transition [196], so that the active Cdk1/cyclin B complex does not form and is therefore unable to phosphorylate Bcl-2/Bcl-xL.

The current working model summarizing the effects of 6-MOMIPP on glioblastoma cells is depicted in Fig. 2-25.

To further evaluate the efficacy of 6-MOMIPP as an anti-tumor agent and to identify which tumors are most likely to respond to these agents, cytotoxic analysis of 6-MOMIPP against 19 cancer cell lines and 3 non-malignant cell lines was performed. ATP assays revealed that 6-MOMIPP displays a broad-spectrum anti-tumor activity in multiple cancer cell lines, including glioblastoma, melanoma, and lung cancer. However, there were significant differences in sensitivity observed among the various cell lines. The basis for the differential sensitivity will be an important topic for future study. Possibilities include variations in cell doubling times, tubulin isoform expression, or apoptotic signaling pathways. Toxicity of 6-MOMIPP was substantially reduced in quiescent human fibroblasts, HUVEC, and differentiated rat neuronal progenitor cells. These findings indicate that 6-MOMIPP merits further evaluation as an anti-tumor agent for treatment of primary and secondary brain tumors.
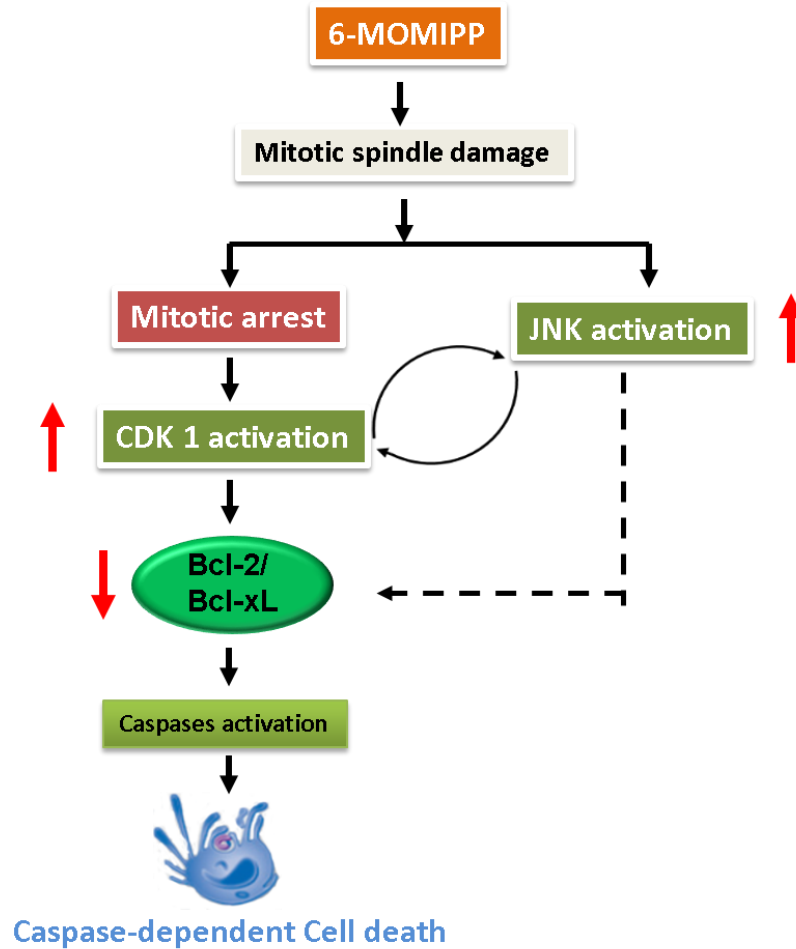
Figure 2-25. A working model of 6-MOMIPP-induced cell death. 6-MOMIPP binds to tubulin on colchicine binding site and causes destabilizes the microtubule network in cells. Depolymerization of spindle microtubules triggers the spindle assembly checkpoint (SAC) resulting in sustained activity of Cdk1 and phosphorylation (inactivation) of anti-apoptotic Bcl-2 family members, ultimately leading to activation of caspases and cell death. JNK is also activated when cells are treated with 6-MOMIPP, but it is not clear whether it is involved in directly phosphorylating Bcl-2/Bcl-xL or in promoting G2 → M transition to allow activation of Cdk1.

Chapter 3

In vivo Evaluation of 6-MOMIPP as a Brain Cancer Therapy

3.1 Abstract

Although microtubule targeting agents (MTAs), such as *Vinca* alkaloids and taxanes, are widely used as anti-neoplastic agents, they have shown little efficacy in treating primary and metastatic brain tumors, partly due to their limited penetrance of the blood-brain barrier (BBB). Pharmacokinetic studies of a new MTA, termed 6-MOMIPP, showed that administration of a single 20 mg/kg dose via i.p. injection in mice, resulted in brain concentrations above 0.5 μM for 8 h, closely approximating plasma concentrations of the compound. This suggests that 6-MOMIPP readily cross the BBB and can reach a tissue concentration that was previously shown to be effective in killing glioblastoma, melanoma, and lung carcinoma cells *in vitro* (Chapter 2). Evaluation of 6-MOMIPP in mouse glioblastoma xenograft models showed 6-MOMIPP treatment significantly inhibits the growth rate of both subcutaneous and intracranial tumors without notable general toxicity. These studies provide evidence that 6-MOMIPP could serve as a

prototype for a new generation of MTAs that may be useful in treating primary and metastatic brain tumors.

3.2 Introduction

Glioblastoma multiforme is among the most devastating types of human brain cancer, with only 15 months average survival after diagnosis [7]. Therapeutic approaches that can prolong survival with minimal side effects are desperately needed. MTAs are among the most successful chemotherapeutic agents for many cancers. However, due to low bioavailability, poor solubility, and limited penetrance of the BBB, toxicity of these compounds (e.g. myelosuppression, neurotoxicity [58]) can be dose-limiting when trying to use them for brain tumor therapy. Acquired drug resistance [59-61] is another factor that limits the efficacy of current MTAs for some cancers. For all of these reasons, there is considerable interest in developing new generations of MTAs.

The colchicine binding site is one of the important pockets for potential tubulin depolymerization compounds. However, among the different types of anti-tubulin agents, colchicine itself has not been widely used to treat cancer despite its potency in killing cancer cells. Colchicine is used to treat familial Mediterranean fever and acute gout, but clinical cancer treatment was hampered due to its significant toxicity. Similarly, the use of ZD6126 and nocodazole for cancer treatment was terminated due to the development of various side effects in patients [197]. Newer colchicine domain binding drugs, such as the combretastatin-A4 analogs, ombrabulin, and phenstatin, have been used as anti-angiogenesis agents [198] and have shown promising anti-tumor activity

[56, 199, 200]. However, these compounds remain to be fully evaluated in clinical trials.

Chapter 2 described our work leading to the identification of a group of novel MTAs that bind to the colchicine domain on tubulin and induce mitotic arrest and cell death in glioblastoma and other cancer cells at micromolar concentrations *in vitro*. However, there are fundamental differences between cultured cells and whole organisms when it comes to the administration and pharmacokinetics of drugs. Thus, in this chapter, studies aimed at evaluating the pharmacokinetic (PK) properties and anti-tumor efficacy of our lead compound, 6-MOMIPP, in mice were described. The results demonstrate that 6-MOMIPP crosses the BBB efficiently and has significant inhibitory effects on the growth of subcutaneous and intracranial glioblastoma xenografts.

3.3 Materials and methods

3.3.1   Cell line

U251 human glioblastoma cells were transfected with a pCMV5-Neo-pGL3 vector and selected in medium containing G418 to generate a stable cell line that expresses firefly luciferase. The resulting cell line, termed, U251-LUC, was maintained in DMEM supplemented with 10% (v/v) fetal bovine serum (FBS) and 200 µg/ml G418 at 37 °C with 5% CO_2/95% air.

3.3.2   Chemicals

6-MOMIPP was synthesized by Dr. Christopher Trabbic as described previously [168] and stored at -20^0C as a 2 mg/ml stock in NSP vehicle, which is comprised of 7.5% n-methyl-2-pyrrolidone (NMP, Sigma Cat. No. 328634), 15% Solutol HS15 (Sigma Cat.

No. 42966) and 77.5% phosphate-buffered saline (PBS). The other two vehicles that were tested in PK studies were, MTD (2% methylcellulose, 0.2% Tween 80, and 0.2% DMSO) and NSP300 (5% NMP, 15% Solutol HS15, and 80% polyethyleneglycol (PEG) 300 (Spectrum Chemicals Cat. No. PO108). For assay of drug levels, tissues were homogenized in RIPA buffer (50 mM Tris, 150 mM NaCl, 1% NP40, 0.5% sodium deoxycholate, 1% SDS, pH 7.5). Matrigel was purchased from Corning Life Science (Cat. No. 356230) and kept on ice during the subcutaneous tumor implantation. XenoLight D-Luciferin (K+ salt) Bioluminescent Substrate was purchased from Perkin Elmer (Cat. No. 122799) and stored at -20^0C as a 15 mg/ml stock in deionized water. Surgical glue (Cat. No.NC0621124), MD bone wax (Cat. No. 50-854-876), and Vet Ointment (Cat. No. NC0138063) were obtained from Fisher Scientific. Buprenorphine (Cat. No. 059122), Xylazine (Cat. No. 033198) and Ketamine were purchased from Henry Schein.

3.3.3 Pharmacokinetic study of 6-MOMIPP

Swiss Webster mice (8-10 weeks, female) were purchased from Charles River Laboratories and housed in ventilated cages on a 12 h light-dark cycle. 6-MOMIPP was formulated in MTD or NSP300 was administered to the mice at a dose of 20 mg/kg by P.O. using gavage. 6-MOMIPP was formulated in NSP and administered to mice via I.P. injection at a dose of 20 mg/kg. Mice in control groups received an equivalent volume of vehicle in the same manner. Mice were euthanized and blood, brain, and liver were harvested at intervals of 30 min, 1 h, 2 h, 4 h or 8 h after drug administration. Blood was collected by cardiac puncture, stored on ice in EDTA-coated collection tubes

(Fisher, Cat.No.365794), and centrifuged at 10,000g for 20 min to obtain plasma. Thereafter, plasma was stored at -80^{0}C until analysis. Brain and liver were snap-frozen in liquid nitrogen and stored at -80°C until analysis. Frozen tissue was weighed and added to RIPA buffer (1:9 dilution) for homogenization. For tissue samples, the 6-MOMIPP levels were expressed as nmol/kg tissue.

To determine the level of 6-MOMIPP, plasma (200 µl) or tissue homogenate (500 µl) were extracted with ethyl acetate (1000 µl) by incubating at 37°C for 20 min followed by centrifugation for 2 mins at 16,000 x g. The 800 µl of supernatant, which contains 6-MOMIPP, was vacuum centrifuged at 30°C for 1 h followed by suspending in 30 µl acetonitrile plus 70 µl water containing 0.1% formic acid. Thereafter, the mixture was centrifuged and the supernatant was transferred to autosampler vials and stored at 4°C until LC-MS analysis. Liquid chromatography (LC) separations were performed by Dr. Jeff Sarver on a Waters 2795 HT-Alliance LC Separations Module with a 10 µl sample injection onto a Waters Ascentis Express C18 column (75 x 21 mm, 2.7 µm) with matching guard column. An isocratic elution method was used with a flow rate of 0.3 ml/min of 70% water containing 0.1% formic acid and 30% acetonitrile. MOMIPP and three metabolites (not discussed elsewhere in this document) were detected via multiple reaction monitoring (MRM) on a Micromass Quattro Micro Mass Spectrometer (MS) in ESI+ mode with capillary voltage 3.0 kV, source temperature 100°C, desolvation temperature 400°C, desolvation gas flow 650 L/hr, cone gas flow 40 L/hr, and dwell time 0.2 sec. MOMIPP was detected as 293.1 > 95.9 at cone voltage 40V, collision energy 23V, and at a column retention time of 2.1 min. While not discussed elsewhere in this

document, three metabolites formed by the reduction of the α,β-unsaturated chalcone bridge can also be detected using this same method with a cone voltage of 30V and collision energy of 23V as follows: Metabolite M2A (reduced at the carbon-oxygen double-bond) was detected as 295.1 > 174.1 at a retention time of 1.0 min, Metabolite M2B (reduced at the carbon-carbon double-bond) as 295.1 > 122.0 at a retention of 3.7 min, and Metabolite M1 (reduced at both the carbon-carbon and carbon-oxygen double-bond) as 297.1 > 174.1 at 0.9 min retention. Nitrogen gas is used as the carrier gas through the mass spectrometer, while Argon gas is used in the collision chamber. All animal protocols were reviewed and approved by the University of Toledo Institutional Animal Care and Use Committee.

3.3.4 *In vivo* subcutaneous tumor xenograft study

CrTac: NCR-Foxn1<nu> mice (female, 7-10 Weeks) were purchased from Taconic Biosciences, Inc. and housed in ventilated cages on a 12 h light-dark cycle. Each mouse was inoculated subcutaneously in the right flank with 5,000,000 (10,000,000 for the second study) U251-LUC cells in 100 μl DMEM/Matrigel (1:1) using a 27 g needle. When the tumors were palpable and detectable by bioluminescence imaging (4 to 5 d), mice were sorted randomly into control and treatment groups. 6-MOMIPP was administered in NSP vehicle at a dose of 20 mg/kg via I.P. injection every 12 h for 15 consecutive days and control mice received injections of an equivalent volume of vehicle. Tumor growth was assessed on the indicated days by bioluminescence imaging with an IVIS Spectrum System (PerkinElmer). Mice were injected with 200 μl of 15 mg/ml Luciferin solution 15 min before imaging. After 15 days (14 days for the second

study) of treatment, all mice were euthanized and tumors were weighed and fixed in 10% neutral buffered formalin for 24 h (20:1, formalin to tissue). Finally, the tumors were transferred to 70% ethanol and processed for histology. All animal protocols were reviewed and approved by University of Toledo Institutional Animal Care and Use Committee.

3.3.5 *In vivo* intracranial tumor xenograft study

The intracranial xenograft tumor model was established based on the method described previously [201]. CrTac: NCR-Foxn1<nu> mice (female, 7-10 Weeks) were purchased from Taconic Biosciences, Inc. and housed in ventilated cages on a 12 h light-dark cycle. Anesthesia of mice was achieved by I.P. injection of 80 mg/kg ketamine and 5 mg/kg xylazine mixture. Thereafter, each mouse received 0.06 mg/kg buprenorphine through S.C. injection. Before surgery, the skin on top of the head was scrubbed with 10% povidone-iodine topical solutions followed by 70% alcohol. A 1 cm incision was made down the midline of the scalp and a small hole was drilled in the skull using a 25 g needle at a point 1 mm anterior and 2 mm lateral to the bregma. 400,000 cells (suspended in 3 µl of DMEM medium) were drawn into a sterile 10 microliter Hamilton syringe with a plastic cuff placed 3 mm from the tip of the 27 g needle. After injection of 3 µl cell suspension, the hole in the skull was sealed with sterile bone wax and the skin incision was closed with surgical glue. 0.06 mg/kg buprenorphine was given to mice via S.C. injection on the day after surgery. Tumor growth was monitored by bioluminescence imaging, as described in the previous section. By the fifth day all of the mice had tumors that emitted 10^7 - 10^8 photons. Mice bearing tumors were grouped randomly into control

and treatment groups and treatment with 6-MOMIPP (20 mg/kg) or vehicle started, with I.P. injections administered every 12 h for 12 consecutive days. Tumor growth was monitored by IVIS imaging on the indicated days, starting from the first day of treatment as day 1. After 12 days, the control and 6-MOMIPP-treated mice were euthanized and the brains fixed in 10% neutral buffered formalin for 24 h and processed for histology. At the same time, blood was collected by the cardiac puncture, stored in lithium heparin-coated collection tubes (Fisher, Cat.No.0265729), and centrifuged at 10,000g for 20 min for plasma isolation. The plasma samples were stored at -80^0C until they were used for toxicity screens.

3.3.6   H&E staining and immunohistochemistry

Fixed and dehydrated subcutaneous tumors were embedded in paraffin and serial sections were prepared. Three 5 µm sections were mounted on each slide and stained with hematoxylin and eosin (H&E). The histology procedures were carried out by Allen Schroering in the UT Microscopy and Imaging Core Facility.

To assess apoptosis in tumor xenografts, immunohistochemistry was carried out to detect active caspase 3. Unstained sections were deparaffinized with xylene for 5 min, followed by sequential rehydration with double-distilled water. Sections were then subjected to heat-induced antigen retrieval by boiling in Tris-EDTA buffer for 20 min. Thereafter, the samples were incubated with 10% FBS for 2 h followed by overnight incubation with a primary antibody that specifically detects the large fragment (17/19 kD) of activated caspase-3 (Cell Signaling Technology, Cat. No. 9661S) in 10% FBS in TBS (50mM Tris Base, 0.9% NaCl, PH 7.6) at 4^0C. On the second day, samples were

incubated with 3% H_2O_2 in TBS for 15 min followed by 1 h incubation with biotinylated goat anti-rabbit IgG secondary antibody (Vector. Cat. No. BA-1000). Slides were developed by incubation with Sigmafast 3, 3'-Diaminobenzidine (Cat. No. D4293), mounted and analyzed with a Cytation 5 image reader (BioTek).

Fixed brains bearing intracerebral tumors were embedded in paraffin and serial coronal sections were prepared, moving anterior to posterior in 100 µm steps. At each step three 5 µm sections were mounted and stained with H & E. Central regions of the tumors were identified and images were obtained with an Olympus Virtual Slide Microscope VS120. CellSense software was used to draw contours around the tumor to determine the tumor area. For each brain the areas were determined for four separate sections in the central part of the tumor and the values were averaged.

3.3.7 Blood tests to assess potential toxicity of 6-MOMIPP

Plasma samples obtained from control and 6-MOMIPP-treated mice at the time of euthanasia were analyzed to determine alanine aminotransferase (ALT), albumin (ALB), alkaline phosphatase (ALP), amylase (AMY), total calcium (Ca^{++}), globulin (GLOB), glucose (GLU), phosphorus (PHOS), sodium (Na^+), total protein (TP), and blood urea nitrogen (BUN) using a comprehensive diagnostic profile kit (Abaxis, Cat. No. 500003824) using a VetScan VS2 Analyzer (Abaxis), following standard procedures detailed in the manufacturer's instructions.

3.3.8 Statistical analysis

GraphPad Prism 7 was used for statistical analysis. Data are presented as the means ± S.D., and statistical significance of end-point differences between control and treated groups was determined using a Student's unpaired t-test.

3.4 Results

3.4.1 Tissue distribution and pharmacokinetic properties of 6-MOMIPP

To assess the *in vivo* PK properties of 6-MOMIPP and evaluate its ability to penetrate the BBB, 6-MOMIPP was formulated in three different solvents, MTD, NSP300, and NSP, and administered to mice via P.O. or I.P. at a dose of 20 mg/kg. Quantification of 6-MOMIPP by LC-MS showed that plasma concentrations were below 1 µM after a single oral dose in MTD or NSP300 (Fig 3-1A and B). Consistent with the PK behavior of many drugs, liver concentrations of the 6-MOMIPP were substantially higher than the plasma levels at all time points. In accord with the low circulating drug levels, the concentration of 6-MOMIPP in the brain was at or below 0.1 µM following oral dosing (Fig. 3-1 A and B). Based on results obtained with cultured cells in Chapter 2, this would not be expected to be a therapeutic concentration. Therefore, we next tried administering 6-MOMIPP via I.P. injection using the NSP formulation. The results showed that a 20 mg/kg injection yielded a plasma concentration above 10 µM after 30 min. The plasma concentration gradually dropped over 8 h, but remained above the 0.5 µM threshold previously shown to cause mitotic arrest and cell death in culture U251 cells (Fig. 3-1 C). Of particular note, the concentration of 6-MOMIPP in the brain mirrored the concentration in the plasma throughout the time-course. This suggested that 6-MOMIPP is able to cross the BBB freely and reach a potential therapeutic concentration (≥0.5 µM)

111

for at least 8 h after a single I.P. injection. Observation of the behavior of the mice during the period of the PK study did not reveal any behavioral changes indicative of acute toxicity.
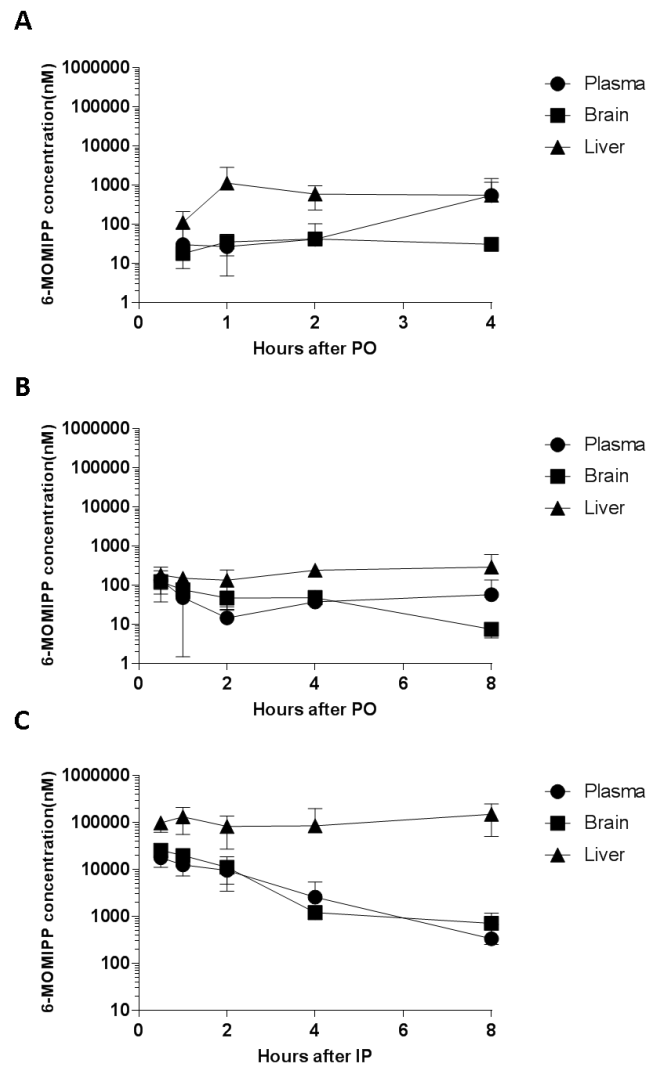

Figure 3-1. PK studies with 6-MOMIPP in mice. A and B. Mice received a single 20 mg/kg dose of 6-MOMIPP that was formulated in MTD (A) or NSP300 (B) by P.O.

112

administration. Blood, brain, and liver were harvested from the mice at the indicated time points after drug administration. Each point represents mean ± S.D. of values derived from 3 mice. C. Mice received a single 20 mg/kg of 6-MOMIPP formulated in NSP by I.P injection and tissues were harvested at the indicated time points. 6-MOMIPP concentration was determined as described in the Methods. Each value represents the mean ± S.D. derived from 6 mice.

3.4.2   Anti-tumor activity of 6-MOMIPP in subcutaneous xenograft model

To determine if 6-MOMIPP affects glioblastoma growth *in vivo*, a subcutaneous xenograft mouse model was used to assess the anti-tumor activity of 6-MOMIPP. U251-LUC cells were subcutaneously implanted into immune compromised mice and allowed to grow for 4 days. Thereafter, mice were treated twice daily with 20 mg/kg 6-MOMIPP via I.P. injection for 15 days. 6-MOMIPP was well tolerated, with no signs of systemic or local toxicity in the treated animals. Body weight of mice in the drug treatment group did not decrease during the experiment (Appendix B Fig. 1). Tumor growth was monitored by bioluminescence imaging system and the result showed that 6-MOMIPP significantly decreased tumor growth, as measured by luminescence intensity ($p < 0.01$) (Fig. 3-2) and tumor weight ($p < 0.01$) (Fig. 3-3). The study was repeated a second time, with consistent results (Fig. 3-4, Fig. 3-5 and Appendix B, Fig. 2). H&E staining shows that the tumors from the vehicle-treated control mice contained abundant, densely packed cells with predominant euchromatic nuclei and abundant mitotic figures. The cells were mostly negative when stained for active caspase 3 (Fig. 3-6A). In contrast, the tumors from the 6-MOMIPP-treated mice contained large areas of fluid and necrosis,

surrounded by cells with pyknotic nuclei (Fig. 3-6B). Areas that stained positively for active caspase-3 were readily detected by immunohistochemistry, consistent with massive cellular death in the treated tumors. (Fig. 3-6B).

A

B
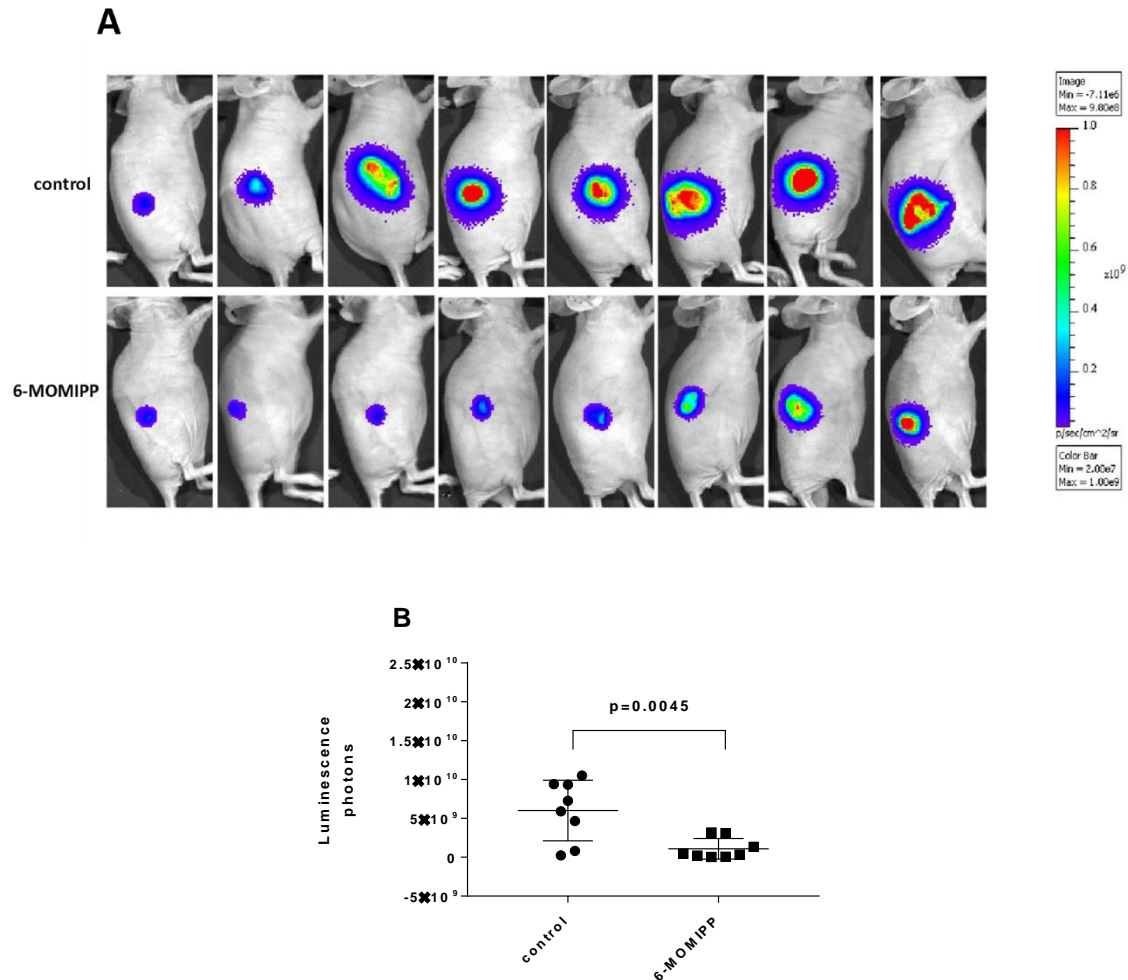
Figure 3-2. 6-MOMIPP inhibits tumor growth in subcutaneous human glioblastoma xenografts in nude mice.

A. Mice were subcutaneously implanted with 5×10^6 U251-LUC cells. After tumors were established (4 days), treatment with 6-MOMIPP commenced (I.P. 20 mg/kg, every 12 hours for 15 days). Control mice received an equivalent volume of NSP vehicle. The

picture shows the results of bioluminescence imaging of the mice after the 15 days of treatment. B. The graph represents mean ± S.D. of the day-15 luminescence signals from the control and treated mice (n=8 for each group).
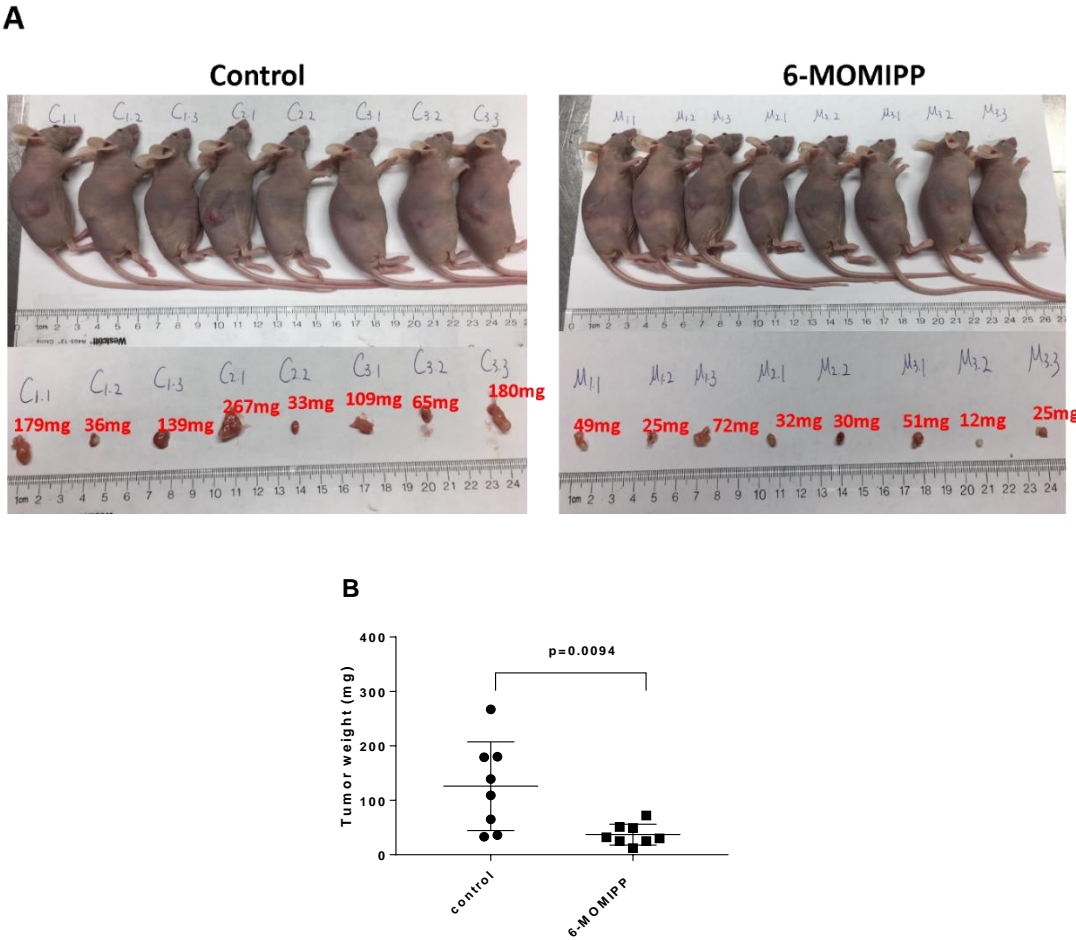
Figure 3-3. 6-MOMIPP reduces tumor weight in subcutaneous xenograft mice.

Immunocompromised mice bearing subcutaneous U251-LUC tumors were treated with 20 mg/kg 6-MOMIPP every 12 hours for 15 days by I.P. injection and the control group received same volume of vehicle. After bioluminescence imaging on day-15 (see Fig. 3-2) the mice were euthanized and tumor wet weight was measured. Panel A shows the

115

gross appearance of the mice and the excised tumors. Panel B depicts the mean ± S.D.

of the tumor weights in the control and 6-MOMIPP treated groups (n=8 for each group).
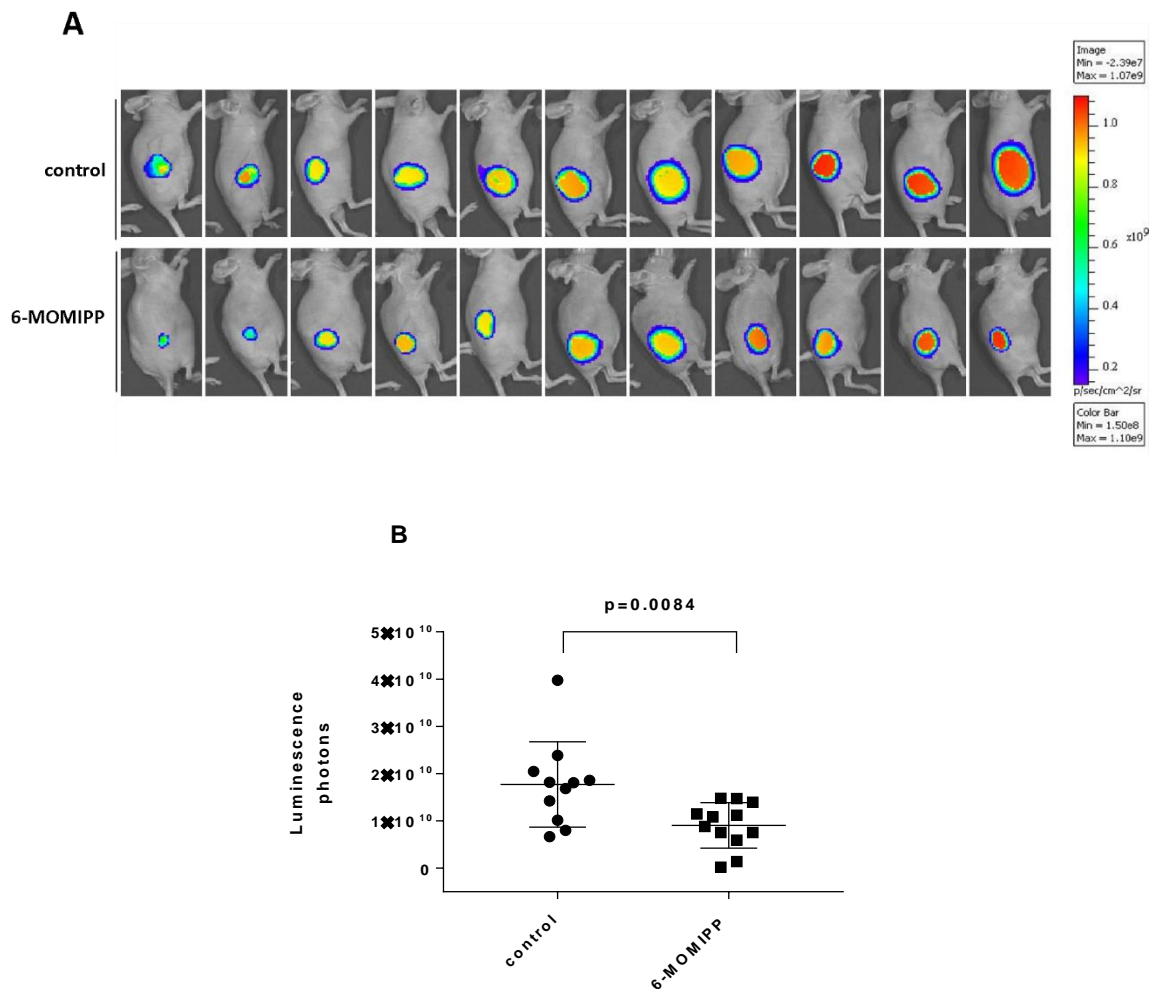
Figure 3-4. 6-MOMIPP inhibits the growth of subcutaneous glioblastoma xenografts in

nude mice. This was a replication of the study described in Fig. 3-2 A&B, with the

following minor modifications: Tumors were initiated with 10^7 cells instead of 5×10^6

cells. Eleven mice were included in the control and treatment groups, instead of eight.

The study was concluded after 14 days of treatment, instead of 15 days.

Figure 3-5. 6-MOMIPP reduces tumor weight in subcutaneous xenograft mice.

The results are from the experiment described in Fig. 3-4. Panel A shows the gross appearance of the mice and the excised tumors. Panel B depicts the mean ± S.D. of the tumor weights in the control and 6-MOMIPP treated groups (n = 11 for each group).
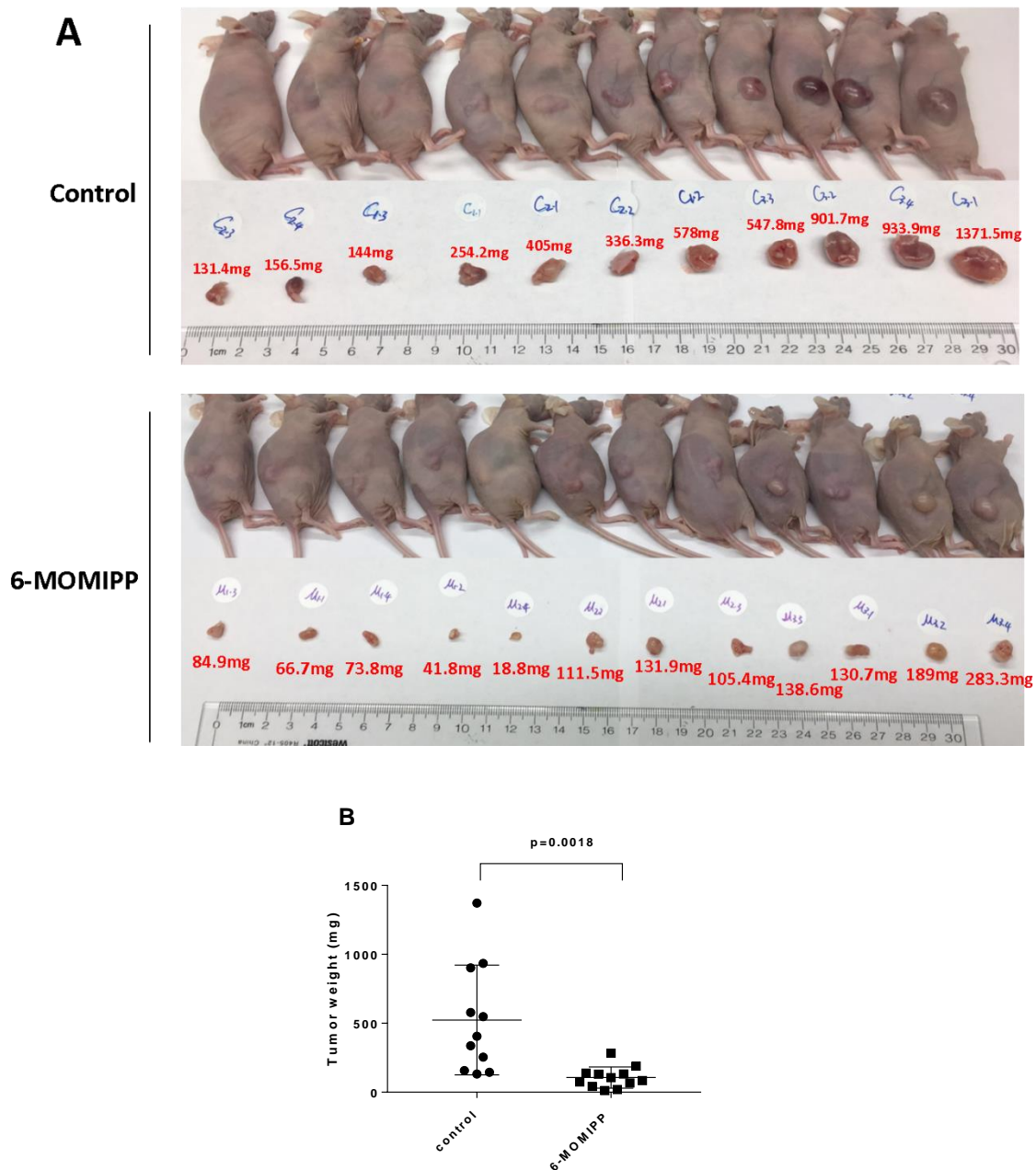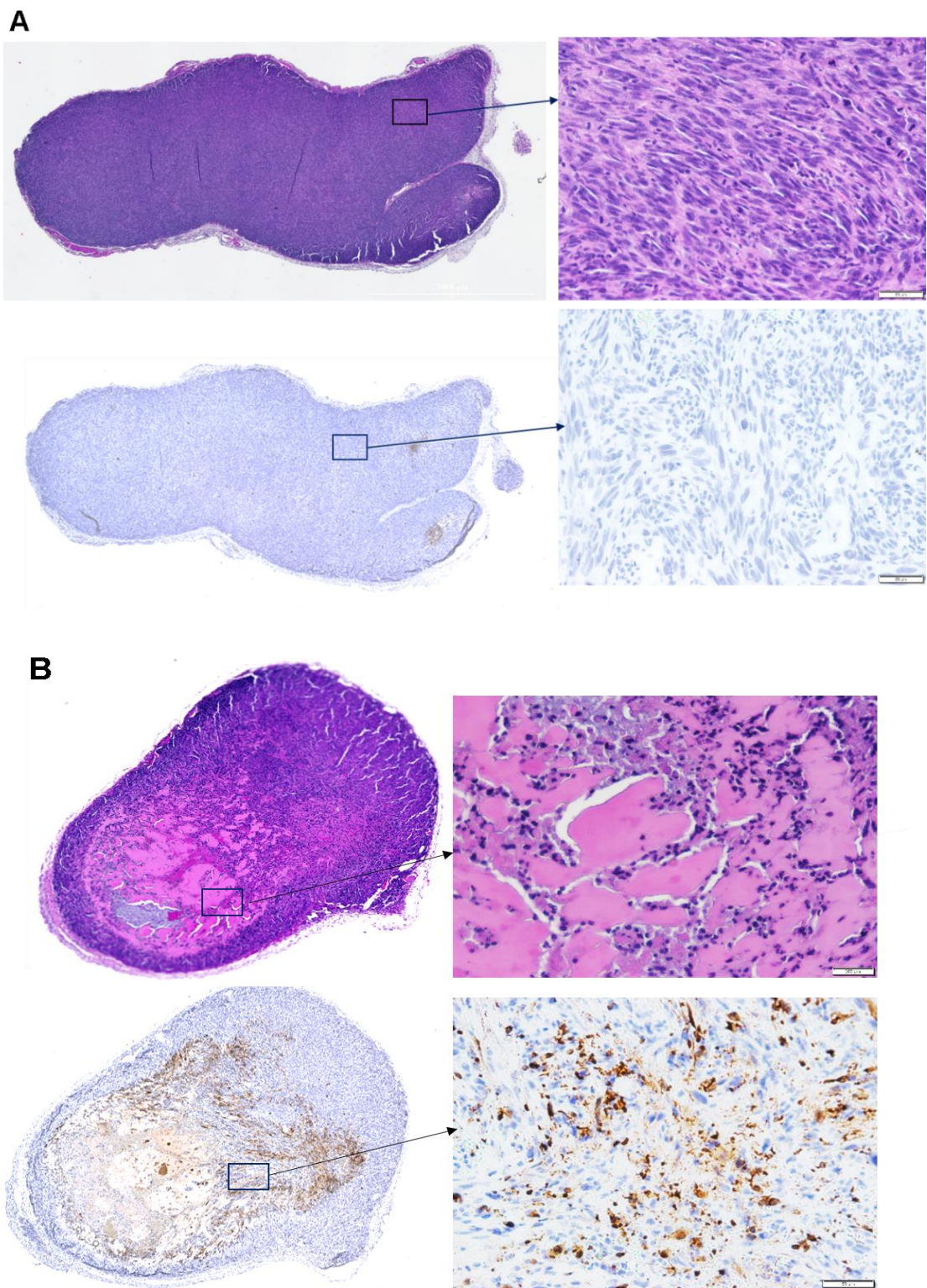
Figure 3-6. H&E staining of subcutaneous tumors. Subcutaneous tumors derived from the experiment described in Figures 3-2 and 3-3 were stained with H&E (upper panels) or antibody to detect activated caspase-3 by peroxidase staining (lower panel). A. Control tumor (C3.3). B. 6-MOMIPP-treated tumor (M2.2)

3.4.3 Anti-tumor activity of 6-MOMIPP in an intracranial xenograft model

Having shown that 6-MOMIPP can inhibit subcutaneous tumor growth and can readily cross the BBB, the next logical step was to determine if 6-MOMIPP can inhibit brain tumor progression. Immunocompromised mice bearing intracranial U251-LUC glioblastoma implants were treated with 20 mg/kg 6-MOMIPP every 12 hours via I.P. administration beginning 5 days after tumor implantation. By 12 days following the start of drug treatment, all animals were euthanized due to morbidity in control group. Within the 12 days of drug treatment, 6-MOMIPP was well tolerated, with no signs of systemic or local toxicity, and no detectable weight loss during the first 9 days of drug treatment, as shown in Appendix B Fig. 3. With brain tumor progression, control mice exhibited significant weight loss between day 10 and day 12, and the 6-MOMIPP-treated group also showed weight loss, but less than the control. Tumor growth was monitored by bioluminescence imaging. As shown in Fig. 3-7, the bioluminescence signals indicated that 6-MOMIPP caused a significant reduction in tumor growth compared to the control group after 12 days of treatment.

Analysis of blood samples collected at the end of the study indicated that the 12-day treatment with 6-MOMIPP did not cause major toxicity in the mice. No significant changes were observed in alanine aminotransferase (ALT), blood urea nitrogen (BUN),

total calcium (Ca^{++}), glucose (GLU), and total protein (TP) levels in plasma (Fig. 3-8). There were small decreases in albumin (ALB), phosphorus (PHOS), and amylase (AMY) and a slight increase in globulin (GLOB).

The only parameter that was substantially altered was alkaline phosphatase (ALP), which was decreased by about 80% in the 6-MOMIPP treated mice. No obvious gross pathologic changes were observed upon visual examination of organs and tissues including heart, lung, kidney, spleen, small and large intestine, liver.

Fixed brains bearing intracerebral tumors were sectioned and stained with H & E. Fig. 3-9A shows size of the tumors area obtained by CellSense software were significantly smaller in 6-MOMIPP treated mice compare to control group.
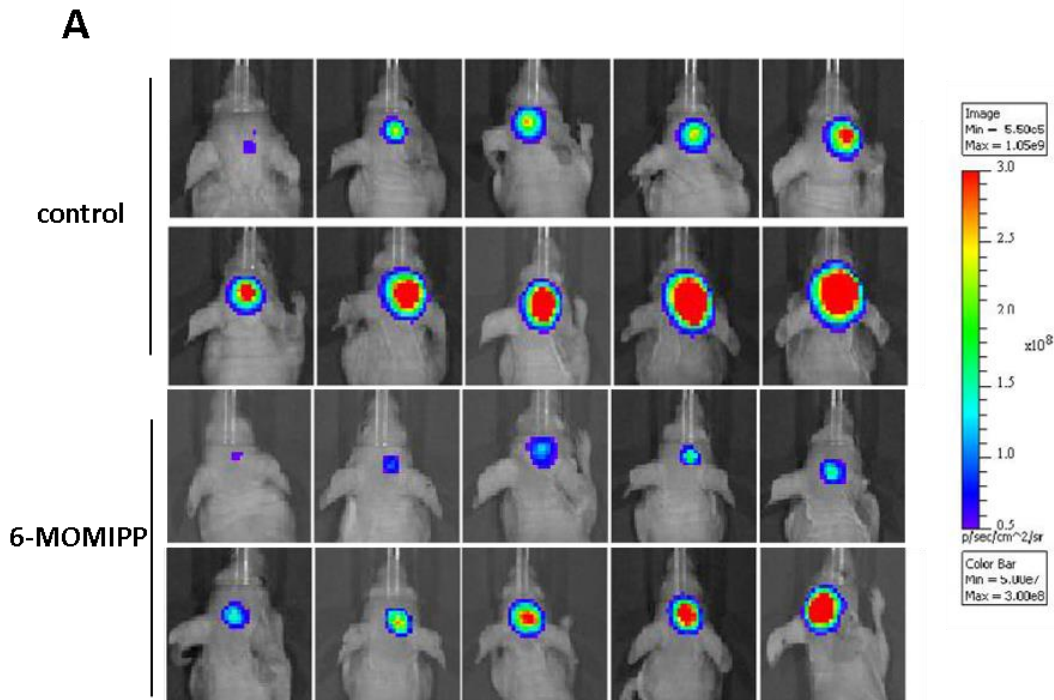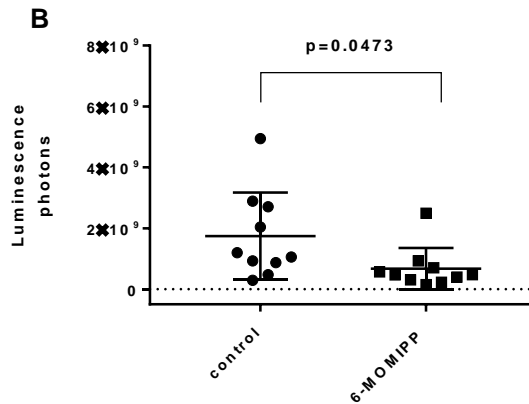
Figure 3-7. 6-MOMIPP inhibits growth of intracranial glioblastoma xenografts in mice.

Immunocompromised mice received intracranial implants of U251-LUC as described in the Methods. After 4 days treatment was initiated with 6-MOMIPP (20 mg/kg, I.P., every 12 h) and continued for 12 d. Panel A shows the individual bioluminescence images captured just prior to euthanasia of the mice on day-12 of treatment. The quantitative results (photons) are graphed in panel B, with the mean $\pm$ S.D. derived from 10 mice in each group.

A

Control   6-MOMIPP

B
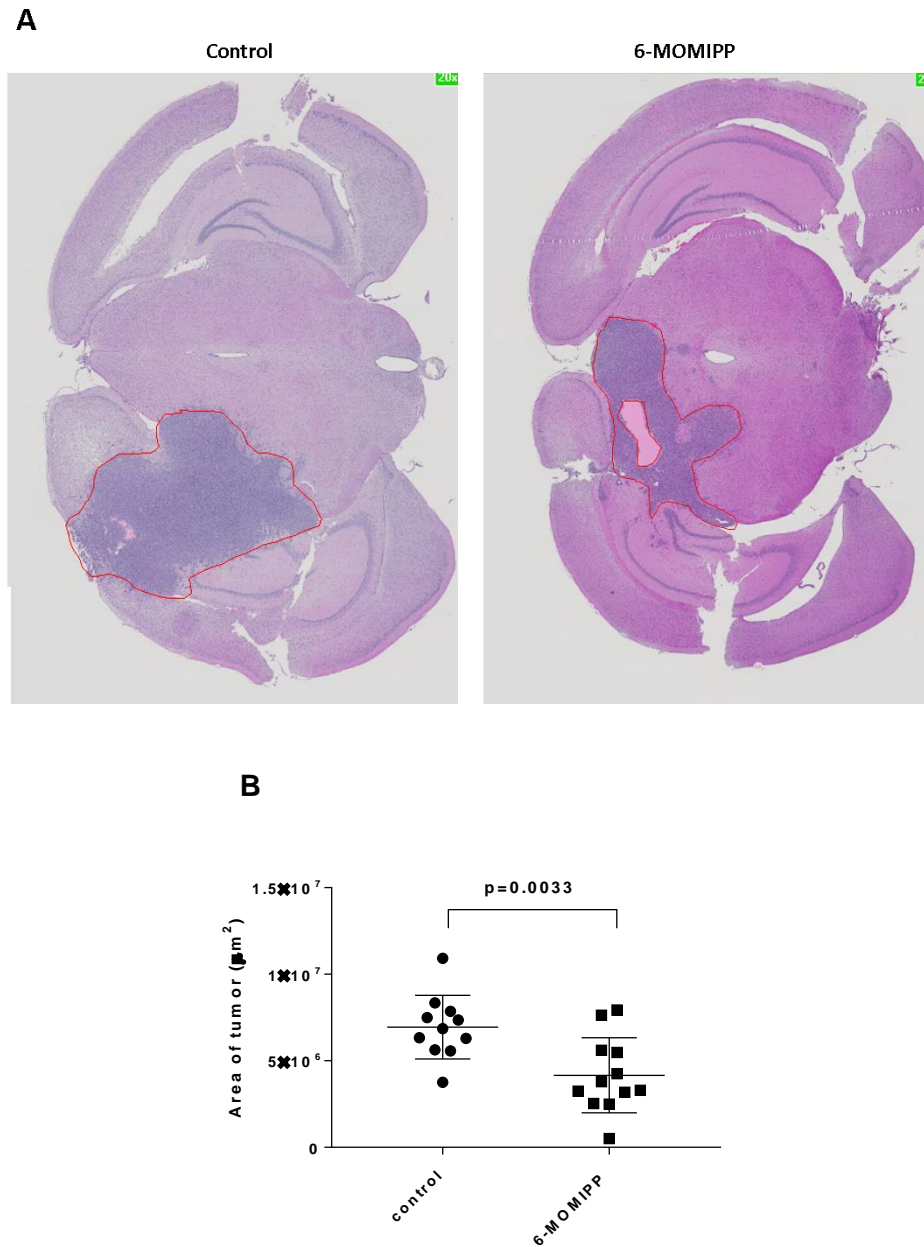
Figure 3-8. 6-MOMIPP reduces the size of intracranial glioblastoma xenografts in

mice. The brains from the mice described in Fig. 3-7 were processed for histology.

Central tumor regions of the brain tumors in each mouse were identified in serial

coronal sections stained with H&E and tumor areas were calculated as described in the

Methods. The graph shows mean ± S.D. calculated for the 10 control and 10 treated
mice.
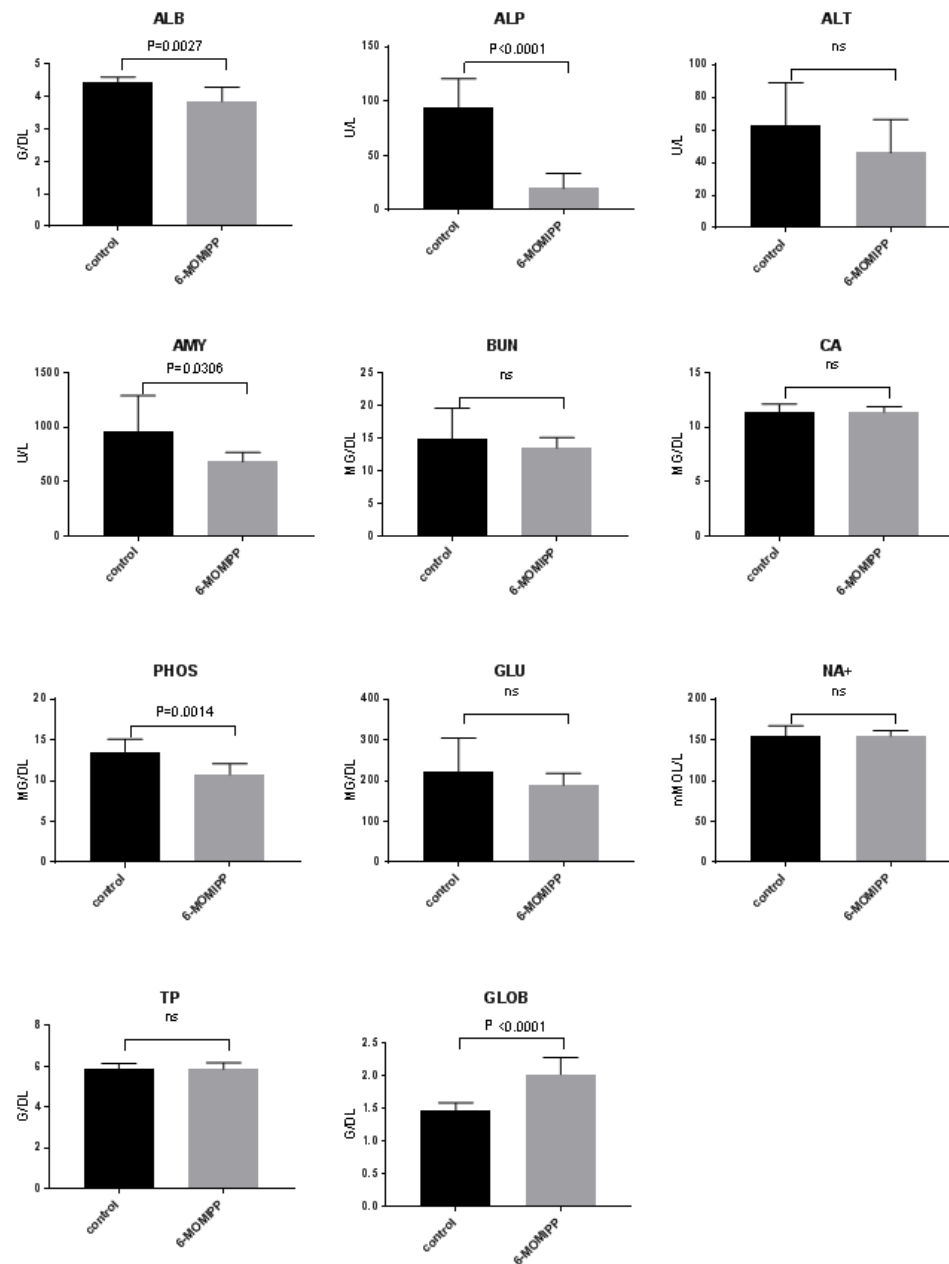
Figure 3-9. Blood chemistry profiles obtained after 12 days of treatment with 6-
MOMIPP or vehicle.

At the time of euthanasia, blood was collected from 8 control and 8 treated mice in the study described in Fig. 3-7. Plasma samples were analyzed using a VetScan VS2 instrument as indicated in the Methods. Each graph depicts the mean ± S.D. and significant differences are between control and treated groups are noted above each graph. All control values were within the normal range for NCR-Foxn1 female nude mice.

3.5 Discussion

In studies presented in Chapter 2, I described a group of novel indole-based chalcones with microtubule-depolymerization activity. The lead compound, 6-MOMIPP, causes mitotic arrest and cell death in a broad spectrum of cancer cell lines, with comparatively low toxicity in normal cell lines. In this chapter, the *in vivo* anti-tumor activity of 6-MOMIPP was evaluated. Pharmacokinetic studies using three different formulations and two different routes of administration (P.O. and I.P.) indicated that a single I.P. injection of 6-MOMIPP (formulated in NSP) could produce optimal sustained concentrations above 0.5 µM in the plasma for at least 8 h. Concentrations above 0.5 µM were optimal for microtubule disruption, mitotic arrest and cell death *in vitro* (see Chapter 2). Since the concentration of 6-MOMIPP in the brain mirrored the concentration in plasma, the results suggested that 6-MOMIPP freely cross the BBB. The BBB is composed of endothelial and neuron cells, which function as a physical and enzymatic barrier at the brain-blood interface to regulate the entry of molecules into the CNS [202]. Common

anti-cancer drugs have limitations in treating GBM and brain metastasis due to the poor distribution caused by BBB [203]. Thus, during new drug development for brain cancer, the ability of drug to cross the BBB is important. The results of our PK studies provided a strong rationale for moving forward with studies to evaluate the antitumor efficacy of 6-MOMIPP in glioblastoma xenograft models.

The *in vivo* studies used U251-LUC cells in two mouse xenograft models; subcutaneous and intracranial. The results in both models revealed that 6-MOMIPP inhibited tumor growth in a statistically significant manner when administered at a dose of 20 mg/kg. MTAs, especially colchicine-domain binding agents, remain controversial in regard to their toxicity in biological systems [204]. During treatment periods of 12-15 days, 6-MOMIPP did not cause significant changes in body weight or other behavioral signs of toxicity (e.g. hunched posture, lethargy, and ataxia). In addition, no significant changes were observed in several blood chemistry parameters such as ALT, BUN, and Na^+. ALT is typically used to detect liver dysfunction, including viral hepatitis and cirrhosis. BUN measurement is used to detect liver and kidney failure. Na^+ is a factor that is used to determine dehydration and diabetes. We did detect small but significant decreases in ALP, ALB, AMY, and PHOS in plasma of 6-MOMIPP-treated mice, however the decreases in ALB, PHOS are still within normal range. Elevations of ALP may reflect liver, bone, parathyroid, and intestinal disorders, but decreases of ALP are relatively uncommon. Decreased ALB level in serum indicate liver and kidney diseases. AMY is the measurement used to determine kidney and pancreatic function, and the disease is indicated by increasing in serum AMY. PHOS elevation is a biomarker for kidney

disease, hypoparathyroidism and nutritional disorders. Therefore, the slightly decreased levels of ALB may be related to minor liver and kidney damages. There were no statistically significant differences in the TP, glucose, and Ca^{++} after 6-MOMIPP exposure. TP level reflects the dehydration, kidney and liver disease, metabolic and nutritional disorders; GLU levels reflects diabetes, hyperglycemia, hypoglycemia, diabetes and liver disease; and Ca^{++} is the measurements for parathyroid, bone and chronic renal disease. Over all, the blood biochemical parameters measured in this study suggested that 6-MOMIPP long-term treatment did not result in a significant metabolic alterations and organ damage. The principle findings from the nude mouse xenograft models provide valuable evidence to support additional study of and further development of 6-MOMIPP as an anti-tumor drug, particularly for brain tumors that are not usually treatable with other MTAs.

Chapter 4

Summary and Future Direction

The current standard treatments for GBM can only provide patients with a median survival of 15 months and recurrence occurs in almost all patients. Secondary brain tumors arising from metastases from cancers in distant tissues (e.g., lung, breast, skin) also represent an intractable clinical problem. Therefore, new therapeutic agents are desperately needed to treat brain cancers. In this study we have identified several new indolyl-pyridinyl-propenones that act as microtubule destabilizing agents and exhibit significant inhibitory activity against the proliferation and survival of glioblastoma and other cancer cells. The goals of the studies in this dissertation were 1) to understand the mechanism of action of these newly synthesized IPPs and 2) to conduct a preclinical evaluation of the translational potential of these compounds as anti-tumor drugs.

In the studies presented in Chapter 2, I have established that the IPPs function as novel microtubule-targeting agents that kill cancer cells by binding to colchicine site on tubulin, disrupting microtubule dynamics and blocking cell cycle in M phase. I also noted

that cell death is caspase-dependent and occurs after the prolonged metaphase-anaphase transition, which may be mediated by Cdk1. Increased phosphorylation of anti-apoptotic members of the Bcl-2 family of proteins is closely associated with M phase arrest and activation of Cdk1, but precedes cell death. I next provided evidence that activity of the stress-activated kinase, JNK, is increased in connection with microtubule disruption, and that JNK activation plays an important role in cell death. Cytotoxicity analyses showed that our lead microtubule-disrupting IPP, 6-MOMIPP, displays a broad-spectrum of anti-tumor activity in glioblastoma, melanoma, and lung cancer cell lines. Toxicity of 6-MOMIPP is substantially lower in quiescent human fibroblasts, HUVEC, and rat neuronal progenitor cells. Two drug resistant cancer cell lines exhibited reduced sensitivity to 6-MOMIPP, although the compound was still partly effective. In the future, it will be worthwhile to evaluate 6-MOMIPP activity in additional multidrug resistance cell lines, and to determine whether the compound is a substrate for drug efflux via ABC transporters. Pharmacokinetic studies presented in Chapter 3 show that 6-MOMIPP freely crosses the BBB and maintains a therapeutic concentration above 0.5 µM for at least 8 h. In this respect, 6-MOMIPP offers a major advantage over other established MTAs, such as vinblastine, vincristine and taxol. During the PK studies, we found that 6-MOMIPP has low bioavailability through P.O. administration. I.P. injection increases the bioavailability of 6-MOMIPP, permitting preclinical studies in mice. However, to make 6-MOMIPP a better candidate as an anti-tumor drug, future studies will be required to design new formulations and/or different analogues that can be administered by methods more amenable to human trials. Orally available chemotherapeutic drugs can

help avoid complications such as hypersensitivity reactions, toxic reactions, and variable blood flow to the intraperitoneal cavity.

The *in vivo* study described in Chapter 3, two mouse xenograft models, (subcutaneous and intracranial U251 glioblastoma) showed that 6-MOMIPP significantly inhibited tumor growth in both cases. Currently available anti-cancer drugs are known to depress bone marrow function, damage immune system, cause severe peripheral neuropathies, and lead to gastrointestinal toxicity. During the course of our studies, we did not detect significant changes in body weight or behavior, and blood chemistry changes were generally minor, arguing against major toxic effects on liver or kidney function. Preliminary studies with rat neural progenitor cells *in vitro* (Chapter 2) indicate that 6-MOMIPP may not trigger substantial neurotoxicity, but future evaluation of neurotoxicity and potential bone marrow suppression needs to be conducted *in vivo*.

The cumulative results from these studies demonstrate that 6-MOMIPP has promising efficacy as an anti-tumor agent in treating glioblastoma and brain cancer metastases. 6-MOMIPP exhibits a number of properties that make it an excellent candidate for preclinical development. The novelty of our drug lies in its penetration of BBB and absence of systemic toxicity, compared to other MTAs. Our results compel us to continue to examine the effects of 6-MOMIPP on other human neoplasms and designing better analogues/formulations with the final goal of taking them to the clinic. In the future, the utility of 6-MOMIPP and related compounds should also be evaluated in combination with other drugs. Specifically, combining 6-MOMIPP with exist MTAs,

such as paclitaxel or vinblastine that bind to different binding sites, might have synergistic effects and increase the therapeutic index.

References

1. Holland, E.C., *Glioblastoma multiforme: the terminator.* Proc Nat Acad of Sci, 2000. **97**(12): p. 6242-6244.

2. Maher, E.A., et al., *Malignant glioma: genetics and biology of a grave matter.* Genes Dev, 2001. **15**(11): p. 1311-33.

3. Schwartzbaum, J.A., et al., *Epidemiology and molecular pathology of glioma.* Nat Clin Pract Neurol, 2006. **2**(9): p. 494-503; quiz 1 p following 516.

4. Agnihotri, S., et al., *Glioblastoma, a brief review of history, molecular genetics, animal models and novel therapeutic strategies.* Arch Immunol Ther Exp (Warsz), 2013. **61**(1): p. 25-41.

5. Louis, D.N., et al., *The 2007 WHO classification of tumours of the central nervous system.* Acta Neuropathologica, 2007. **114**(2): p. 97-109.

6. Rock, K., et al., *A clinical review of treatment outcomes in glioblastoma multiforme—the validation in a non-trial population of the results of a randomised Phase III clinical trial: has a more radical approach improved survival?* The British Journal of Radiology, 2014.

7.   Thakkar, J.P., et al., *Epidemiologic and molecular prognostic review of glioblastoma.* Cancer Epidemiol Biomarkers Prev, 2014. **23**(10): p. 1985-96.

8.   Johnson, D.R. and B.P. O'Neill, *Glioblastoma survival in the United States before and during the temozolomide era.* J Neurooncol, 2012. **107**(2): p. 359-64.

9.   Wilson, T.A., M.A. Karajannis, and D.H. Harter, *Glioblastoma multiforme: State of the art and future therapeutics.* Surg Neurol Int, 2014. **5**: p. 64.

10.   Ohgaki, H. and P. Kleihues, *Genetic pathways to primary and secondary glioblastoma.* Am J Pathol, 2007. **170**(5): p. 1445-53.

11.   Aldape, K., et al., *Glioblastoma: pathology, molecular mechanisms and markers.* Acta Neuropathol, 2015. **129**(6): p. 829-48.

12.   Stupp, R., et al., *Radiotherapy plus concomitant and adjuvant temozolomide for glioblastoma.* N Engl J Med, 2005. **352**(10): p. 987-96.

13.   Ma, W., et al., *Effects of Temozolomide and Radiotherapy on Brain Metastatic Tumor: A Systematic Review and Meta-Analysis.* World Neurosurg, 2016. **92**: p. 197-205.

14.   Iacob, G. and E.B. Dinca, *Current data and strategy in glioblastoma multiforme.* J Med Life, 2009. **2**(4): p. 386-93.

15.   Bryukhovetskiy, I., et al., *Novel cellular and post-genomic technologies in the treatment of glioblastoma multiforme (Review).* Oncol Rep, 2016. **35**(2): p. 639-48.

132

16.   Stupp, R., et al., *Effects of radiotherapy with concomitant and adjuvant temozolomide versus radiotherapy alone on survival in glioblastoma in a randomised phase III study: 5-year analysis of the EORTC-NCIC trial.* Lancet Oncol, 2009. **10**(5): p. 459-66.

17.   Liu, G., et al., *Analysis of gene expression and chemoresistance of CD133+ cancer stem cells in glioblastoma.* Mol Cancer, 2006. **5**: p. 67.

18.   Salmaggi, A., et al., *Glioblastoma-derived tumorospheres identify a population of tumor stem-like cells with angiogenic potential and enhanced multidrug resistance phenotype.* Glia, 2006. **54**(8): p. 850-60.

19.   Malmstrom, A., et al., *Temozolomide versus standard 6-week radiotherapy versus hypofractionated radiotherapy in patients older than 60 years with glioblastoma: the Nordic randomised, phase 3 trial.* Lancet Oncol, 2012. **13**(9): p. 916-26.

20.   Hanif, F., et al., *Glioblastoma Multiforme: A Review of its Epidemiology and Pathogenesis through Clinical Presentation and Treatment.* Asian Pac J Cancer Prev, 2017. **18**(1): p. 3-9.

21.   Hegi, M.E., et al., *MGMT gene silencing and benefit from temozolomide in glioblastoma.* N Engl J Med, 2005. **352**(10): p. 997-1003.

22.   Eckel-Passow, J.E., et al., *Glioma Groups Based on 1p/19q, IDH, and TERT Promoter Mutations in Tumors.* N Engl J Med, 2015. **372**(26): p. 2499-508.

23.   Klos, K.J. and B.P. O'Neill, *Brain metastases.* Neurologist, 2004. **10**(1): p. 31-46.

24.   Schouten, L.J., et al., *Incidence of brain metastases in a cohort of patients with carcinoma of the breast, colon, kidney, and lung and melanoma.* Cancer, 2002. **94**(10): p. 2698-705.

25.   Barnholtz-Sloan, J.S., et al., *Incidence proportions of brain metastases in patients diagnosed (1973 to 2001) in the Metropolitan Detroit Cancer Surveillance System.* J Clin Oncol, 2004. **22**(14): p. 2865-72.

26.   Posner, J.B., *Management of brain metastases.* Rev Neurol (Paris), 1992. **148**(6-7): p. 477-87.

27.   Buckner, J., *Surgery, radiation therapy, and chemotherapy for metastatic tumors to the brain.* Curr Opin Oncol, 1992. **4**(3): p. 518-24.

28.   Abe, E. and H. Aoyama, *The role of whole brain radiation therapy for the management of brain metastases in the era of stereotactic radiosurgery.* Curr Oncol Rep, 2012. **14**(1): p. 79-84.

29.   Yamamoto, M., et al., *Stereotactic radiosurgery for patients with multiple brain metastases (JLGK0901): a multi-institutional prospective observational study.* Lancet Oncol, 2014. **15**(4): p. 387-95.

30.   Shah, S.P., et al., *Mutational evolution in a lobular breast tumour profiled at single nucleotide resolution.* Nature, 2009. **461**(7265): p. 809-13.

31.   Pardridge, W.M., *The blood-brain barrier: bottleneck in brain drug development.* NeuroRx, 2005. **2**(1): p. 3-14.

32.   Mollinedo, F. and C. Gajate, *Microtubules, microtubule-interfering agents and apoptosis.* Apoptosis, 2003. **8**(5): p. 413-50.

33. Nogales, E., *Structural insights into microtubule function.* Annu Rev Biochem, 2000. **69**: p. 277-302.

34. Field, J.J., A. Kanakkanthara, and J.H. Miller, *Microtubule-targeting agents are clinically successful due to both mitotic and interphase impairment of microtubule function.* Bioorg Med Chem, 2014. **22**(18): p. 5050-9.

35. Jordan, M.A., *Mechanism of action of antitumor drugs that interact with microtubules and tubulin.* Curr Med Chem Anticancer Agents, 2002. **2**(1): p. 1-17.

36. Wilson, L. and M.A. Jordan, *Microtubule dynamics: taking aim at a moving target.* Chem Biol, 1995. **2**(9): p. 569-73.

37. Akhmanova, A. and M.O. Steinmetz, *Control of microtubule organization and dynamics: two ends in the limelight.* Nat Rev Mol Cell Biol, 2015. **16**(12): p. 711-26.

38. Mitchison, T. and M. Kirschner, *Dynamic instability of microtubule growth.* Nature, 1984. **312**(5991): p. 237-42.

39. Jordan, M.A. and L. Wilson, *Microtubules as a target for anticancer drugs.* Nat Rev Cancer, 2004. **4**(4): p. 253-65.

40. Wilson, M.A.J.a.L., *Microtubules as a target for anticancer drugs.* Nat Rev Cancer, 2004. **4**: p. 253-265.

41. Yvon, A.M., P. Wadsworth, and M.A. Jordan, *Taxol suppresses dynamics of individual microtubules in living human tumor cells.* Mol Biol Cell, 1999. **10**(4): p. 947-59.

42. Zhai, Y., et al., *Microtubule dynamics at the G2/M transition: abrupt breakdown of cytoplasmic microtubules at nuclear envelope breakdown and implications for spindle morphogenesis.* J Cell Bio, 1996. **135**(1): p. 201-214.

43. Rieder, C.L., et al., *Anaphase onset in vertebrate somatic cells is controlled by a checkpoint that monitors sister kinetochore attachment to the spindle.* J Cell Bio, 1994. **127**(5): p. 1301-1310.

44. Rodionov, V., E. Nadezhdina, and G. Borisy, *Centrosomal control of microtubule dynamics.* Proc Natl Acad Sci U S A, 1999. **96**(1): p. 115-20.

45. Checchi, P.M., et al., *Microtubule-interacting drugs for cancer treatment.* Trends Pharmacol Sci, 2003. **24**(7): p. 361-5.

46. Mukhtar, E., V.M. Adhami, and H. Mukhtar, *Targeting microtubules by natural agents for cancer therapy.* Mol Cancer Ther, 2014. **13**(2): p. 275-84.

47. Bates, D. and A. Eastman, *Microtubule destabilising agents: far more than just antimitotic anticancer drugs.* Br J Clin Pharmacol, 2017. **83**(2): p. 255-268.

48. Schiff, P.B., J. Fant, and S.B. Horwitz, *Promotion of microtubule assembly in vitro by taxol.* Nature, 1979. **277**(5698): p. 665-7.

49. Parness, J. and S.B. Horwitz, *Taxol binds to polymerized tubulin in vitro.* J Cell Biol, 1981. **91**(2 Pt 1): p. 479-87.

50. Beck, W.T., C.E. Cass, and P.J. Houghton, *Microtubule-targeting anticancer drugs derived from plants and microbes: vinca alkaloids, taxanes, and epothilones.* 2000.

51. Moudi, M., et al., *Vinca alkaloids.* Inter J Prevent Med, 2013. **4**(11): p. 1231.

52.   Zhao, Y., X. Mu, and G. Du, *Microtubule-stabilizing agents: New drug discovery and cancer therapy.* Pharmacol Ther, 2016. **162**: p. 134-43.

53.   Dostál, V. and L. Libusová, *Microtubule drugs: action, selectivity, and resistance across the kingdoms of life.* Protoplasma, 2014. **251**(5): p. 991-1005.

54.   Feyen, F., et al., *Epothilones as lead structures for the synthesis-based discovery of new chemotypes for microtubule stabilization.* Acc Chem Res, 2008. **41**(1): p. 21-31.

55.   Snow, J.W., L.W. Kao, and R.B. Furbee, *Antitubulin Agents: Colchicine, Vinca Alkaloids, and Podophyllin.* Critical Care Toxicology, 2016: p. 1-23.

56.   Kumar, A., P.R. Sharma, and D.M. Mondhe, *Potential anticancer role of colchicine-based derivatives: an overview.* Anti-cancer drugs, 2017. **28**(3): p. 250-262.

57.   Dumontet, C. and M.A. Jordan, *Microtubule-binding agents: a dynamic field of cancer therapeutics.* Nat Rev Drug Discov, 2010. **9**(10): p. 790-803.

58.   Gascoigne, K.E. and S.S. Taylor, *How do anti-mitotic drugs kill cancer cells?* Journal of cell science, 2009. **122**(15): p. 2579-2585.

59.   Krishna, R. and L.D. Mayer, *Multidrug resistance (MDR) in cancer. Mechanisms, reversal using modulators of MDR and the role of MDR modulators in influencing the pharmacokinetics of anticancer drugs.* Eur J Pharm Sci, 2000. **11**(4): p. 265-83.

60.   Cai, P., et al., *A semisynthetic taxane Yg-3-46a effectively evades P-glycoprotein and beta-III tubulin mediated tumor drug resistance in vitro.* Cancer Lett, 2013. **341**(2): p. 214-23.

61.   Seve, P. and C. Dumontet, *Is class III beta-tubulin a predictive factor in patients receiving tubulin-binding agents?* Lancet Oncol, 2008. **9**(2): p. 168-75.

62.   Gertsch, J., et al., *Differential effects of natural product microtubule stabilizers on microtubule assembly: single agent and combination studies with taxol, epothilone B, and discodermolide.* Chembiochem, 2009. **10**(1): p. 166-75.

63.   Chen, J., et al., *Synthesis, biological evaluation and mechanism study of chalcone analogues as novel anti-cancer agents.* RSC Advances, 2015. **5**(83): p. 68128-68135.

64.   Zhang, S., et al., *Synthesis and Evaluation of Selenium-containing Indole Chalcone and Indole Benzophenone Derivatives as Tubulin Polymerization Inhibition Agents.* Organic & Biomolecular Chemistry, 2017.

65.   Yan, J., et al., *Synthesis, evaluation, and mechanism study of novel indole-chalcone derivatives exerting effective antitumor activity through microtubule destabilization in vitro and in vivo.* Journal of medicinal chemistry, 2016. **59**(11): p. 5264-5283.

66.   Canela, M.-D., et al., *Antivascular and antitumor properties of the tubulin-binding chalcone TUB091.* Oncotarget, 2017. **8**(9): p. 14325.

67. Fogaca, T.B., et al., *Apoptotic effect of chalcone derivatives of 2-acetylthiophene in human breast cancer cells.* Pharmacol Rep, 2017. **69**(1): p. 156-161.

68. Bortolotto, L.F., et al., *Cytotoxicity of trans-chalcone and licochalcone A against breast cancer cells is due to apoptosis induction and cell cycle arrest.* Biomed Pharmacother, 2017. **85**: p. 425-433.

69. Tajuddin, Y., et al., *Synthesis of chalcone derivatives and their effects on proliferation and tubulin dynamics instability of HT-29 Cells.* Letters in Drug Design & Discovery, 2016. **13**(7): p. 662-667.

70. Ducki, S., et al., *Combretastatin-like chalcones as inhibitors of microtubule polymerization. Part 1: Synthesis and biological evaluation of antivascular activity.* Bioorgan & Med Chem, 2009. **17**(22): p. 7698-7710.

71. Rao, Y.K., S.-H. Fang, and Y.-M. Tzeng, *Differential effects of synthesized 2′-oxygenated chalcone derivatives: modulation of human cell cycle phase distribution.* Bioorgan & Med Chem, 2004. **12**(10): p. 2679-2686.

72. Kumar, D., et al., *Synthesis and biological evaluation of indolyl chalcones as antitumor agents.* Bioorgan & Med Chem Lett, 2010. **20**(13): p. 3916-3919.

73. Topham, C.H. and S.S. Taylor, *Mitosis and apoptosis: how is the balance set?* Curr Opin Cell Biol, 2013. **25**(6): p. 780-5.

74. Musacchio, A. and E.D. Salmon, *The spindle-assembly checkpoint in space and time.* Nature reviews. Mole Cell Biol, 2007. **8**(5): p. 379.

75. Malumbres, M., *Cyclin-dependent kinases.* Genome Biol, 2014. **15**(6): p. 122.

76.   Harper, J. and P. Adams, *Cyclin-dependent kinases.* Chem Rev, 2001. **101**(8): p. 2511-2526.

77.   Hochegger, H., S. Takeda, and T. Hunt, *Cyclin-dependent kinases and cell-cycle transitions: does one fit all?* Nat Rev. Molecular cell biology, 2008. **9**(11): p. 910.

78.   Ohi, R. and K.L. Gould, *Regulating the onset of mitosis.* Current opinion in cell biology, 1999. **11**(2): p. 267-273.

79.   Castedo, M., et al., *Cell death by mitotic catastrophe: a molecular definition.* Oncogene, 2004. **23**(16): p. 2825-37.

80.   Lolli, G. and L.N. Johnson, *CAK—cyclin-dependent activating kinase: a key kinase in cell cycle control and a target for drugs?* Cell Cycle, 2005. **4**(4): p. 565-570.

81.   Sacristan, C. and G.J. Kops, *Joined at the hip: kinetochores, microtubules, and spindle assembly checkpoint signaling.* Trends Cell Biol, 2015. **25**(1): p. 21-28.

82.   Porter, L.A. and D.J. Donoghue, *Cyclin B1 and CDK1: nuclear localization and upstream regulators.* Prog Cell Cycle Res., 2003. **5**: p. 335-348.

83.   Gould, K.L. and P. Nurse, *Tyrosine phosphorylation of the fission yeast cdc2+ protein kinase regulates entry into mitosis.* Nature, 1989. **342**(6245): p. 39-45.

84.   Donzelli, M. and G.F. Draetta, *Regulating mammalian checkpoints through Cdc25 inactivation.* EMBO Rep, 2003. **4**(7): p. 671-677.

85.   Lundgren, K., et al., *mik1 and wee1 cooperate in the inhibitory tyrosine phosphorylation of cdc2.* Cell, 1991. **64**(6): p. 1111-1122.

86.   Potapova, T.A., et al., *Fine tuning the cell cycle: activation of the Cdk1 inhibitory phosphorylation pathway during mitotic exit.* Mol. Biol. Cell, 2009. **20**(6): p. 1737-1748.

87.   Konishi, Y., et al., *Cdc2 phosphorylation of BAD links the cell cycle to the cell death machinery.* Mol Cell, 2002. **9**(5): p. 1005-1016.

88.   Perfettini, J.-L., et al., *NF-κB and p53 are the dominant apoptosis-inducing transcription factors elicited by the HIV-1 envelope.* J. Exp. Med, 2004. **199**(5): p. 629-640.

89.   Vitale, I., et al., *Mitotic catastrophe: a mechanism for avoiding genomic instability.* Nat Rev Mol Cell Biol, 2011. **12**(6): p. 385-92.

90.   Galluzzi, L., et al., *Molecular definitions of cell death subroutines: recommendations of the Nomenclature Committee on Cell Death 2012.* Cell Death Differ, 2012. **19**(1): p. 107.

91.   Russell, P. and P. Nurse, *cdc25+ functions as an inducer in the mitotic control of fission yeast.* Cell, 1986. **45**(1): p. 145-153.

92.   Vakifahmetoglu, H., M. Olsson, and B. Zhivotovsky, *Death through a tragedy: mitotic catastrophe.* Cell Death Differ, 2008. **15**(7): p. 1153-62.

93.   Weaver, B.A. and D.W. Cleveland, *Decoding the links between mitosis, cancer, and chemotherapy: The mitotic checkpoint, adaptation, and cell death.* Cancer Cell, 2005. **8**(1): p. 7-12.

94.   Rieder, C.L. and H. Maiato, *Stuck in division or passing through: what happens when cells cannot satisfy the spindle assembly checkpoint.* Dev. Cell, 2004. **7**(5): p. 637-651.

95.   Brito, D.A. and C.L. Rieder, *Mitotic checkpoint slippage in humans occurs via cyclin B destruction in the presence of an active checkpoint.* Curr Biol, 2006. **16**(12): p. 1194-200.

96.   Galluzzi, L., O. Kepp, and G. Kroemer, *TP53 and MTOR crosstalk to regulate cellular senescence.* Aging (Albany NY), 2010. **2**(9): p. 535.

97.   Dimri, G.P., *What has senescence got to do with cancer?* Cancer cell, 2005. **7**(6): p. 505-512.

98.   Stepień, A., M. Izdebska, and A. Grzanka, *The types of cell death.* Postepy Hig Med Dosw (Online), 2007. **61**: p. 420-428.

99.   Kroemer, G., et al., *Classification of cell death: recommendations of the Nomenclature Committee on Cell Death 2009.* Cell Death Differ, 2009. **16**(1): p. 3-11.

100.   Castedo, M. and G. Kroemer, *[Mitotic catastrophe: a special case of apoptosis].* J Soc Biol, 2004. **198**(2): p. 97-103.

101.   Nabha, S.M., et al., *Combretastatin-A4 prodrug induces mitotic catastrophe in chronic lymphocytic leukemia cell line independent of caspase activation and poly(ADP-ribose) polymerase cleavage.* Clin Cancer Res, 2002. **8**(8): p. 2735-41.

102. Jordan, M.A., et al., *Mitotic block induced in HeLa cells by low concentrations of paclitaxel (Taxol) results in abnormal mitotic exit and apoptotic cell death.* Cancer Res, 1996. **56**(4): p. 816-25.

103. Waldman, T., et al., *Uncoupling of S phase and mitosis induced by anticancer agents in cells lacking p21.* Nature, 1996. **381**(6584): p. 713-6.

104. Roninson, I.B., E.V. Broude, and B.D. Chang, *If not apoptosis, then what? Treatment-induced senescence and mitotic catastrophe in tumor cells.* Drug Resist Updat, 2001. **4**(5): p. 303-13.

105. Nakayama, Y. and T. Inoue, *Antiproliferative Fate of the Tetraploid Formed after Mitotic Slippage and Its Promotion; A Novel Target for Cancer Therapy Based on Microtubule Poisons.* Molecules, 2016. **21**(5).

106. Elmore, S., *Apoptosis: a review of programmed cell death.* Toxicologic pathology, 2007. **35**(4): p. 495-516.

107. Ouyang, L., et al., *Programmed cell death pathways in cancer: a review of apoptosis, autophagy and programmed necrosis.* Cell Prolif, 2012. **45**(6): p. 487-498.

108. Geske, F.J. and L.E. Gerschenson, *The biology of apoptosis.* Hum Pathol, 2001. **32**(10): p. 1029-1038.

109. Parrish, A.B., C.D. Freel, and S. Kornbluth, *Cellular mechanisms controlling caspase activation and function.* Cold Spring Harb Perspect Biol, 2013. **5**(6): p. a008672.

110. Favaloro, B., et al., *Role of apoptosis in disease.* Aging (Albany NY), 2012. **4**(5): p. 330.

111. Vucic, D., V.M. Dixit, and I.E. Wertz, *Ubiquitylation in apoptosis: a post-translational modification at the edge of life and death.* Nat. Rev. Mol. Cell Biol, 2011. **12**(7): p. 439.

112. Chen, M. and J. Wang, *Initiator caspases in apoptosis signaling pathways.* Apoptosis, 2002. **7**(4): p. 313-319.

113. Fulda, S. and K. Debatin, *Extrinsic versus intrinsic apoptosis pathways in anticancer chemotherapy.* Oncogene, 2006. **25**(34): p. 4798.

114. Chipuk, J., L. Bouchier-Hayes, and D. Green, *Mitochondrial outer membrane permeabilization during apoptosis: the innocent bystander scenario.* Cell Death Differ, 2006. **13**(8): p. 1396-1402.

115. Green, D.R. and G. Kroemer, *The pathophysiology of mitochondrial cell death.* Science, 2004. **305**(5684): p. 626-629.

116. Ichim, G. and S.W. Tait, *A fate worse than death: apoptosis as an oncogenic process.* Nat. Rev. Cancer, 2016. **16**: p. 539-548.

117. Brentnall, M., et al., *Caspase-9, caspase-3 and caspase-7 have distinct roles during intrinsic apoptosis.* BMC Cell Biol, 2013. **14**(1): p. 32.

118. Nikoletopoulou, V., et al., *Crosstalk between apoptosis, necrosis and autophagy.* Biochim Biophys Acta -Mol Cell Res, 2013. **1833**(12): p. 3448-3459.

119.   Vanden Berghe, T., et al., *Regulated necrosis: the expanding network of non-apoptotic cell death pathways.* Nat Rev Mol Cell Biol, 2014. **15**(2): p. 135-47.

120.   Los, M., et al., *Activation and caspase-mediated inhibition of PARP: a molecular switch between fibroblast necrosis and apoptosis in death receptor signaling.* Mol. Biol. Cell , 2002. **13**(3): p. 978-988.

121.   Skulachev, V., *Bioenergetic aspects of apoptosis, necrosis and mitoptosis.* Apoptosis, 2006. **11**(4): p. 473-485.

122.   Matsumura, H., et al., *Necrotic death pathway in Fas receptor signaling.* J. Cell Biol, 2000. **151**(6): p. 1247-1256.

123.   He, S., et al., *Receptor interacting protein kinase-3 determines cellular necrotic response to TNF-α.* Cell, 2009. **137**(6): p. 1100-1111.

124.   Ling, Y.-H., C. Tornos, and R. Perez-Soler, *Phosphorylation of Bcl-2 is a marker of M phase events and not a determinant of apoptosis.* J. Biol. Chem, 1998. **273**(30): p. 18984-18991.

125.   Zinkel, S., A. Gross, and E. Yang, *BCL2 family in DNA damage and cell cycle control.* Cell Death Differ, 2006. **13**(8): p. 1351.

126.   Lu, Q.-L., et al., *Bcl-2 protein localizes to the chromosomes of mitotic nuclei and is correlated with the cell cycle in cultured epithelial cell lines.* J. Cell Sci, 1994. **107**(2): p. 363-371.

127.   Basu, A. and S. Haldar, *Microtubule-damaging drugs triggered bcl2 phosphorylation-requirement of phosphorylation on both serine-70 and serine-87 residues of bcl2 protein.* Int. J. Oncol., 1998. **13**(4): p. 659-723.

128. Haldar, S., A. Basu, and C.M. Croce, *Serine-70 is one of the critical sites for drug-induced Bcl2 phosphorylation in cancer cells.* Cancer Res., 1998. **58**(8): p. 1609-1615.

129. Correia, C., et al., *Emerging understanding of Bcl-2 biology: Implications for neoplastic progression and treatment.* Biochimica et Biophysica Acta -Mole Cell Res., 2015. **1853**(7): p. 1658-1671.

130. Du, L., C.S. Lyle, and T.C. Chambers, *Characterization of vinblastine-induced Bcl-xL and Bcl-2 phosphorylation: evidence for a novel protein kinase and a coordinated phosphorylation/dephosphorylation cycle associated with apoptosis induction.* Oncogene, 2005. **24**(1): p. 107-17.

131. Upreti, M., et al., *Identification of the major phosphorylation site in Bcl-xL induced by microtubule inhibitors and analysis of its functional significance.* J. Biol. Chem., 2008. **283**(51): p. 35517-35525.

132. Harley, M.E., et al., *Phosphorylation of Mcl‑1 by CDK1‑cyclin B1 initiates its Cdc20‑dependent destruction during mitotic arrest.* EMBO J., 2010. **29**(14): p. 2407-2420.

133. Shi, J., et al., *Navitoclax (ABT-263) accelerates apoptosis during drug-induced mitotic arrest by antagonizing Bcl-xL.* Cancer Res., 2011. **71**(13): p. 4518-4526.

134. Ruth, A.C. and I.B. Roninson, *Effects of the multidrug transporter P-glycoprotein on cellular responses to ionizing radiation.* Cancer Res., 2000. **60**(10): p. 2576-2578.

135. Terrano, D.T., M. Upreti, and T.C. Chambers, *Cyclin-dependent kinase 1-mediated Bcl-xL/Bcl-2 phosphorylation acts as a functional link coupling mitotic arrest and apoptosis.* Mol. Cell. Biol., 2010. **30**(3): p. 640-656.

136. Eichhorn, J., et al., *Critical role of anti-apoptotic Bcl-2 protein phosphorylation in mitotic death.* Cell Death Dis, 2013. **4**(10): p. e834.

137. Fan, M., et al., *Vinblastine-induced phosphorylation of Bcl-2 and Bcl-xL is mediated by JNK and occurs in parallel with inactivation of the Raf-1/MEK/ERK cascade.* J. Biol. Chem., 2000. **275**(39): p. 29980-29985.

138. Yamamoto, K., H. Ichijo, and S.J. Korsmeyer, *BCL-2 is phosphorylated and inactivated by an ASK1/Jun N-terminal protein kinase pathway normally activated at G2/M.* Mol. Cell. Biol., 1999. **19**(12): p. 8469-8478.

139. Johnson, G.L. and K. Nakamura, *The c-jun kinase/stress-activated pathway: regulation, function and role in human disease.* Biochim Biophys Acta-Mole Cell Res., 2007. **1773**(8): p. 1341-1348.

140. Parker, A.L., M. Kavallaris, and J.A. McCarroll, *Microtubules and their role in cellular stress in cancer.* Front Oncol, 2014. **4**.

141. Davis, R.J., *Signal transduction by the JNK group of MAP kinases.* Cell, 2000. **103**(2): p. 239-252.

142. Aoki, H., et al., *Direct activation of mitochondrial apoptosis machinery by c-Jun N-terminal kinase in adult cardiac myocytes.* J Biol Chem, 2002. **277**(12): p. 10244-50.

143.   Kharbanda, S., et al., *Translocation of SAPK/JNK to mitochondria and interaction with Bcl-xL in response to DNA damage.* J. Biol. Chem., 2000. **275**(1): p. 322-327.

144.   Brichese, L., G. Cazettes, and A. Valette, *JNK is associated with Bcl-2 and PP1 in mitochondria: paclitaxel induces its activation and its association with the phosphorylated form of Bcl-2.* Cell Cycle, 2004. **3**(10): p. 1312-1319.

145.   Yamamoto, K., H. Ichijo, and S.J. Korsmeyer, *BCL-2 is phosphorylated and inactivated by an ASK1/Jun N-terminal protein kinase pathway normally activated at G(2)/M.* Mol Cell Biol, 1999. **19**(12): p. 8469-78.

146.   Du, L., et al., *Inhibition of Cell Proliferation and Cell Cycle Progression by Specific Inhibition of Basal JNK Activity Evidence That Mitotic Bcl-2 Phosphorylation Is Jnk-Independent.* J. Biol. Chem., 2004. **279**(12): p. 11957-11966.

147.   Bakiri, L., et al., *Cell cycle‐dependent variations in c‐Jun and JunB phosphorylation: a role in the control of cyclin D1 expression.* EMBO J, 2000. **19**(9): p. 2056-2068.

148.   Oktay, K., et al., *The c-Jun N-terminal kinase JNK functions upstream of Aurora B to promote entry into mitosis.* Cell Cycle, 2008. **7**(4): p. 533-541.

149.   Gutierrez, G.J., et al., *JNK-mediated phosphorylation of Cdc25C regulates cell cycle entry and G(2)/M DNA damage checkpoint.* J Biol Chem, 2010. **285**(19): p. 14217-28.

150.   Zhu, N., et al., *Gadd45-α and Gadd45-γ utilize p38 and JNK signaling pathways to induce cell cycle G2/M arrest in Hep-G2 hepatoma cells.* Mol Biol Rep, 2009. **36**(8): p. 2075.

151.   Zhu, B.-k., et al., *Activation of Jun N-terminal kinase is a mediator of vincristine-induced apoptosis of melanoma cells.* Anti-cancer drugs, 2008. **19**(2): p. 189-200.

152.   Wang, C.C., et al., *Plumbagin induces cell cycle arrest and apoptosis through reactive oxygen species/c-Jun N-terminal kinase pathways in human melanoma A375. S2 cells.* Cancer Lett., 2008. **259**(1): p. 82-98.

153.   Kolomeichuk, S.N., et al., *Distinct signaling pathways of microtubule inhibitors – vinblastine and Taxol induce JNK‐dependent cell death but through AP‐1‐dependent and AP‐1‐independent mechanisms, respectively.* FEBS J, 2008. **275**(8): p. 1889-1899.

154.   Stone, A.A. and T.C. Chambers, *Microtubule inhibitors elicit differential effects on MAP kinase (JNK, ERK, and p38) signaling pathways in human KB-3 carcinoma cells.* Exp. Cell Res., 2000. **254**(1): p. 110-119.

155.   Fan, M., et al., *Modulation of mitogen-activated protein kinases and phosphorylation of Bcl-2 by vinblastine represent persistent forms of normal fluctuations at G2-M.* Cancer Res., 2000. **60**(22): p. 6403-6407.

156.   Wang, T.-H., et al., *Microtubule dysfunction induced by paclitaxel initiates apoptosis through both c-Jun N-terminal kinase (JNK)-dependent and-*

independent pathways in ovarian cancer cells. J. Biol. Chem., 1999. **274**(12): p. 8208-8216.

157. Annovazzi, L., M. Mellai, and D. Schiffer, *Chemotherapeutic Drugs: DNA Damage and Repair in Glioblastoma.* Cancers, 2017. **9**(6): p. 57.

158. Overmeyer, J.H., et al., *A chalcone-related small molecule that induces methuosis, a novel form of non-apoptotic cell death, in glioblastoma cells.* Mol Cancer, 2011. **10**: p. 69.

159. Bhanot, H., et al., *Induction of nonapoptotic cell death by activated Ras requires inverse regulation of Rac1 and Arf6.* Mol Cancer Res, 2010. **8**(10): p. 1358-74.

160. Maltese, W.A. and J.H. Overmeyer, *Methuosis: nonapoptotic cell death associated with vacuolization of macropinosome and endosome compartments.* Am J Pathol, 2014. **184**(6): p. 1630-42.

161. Maltese, W.A. and J.H. Overmeyer, *Non-apoptotic cell death associated with perturbations of macropinocytosis.* Front Physiol, 2015. **6**: p. 38.

162. Trabbic, C.J., et al., *Synthesis and biological evaluation of indolyl-pyridinyl-propenones having either methuosis or microtubule disruption activity.* J Med Chem, 2015. **58**(5): p. 2489-512.

163. Robinson, M.W., et al., *Synthesis and evaluation of indole-based chalcones as inducers of methuosis, a novel type of nonapoptotic cell death.* J Med Chem, 2012. **55**(5): p. 1940-56.

164. Trabbic, C.J., et al., *Synthesis and biological evaluation of isomeric methoxy substitutions on anti-cancer indolyl-pyridinyl-propenones: Effects on potency and mode of activity.* Eur J Med Chem, 2016. **122**: p. 79-91.

165. Stanton, R.A., et al., *Drugs that target dynamic microtubules: a new molecular perspective.* Med. Res. Rev., 2011. **31**(3): p. 443-481.

166. O'Reilly, K.C., et al., *13-cis-Retinoic acid alters intracellular serotonin, increases 5-HT1A receptor, and serotonin reuptake transporter levels in vitro.* Exp Biol Med (Maywood), 2007. **232**(9): p. 1195-203.

167. Maltese, W.A. and D.C. De Vivo, *Cholesterol and phospholipids in cultured skin fibroblasts from patients with dystonia.* Ann Neurol, 1984. **16**(2): p. 250-2.

168. Trabbic, C.J., et al., *Differential Induction of Cytoplasmic Vacuolization and Methuosis by Novel 2-Indolyl-Substituted Pyridinylpropenones.* ACS Med Chem Lett, 2014. **5**(1): p. 73-77.

169. Skehan, P., et al., *New colorimetric cytotoxicity assay for anticancer-drug screening.* J. Natl. Cancer Inst, 1990. **82**(13): p. 1107-1112.

170. Morrison, K.C. and P.J. Hergenrother, *Whole cell microtubule analysis by flow cytometry.* Anal Biochem, 2012. **420**(1): p. 26-32.

171. Tahir, S.K., et al., *Rapid colchicine competition-binding scintillation proximity assay using biotin-labeled tubulin.* Biotechniques, 2000. **29**(1): p. 156-60.

172. Fortin, S., et al., *Quick and simple detection technique to assess the binding of antimicrotubule agents to the colchicine-binding site.* Biol. Proced. Online, 2010. **12**(1): p. 113.

173. Kwon, Y.-G., et al., *Cell cycle-dependent phosphorylation of mammalian protein phosphatase 1 by cdc2 kinase.* Proc. Natl. Acad. Sci., 1997. **94**(6): p. 2168-2173.

174. Morton Bradbury, E., *Reversible histone modification and the chromosome cell cycle.* Bioessays, 1992. **14**(1): p. 9-16.

175. Van Hooser, A., et al., *Histone H3 phosphorylation is required for the initiation, but not maintenance, of mammalian chromosome condensation.* J. Cell Sci., 1998. **111**(23): p. 3497-3506.

176. Prigent, C. and S. Dimitrov, *Phosphorylation of serine 10 in histone H3, what for?* J. Cell Sci., 2003. **116**(18): p. 3677-3685.

177. Hans, F. and S. Dimitrov, *Histone H3 phosphorylation and cell division.* Oncogene, 2001. **20**(24): p. 3021.

178. Bacus, S.S., et al., *Taxol-induced apoptosis depends on MAP kinase pathways (ERK and p38) and is independent of p53.* Oncogene, 2001. **20**(2): p. 147.

179. Fan, M., et al., *The c-Jun NH2-terminal protein kinase/AP-1 pathway is required for efficient apoptosis induced by vinblastine.* Cancer Res., 2001. **61**(11): p. 4450-4458.

180. Bollig-Fischer, A., et al., *The molecular genomics of metastatic brain tumours.* Mol. Oncol, 2013. **1**(1).

181. Dumontet, C. and B.I. Sikic, *Mechanisms of action of and resistance to antitubulin agents: microtubule dynamics, drug transport, and cell death.* J. Clin. Oncol., 1999. **17**(3): p. 1061-1061.

182. Mukhtar, E., V.M. Adhami, and H. Mukhtar, *Targeting microtubules by natural agents for cancer therapy.* Mol. Cancer Ther., 2014. **13**(2): p. 275-284.

183. Blajeski, A.L., et al., *G1 and G2 cell-cycle arrest following microtubule depolymerization in human breast cancer cells.* J. Clin. Investig., 2002. **110**(1): p. 91.

184. Blagosklonny, M.V. and T. Fojo, *Molecular effects of paclitaxel: myths and reality (a critical review).* Int J Cancer, 1999. **83**(2): p. 151-6.

185. Blagosklonny, M.V., *Sequential activation and inactivation of G2 checkpoints for selective killing of p53-deficient cells by microtubule-active drugs.* Oncogene, 2002. **21**(41): p. 6249.

186. O'Connor, D.S., et al., *A p34 cdc2 survival checkpoint in cancer.* Cancer Cell, 2002. **2**(1): p. 43-54.

187. Brown, J.M. and L.D. Attardi, *The role of apoptosis in cancer development and treatment response.* Nat. Rev. Cancer, 2005. **5**(3): p. 231-237.

188. Yu, D., et al., *Overexpression of ErbB2 blocks Taxol-induced apoptosis by upregulation of p21 Cip1, which inhibits p34 Cdc2 kinase.* Mol. Cell., 1998. **2**(5): p. 581-591.

189. Shen, S.C., et al., *Taxol-induced p34cdc2 kinase activation and apoptosis inhibited by 12-O-tetradecanoylphorbol-13-acetate in human breast MCF-7 carcinoma cells.* Cell Growth Differ, 1998. **9**(1): p. 23-29.

190. Maurer, M., O. Komina, and J. Węsierska‑Gądek, *Roscovitine Differentially Affects Asynchronously Growing and Synchronized Human MCF‑7 Breast Cancer Cells.* Ann. N. Y. Acad. Sci., 2009. **1171**(1): p. 250-256.

191. Choi, H.J., M. Fukui, and B.T. Zhu, *Role of cyclin B1/Cdc2 up-regulation in the development of mitotic prometaphase arrest in human breast cancer cells treated with nocodazole.* PLOS One, 2011. **6**(8): p. e24312.

192. Upreti, M., et al., *Vinblastine-induced apoptosis is mediated by discrete alterations in subcellular location, oligomeric structure, and activation status of specific Bcl-2 family members.* J Biol Chem, 2006. **281**(23): p. 15941-50.

193. Sharma, P.S., R. Sharma, and R. Tyagi, *Inhibitors of cyclin dependent kinases: useful targets for cancer treatment.* Curr. Cancer Drug Targets., 2008. **8**(1): p. 53-75.

194. Collins, I. and M.D. Garrett, *Targeting the cell division cycle in cancer: CDK and cell cycle checkpoint kinase inhibitors.* Curr Opin Pharmacol, 2005. **5**(4): p. 366-373.

195. Tanemura, S., et al., *Utility and limitations of SP600125, an inhibitor of stress-responsive c-Jun N-terminal kinase.* Curr Enzym Inhib, 2010. **6**(1): p. 26-33.

196. Kim, J.A., et al., *SP600125 suppresses Cdk1 and induces endoreplication directly from G2 phase, independent of JNK inhibition.* Oncogene, 2010. **29**(11): p. 1702-16.

197. Bates, D. and A. Eastman, *Microtubule destabilising agents: far more than just antimitotic anticancer drugs.* Br. J. Clin. Pharmacol., 2016.

198.   Schwartz, E.L., *Antivascular actions of microtubule-binding drugs.* Clinical Cancer Res., 2009. **15**(8): p. 2594-2601.

199.   Lu, Y., et al., *An overview of tubulin inhibitors that interact with the colchicine binding site.* Pharm. Res., 2012. **29**(11): p. 2943-2971.

200.   Chen, J., et al., *Recent development and SAR analysis of colchicine binding site inhibitors.* Mini Rev Med Chem, 2009. **9**(10): p. 1174-1190.

201.   Ozawa, T. and C.D. James, *Establishing intracranial brain tumor xenografts with subsequent analysis of tumor growth and response to therapy using bioluminescence imaging.* J Vis Exp., 2010(41).

202.   Loscher, W. and H. Potschka, *Blood-brain barrier active efflux transporters: ATP-binding cassette gene family.* NeuroRx, 2005. **2**(1): p. 86-98.

203.   Laquintana, V., et al., *New strategies to deliver anticancer drugs to brain tumors.* Expert Opin. Drug Deliv., 2009. **6**(10): p. 1017-1032.

204.   Attard, G., et al., *Update on tubulin-binding agents.* Pathol. Biol., 2006. **54**(2): p. 72-84.

Appendix A

Supplementary Data for Chapter 2
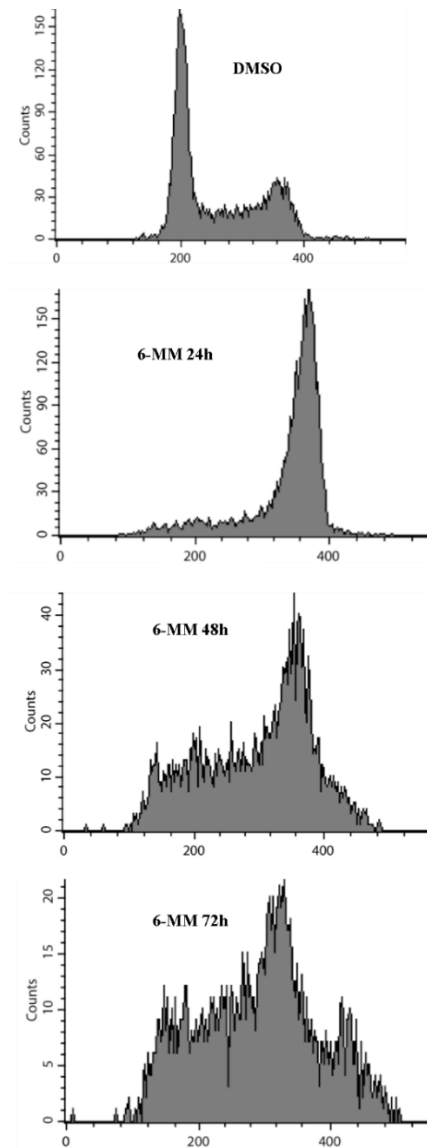
Appendix A Figure 1. Effect of 6-MOMIPP on cell cycle distribution in T98G cells. DNA histone-grams of cells treated with 6-MOMIPP at 1 µM for 24 h, 48 h or 72 h were generated by FACS-Calibur flow cytometry as described in the Material and Methods section. Cells in the G_2/M phase were identified based on the 4N PI stain. DNA histograms were generated with CellQuest Pro software. Experiment was repeated 3 times.
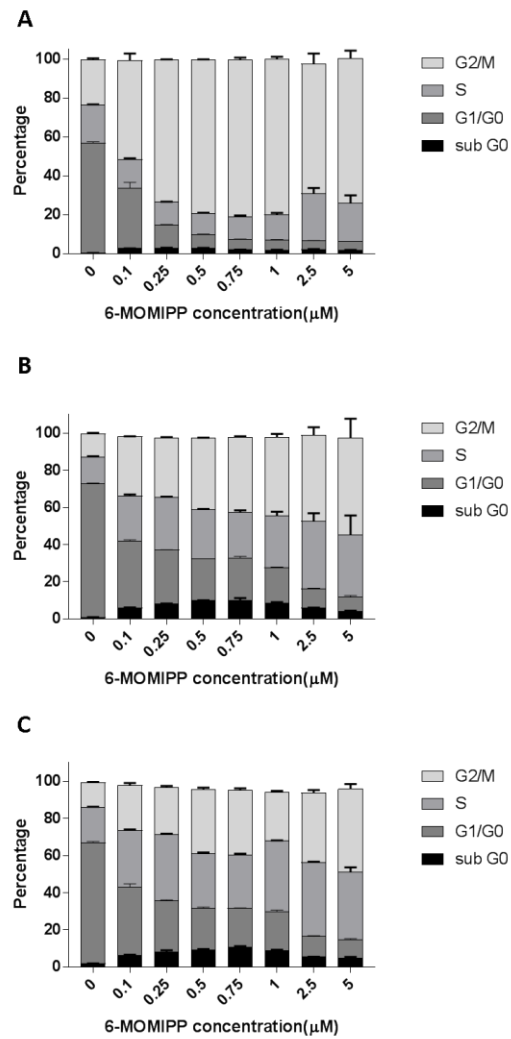
Appendix A Figure 2. Effects of 6-MOMIPP on cell cycle distribution in T98G cells.

A. The assessment of cell cycle distribution was repeated in T98G cells treated with 6-MOMIPP at indicated concentrations. Both attached and detached cells were harvested at 24 h and subjected to FACS-Calibur flow cytometry. Data were analyzed by GraphPad Prism 7 and each point represents mean ± S.D. derived from three separate cultures. B.

DNA histograms of U251 cells that were treated with 6-MOMIPP for 48 h. C. U251

cells were treated with 6-MOMIPP for 72 h.
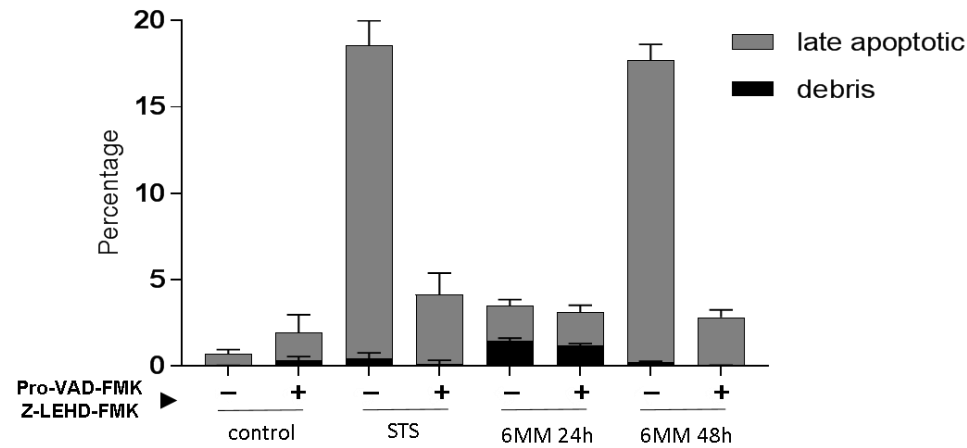
Appendix A Figure 3. Caspase inhibitor study. 100,000 U251 cells were seeded in 35

mm dishes. On the second day, the cells were pretreated with or without Caspase 9

inhibitor Z-LEHD-FMK and Pan-Caspase inhibitor PRO-VAD-FMK for 2 h followed

by 6-MOMIPP treatment for the indicated time. Cells were harvested and stained with

annexin V and 7-ADD before being analyzed. Data were analyzed with GraphPad Prism

7 and each point represents mean ± S.D. of triplicates.
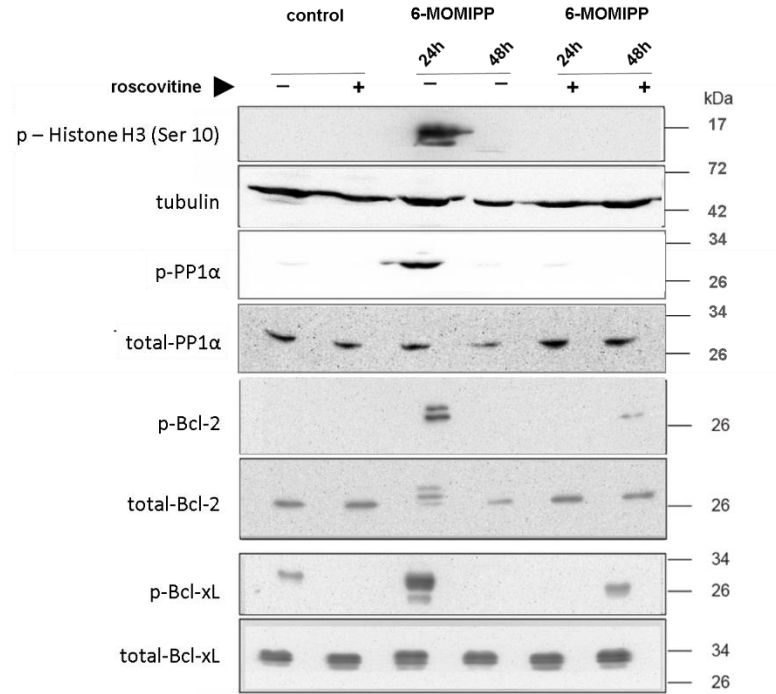
Appendix A Figure 4. 6-MOMIPP-induced Cdk1 activation plays an important role in mitotic arrest and Bcl-xL/Bcl-2 phosphorylation. 10^6 U251 cells were seeded in the 10 cm dishes and treated with 1 μM 6-MOMIPP, or an equivalent volume of DMSO. For the inhibitor study, 15 µM roscovitine was added to the cells 2 h before the addition of 6-MOMIPP. Detaches and attached cells were harvested after 24 h or 48 h subjected to SDS-PAGE and immunoblot analysis for the indicated proteins as described in the Methods. The results shown are representative of three replicate experiments.
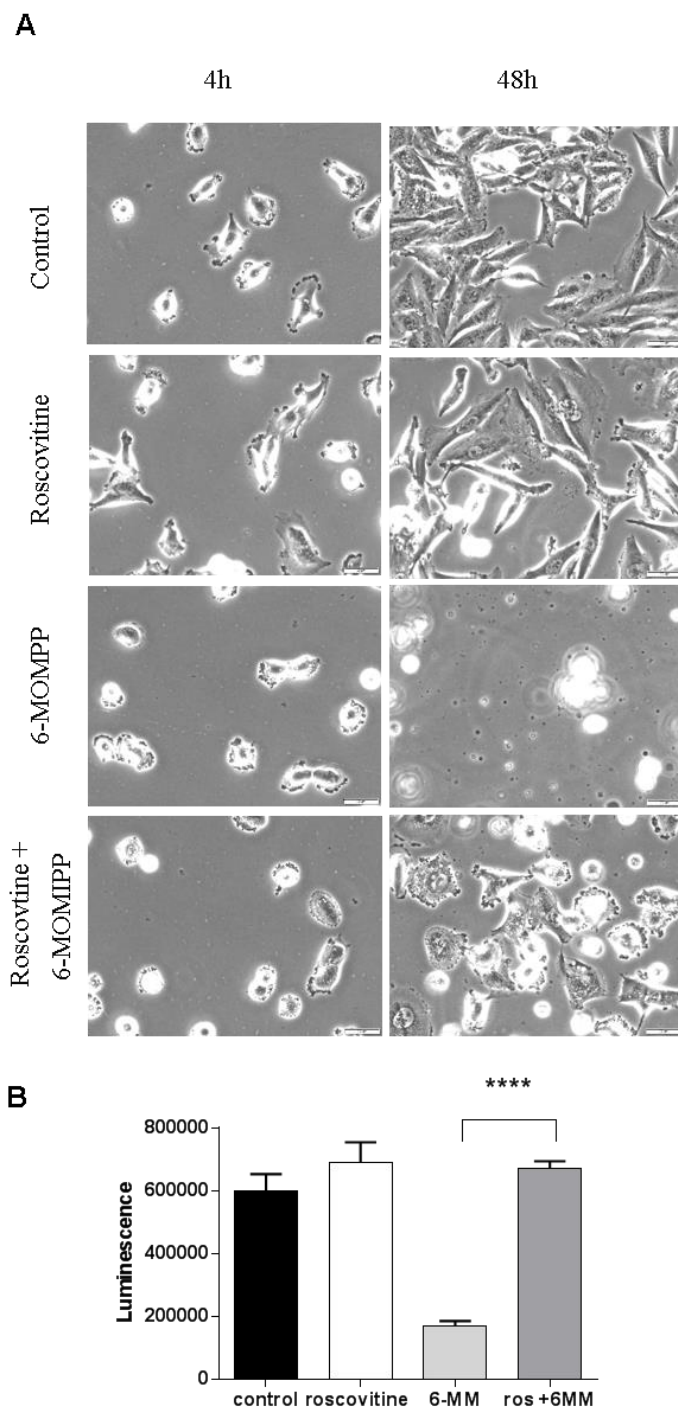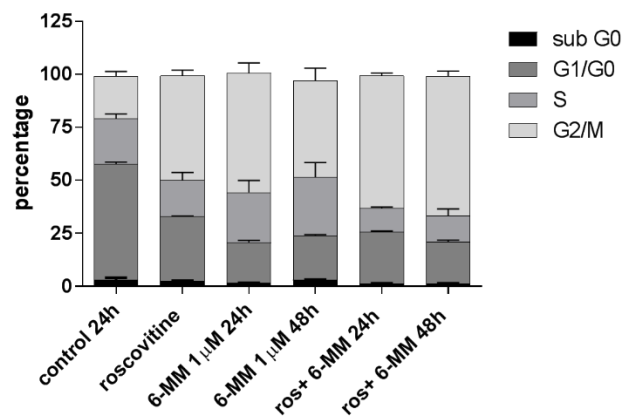
Appendix A Figure 5. CDK1 inhibitor, roscovitine, blocks cell death induced by 6-

MOMIPP. A. 100,000 U251 cells were seeded in 35 mm dishes. The next day, cells were

treated with DMSO, 15 μM roscovitine, 1 μM 6-MOMIPP or combination of roscovitine

(2 h pretreatment with 1 μM 6-MOMIPP. Phase-contrast images were obtained at 4 h

and 48 h B. U251 cells were seeded in a white-walled opaque 96-well plate at a density

of 2,000 cells/well. On the second day, 6-MOMIPP at the indicated concentrations was

added and cell viability was assayed after 48 h. For the inhibitor study, 15 μM of

roscovitine was added 2 h before 6-MOMIPP treatment. Luminescence was determined

as described in the Methods. Values represent the mean ± S.D. of four replicates. ****

$p < 0.0001$.
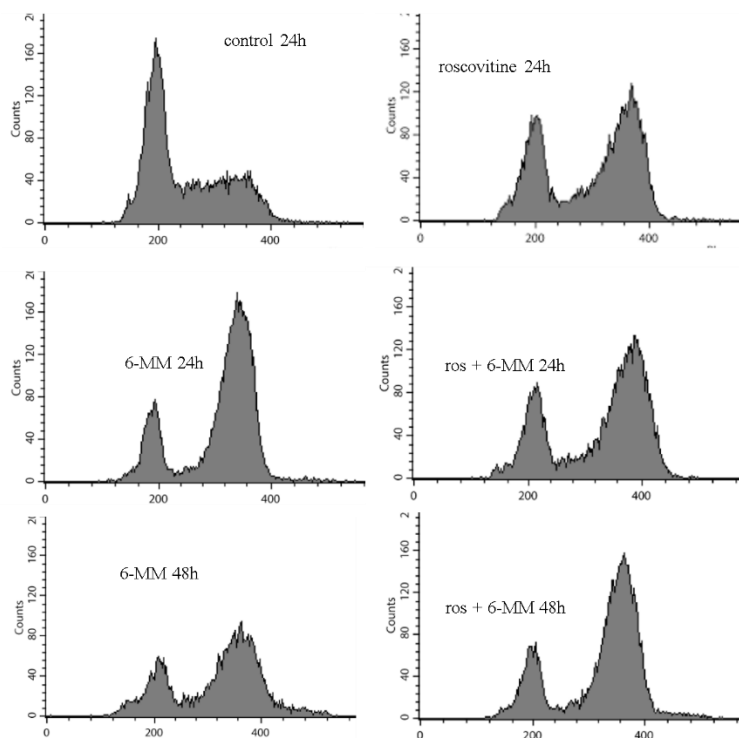
Appendix A Figure 6. Effects of the Cdk1 inhibitor, roscovitine, on the cell cycle arrest induced by 6-MOMIPP. A. U251 cells were seeded at 350,000 cells in 60 mm dishes and treated with 1 µM 6-MOMIPP for 24 h or 48 h. For the inhibitor study, 15 µM

roscovitine was added 2 h before the 6-MOMPP treatment. Then both attached and detached cells were harvested, fixed with 70% ethanol and stained with propidium iodide (PI). The cellular DNA content in each sample was analyzed by flow cytometry as described in the Methods. B. Cell cycle data were quantified and plotted with GraphPad Prism 7. Each point represents mean ± S.D. of triplicates.
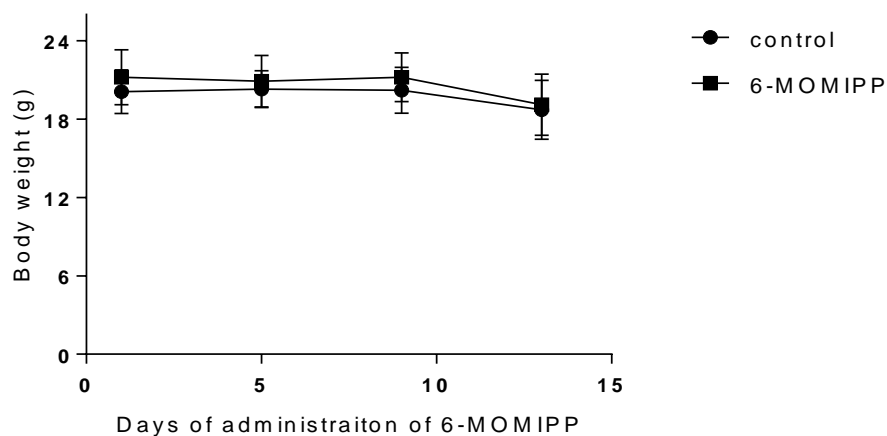
Appendix B

Supplementary Data for Chapter 3
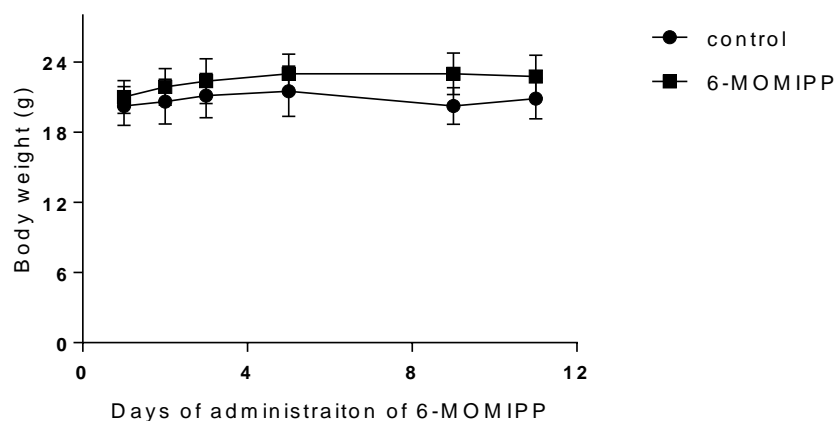
Appendix B Figure 1. 6-MOMIPP does not affect body weight of mice bearing subcutaneous U251 xenografts. Mice from Figure 3-3 were treated with 20 mg/kg 6-MOMIPP every 12 h for 15 d by I.P. injection. The control group received the same volume vehicle. Body weight of each mouse was recorded on the indicated days after the drug treatment. Each point represents mean ± S.D., with n = 8 for each group.
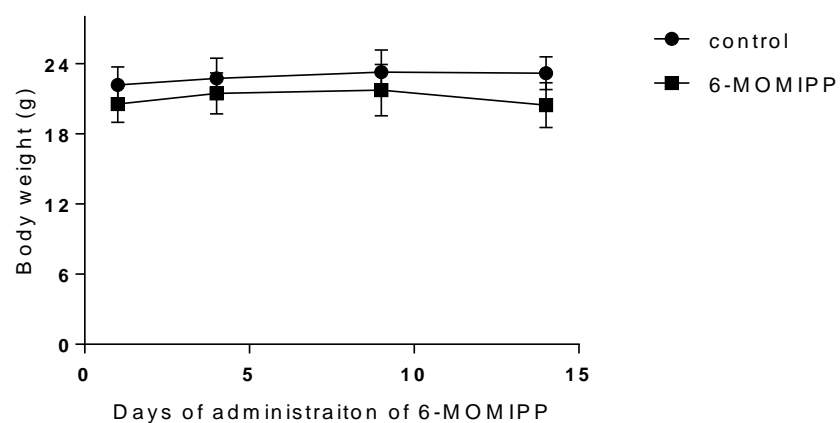
Appendix B Figure 2. 6-MOMIPP does not affect body weight of mice bearing subcutaneous U251 xenografts. Mice from Figure 3-5 were treated with 20 mg/kg 6-MOMIPP every 12 h for 14 days by I.P. injection. The control group received the same volume vehicle. Body weight of each mouse was recorded on the indicated days after the drug treatment. Each point represents mean ± S.D., with n = 11 for each group.

Appendix B Figure 3. 6-MOMIPP does not affect body weight of mice bearing intracranial U251 xenografts. Mice from Figure 3-7 were treated with 20 mg/kg 6-MOMIPP every 12 h for 12 d by I.P. injection. The control group received the same volume vehicle. Body weight of each mouse was recorded on the indicated days after the drug treatment. Each point represents mean ± S.D., with n = 10 for each group.